01 May 1972

The structural behavior of cold-formed steel members with perforated elements

Charles S. Davis

Wei-wen Yu
Missouri University of Science and Technology, wwy4@mst.edu

Department of Civil Engineering

School of Engineering

UNIVERSITY OF MISSOURI-ROLLA

Final Report

THE STRUCTURAL BEHAVIOR OF COLD-FORMED STEEL MEMBERS WITH PERFORATED ELEMENTS

by

Charles S. Davis
Research Assistant

Wei-Wen Yu
Project Director

A Research Project Sponsored by

American Iron and Steel Institute

ROLLA, MISSOURI

May, 1972

PREFACE

This report was originally a dissertation presented to the Faculty of the Graduate School of the University of Missouri-Rolla in partial fulfillment of the requirements for the Degree of Doctor of Philosophy in Civil Engineering, for conferment in May 1972.

The research project described within was sponsored by American Iron and Steel Institute through a Special Engineering Fellowship in the fiscal year 1970-71.

The author wishes to thank Dr. Wei-Wen Yu, Associate Professor of Civil Engineering, University of Missouri-Rolla for his invaluable guidance in his joint capacity as the project director and as major advisor of my advisory committee. Thanks are due to Mr. L.A. Barron, Vice President - Engineering and Dr. A.L. Johnson, Senior Research Engineer of American Iron and Steel Institute for their advice and cooperation. Appreciation should also be expressed to the AISI committee, for which Dr. J.B. Scalzi was the chairman.

TABLE OF CONTENTS

Page

Page

LIST OF FIGURES

Page

LIST OF TABLES

Page

NOTATION

A = cross-sectional area

A = constant

A_a = area of the angles

A_p = area of the plate

a = length of perforation

a = length or width of plate

B = flange width of C-shaped channels

B = constant

b = effective design width

b = length or width of plate

b = distance between perforation and centerline of bolts

b_1 = width of outstanding leg at perforation

$C = \frac{\pi}{\sqrt{3(1-\mu^2)}}$

C = measure of the effectiveness of a plate with respect to the compressive strength

c = spacing between centerlines of perforations

D = total depth of C-shaped channel and channels

d = diameter of perforation

d = width of restraining flange plate

E = modulus of elasticity

E'_p = effective modulus based on gross area for a column with perforated cover plates

E'_s = modulus for a solid column with cover plates

F = total width of channel flange

F_c = maximum allowable compression stress on unstiffened elements

F_u = ultimate tensile strength

F_y = yield point

f = actual stress in the compression element computed on the basis of the effective design width

f = deflection function

f_{max} = maximum stress in compression element

h = height of web

h_s = width of square holes

I = moment of inertia

$K = C\sqrt{E\sigma_y}$

K = axial rigidity factor

K_1 = axial rigidity factor for columns having angles and perforated plates

K_2 = axial rigidity factor for a perforated plate

k = buckling coefficient

k_c = buckling coefficient for a perforated plate having a central circular hole

k_o = buckling coefficient for a solid plate

k_s = buckling coefficient for a perforated plate having a central square hole

k_{co} = buckling coefficient for a solid plate

k_{so} = buckling coefficient for a solid plate

L = column length

LD = overall depth of simple lip

ℓ = length of plate

ℓ = width of distributed load

M = bending moment

M_{comp} = computed bending moment

M_{test} = test bending moment

m = diameter of semi-circle for ovaloid perforations

m = number of half waves

N = actual length of bearing

n = number of perforated plates

P = total load on plate

P_{cr} = critical buckling load

P_{max} = allowable concentrated load to avoid crippling of flat webs of beams

P_{max} = maximum column Load

P_{ult} = ultimate load on a simply supported plate

q_s = load reduction factor for perforated shear webs

$q_{s_{exp}}$ = experimental load reduction factor for perforated shear webs

q_{ub} = stress reduction factor for unstiffened compression elements

$q_{ub_{exp}}$ = experimental stress reduction factor for unstiffened compression elements

q_{uy} = stress reduction factor based on yielding of unstiffened compression elements

q_{wbs} = buckling load reduction factor for perforated webs

q_{wcc} = crippling load reduction factor for a web having a circular perforation

$q_{wcc_{exp}}$ = experimental crippling load reduction factor for a web having a circular perforation

q_{wcs} = crippling load reduction factor for a web having a square perforation

$q_{wcs_{exp}}$ = experimental crippling load reduction factor for a web having a square perforation

R = inside corner radius

r, r_f, r_x = radius of gyration

s = thickness of restraining flange plate

t = thickness

w = flat width

w/t = width - thickness ratio

α, β = terms for determining the critical buckling load of an unstiffened plate

α_c, β_c = terms for determining the $(w/t)_{lim}$ ratio for perforated plates having circular holes

α_s, β_s = terms for determining the $(w/t)_{lim}$ ratio for perforated plates having square holes

ε = strain

ε = critical buckling strain

μ = Poisson's ratio

σ_{cr} = critical buckling stress

σ_{max} = average column stress

σ_y = yield strength

I. INTRODUCTION

A. General

Since the early 1940's, thin-walled cold-formed steel structural members have gained increasing use in building construction, especially for low rise buildings, residences, and for many other different types of structural framing systems. This trend will continue in the future because cold-formed steel members can provide an economical design for relatively light loads or short spans. In addition, unusual sectional configurations can be easily produced by the cold-forming process, and a large strength-to-weight ratio can be obtained for cold-formed steel sections.

In cold-formed steel structural members, holes are sometimes provided in webs and/or flanges of beams and columns for duct work, piping, ease of handling, and for other purposes. The presence of such holes may result in a reduction in strength of individual component elements and/or the overall strength of the member. The load-carrying capacity of the cold-formed steel member with perforated elements depends mainly on the configuration and arrangement of holes, the material properties, and the cross section of the member.

The analysis and design of cold-formed steel sections with perforated elements are rather complex especially when the shape of the holes and their arrangement are unusual. At present, only a limited amount of information on the analysis and design of relatively heavy steel sections with perforated elements can be found in several design guides and specifications (1,2,3,4,5). Such design information has

been developed on the basis of test results of relatively thick built-up compression members (6,7,8,9) supplemented by engineering judgement. This type of design information may not be applicable to the design of perforated cold-formed steel sections due to the fact that local buckling is usually a major concern for thin walled structural members.

Presently, no provisions are included in the American Iron and Steel Institute Specification (10) for the design of this particular type of cold-formed steel section. When perforated sections are used, special tests must be conducted and evaluated in accordance with the test procedures of the AISI Specification to provide design data for use by engineers. This requirement for testing of perforated sections will undoubtedly increase the cost of the new products and limit the use of perforated sections due to lack of design information.

In order to increase the use of perforated cold-formed steel sections, design provisions must be developed on the basis of an extensive research work. The availability of such design recommendations will eliminate or minimize the tests presently required by the AISI Specification.

B. Purpose of Investigation

The purpose of this investigation is to study the structural behavior of cold-formed steel beams and columns with perforated elements. Based on the analytical and experimental investigations, the following design recommendations will be developed to extend the design provisions of the current AISI Specifications:

a) formulas to determine the effective design width of perforated stiffened compression elements,

b) formulas to determine the reduction of the load-carrying capacity of perforated unstiffened compression elements,

c) formulas to determine the allowable shear stresses for perforated webs, and

d) formulas to determine the maximum load capacity to prevent perforated webs from crippling.

C. Scope of Investigation

This study includes both the analytical and experimental investigations on the structural performance of cold-formed steel members with perforated elements.

As the first step of this investigation, available publications were reviewed in detail. Chapter II consists of a summary of the literature survey. All literatures are divided into six major parts.

Local buckling and post-buckling strength of perforated stiffened compression elements are studied in Chapter III. In this chapter, the analytical and experimental results are presented for beams and short column specimens with perforations. In this study, perforations used in short column specimen were circular and square in shape. For the beam specimens, only circular holes were used.

The behavior of unstiffened elements with circular perforations is discussed in Chapter IV. Experimental results of three series of column tests are presented along with analytical results.

Investigation of the shear buckling behavior of webs having a circular hole is presented in Chapter V. Experimental results are

presented and compared with analytical values of other investigators.

The crippling strength of circular and square perforated webs is discussed in Chapter VI. The stability of perforated webs subjected to equal and opposite loads is also discussed.

Finally, Chapter VII summarizes the results of this investigation and includes the conclusions which have been reached with regard to the structural behavior of cold-formed steel members with perforated elements. Recommendations for design are given for perforated stiffened elements, perforated unstiffened compression elements, perforated shear webs, and strength of perforated webs subjected to crippling.

II. REVIEW OF LITERATURE

A. Introduction

Some of the most important work pertaining to buckling and post-buckling strength of plates and members will be discussed first in this chapter. Results of extensive analytical and experimental studies on the compressive strength of perforated cover plates are summarized in Part C.

All available literature pertaining to the stability of perforated plates are summarized in Part D. The theoretical and experimental analyses are discussed.

Previous analytical and experimental studies on shear buckling of perforated plates and members are discussed in Part E.

In Part F, the results of an extensive experimental investigation of web crippling are summarized. Also in Part F, an analytical approach to the problem of web stability problem is discussed.

A summary of available data from current specifications and design guides for steel sections with perforations is given in Part G. The design suggestions are presented in detail.

B. Strength of Thin Plates in Compression

The stability of thin plates has been investigated by numerous researchers. These investigations were originally carried out to improve the design for ship and aircraft structures, in which thin plate components are often loaded beyond the limits of stability. It is well known that thin plates will not fail at the load causing local buckling, but will continue to carry additional load due to the post buckling strength. For this reason, the "effective width" concept has been used in design.

The application of the "effective width" concept seems to have been initiated by William John in 1877 as noted in an article by Murray (11). John pointed out that light deck and top sides plating of ships could not be taken as being fully effective under compression. He suggested that only a portion of the width of plate be considered as fully effective if the width of the plate exceeds a certain value.

The National Bureau of Standards in cooperation with the Bureau of Aeronautics, the Department of Navy, initiated a series of experiments for the purpose of determining the strength of plates under edge compression. In those tests, the ultimate load was found to be independent of the width and length of the plate, and approximately proportioned to the square of the thickness. The results of the experiments can be expressed by the following simple formula.

$$P = Kt^2 \tag{1}$$

where K is a constant depending on the physical properties of the material and t is the plate thickness. The question arose as to how the physical properties of the material enter in the constant K. This question was answered by von Karman and will be discussed later.

The most celebrated study of von Karman, Sechler, and Donnell (12) on the strength of thin plates in compression was published in 1932. An approximate theoretical solution was developed, by which the "effective width" and the ultimate strength of a thin plate can be determined.

Dr. von Karman first derived a simple expression for determining the constant K that was mentioned earlier. It was found that

$$K = C\sqrt{E\sigma_y} \tag{2}$$

where

$$C = \frac{\pi}{\sqrt{3(1-\mu^2)}}$$

Using Equations (1) and (2), the ultimate load on a plate simply supported along the sides can be written as

$$P_{ult} = C\sqrt{E\sigma_y}\ t^2 \tag{3}$$

The "effective width" was to replace the non-uniform stress distribution which occurs after exceeding the stability limit of the plate by two rectangular blocks of constant stress as shown in Fig. 1. In Fig. 1, the solid line is the actual stress distribution over the entire width of the element and the dashed line represents the equivalent uniform stress distribution.

Von Karman, Sechler and Donnell proposed a solution of the classical Bryan elastic buckling equation, to use an effective width b in place of the actual width w when the following critical local buckling stress, σ_{cr}, equals to the yield stress of the material, since experiments had shown that the ultimate strength of a sheet simply supported at the edges was independent of the width of the sheet.

$$\sigma_{cr} = \frac{k\pi^2 E}{12(1-\mu^2)(\frac{w}{t})^2} \tag{4}$$

where σ_{cr} = critical buckling stress

E = modulus of elasticity

μ = Poisson's ratio

t = thickness of the plate

w = flat width of the plate

k = buckling coefficient

If equation (4) is solved for k = 4.0, μ = 0.3, and b = w, equation (5) can be obtained as follows:

$$\frac{b}{t} = 1.90 \sqrt{E/\sigma_y} \tag{5}$$

Additional experiments were conducted on thin plates by Sechler. He found that Eq. (5) holds true except that instead of a definite constant of 1.9, a variable constant C would result in better agreement with his tests. This coefficient C, was found to depend on the parameter $\sqrt{E/\sigma_y}$ $(\frac{t}{w})$.

Karl Marguerre (13) in 1937 presented a very simplified derivation from the results of an investigation entitled: "The Load Capacity of a Plate Strip Stressed in Compression Beyond its Buckling Limit."

Following the discussion of the methods and results of other investigators, Marguerre suggested an extension of the usual stability investigation to include the supercritical range. This extension consists of two parts. Part I considers the buckling form

$$\Delta = f \cos \frac{\pi x}{\ell} \cos \frac{\pi y}{w} \tag{6}$$

known from elementary theory, the higher terms in f are preserved and yields, using the principle of virtual displacements, a relation which gives the decrease of the apparent strain stiffness at the instant of buckling. Part II considers a formula containing several arbitrary values, from which the buckling form, with a greatly exceeded critical

point, can be computed, which is shown to be in sufficient agreement with the actual conditions existing in a zone.

Based on the foregoing extension, the apparent width is conveniently calculable.

George Winter has studied the distribution of longitudinal stresses in the flanges of thin-walled beams of I, T, or Box shape. In his paper (14), Winter indicated that in wide beams the stress distribution considerably deviates from uniformity and that for a rational design of such beams this non-uniformity must be taken into account. Tables and curves are given by Winter (14), from which the equivalent width of any given beam flange can be read directly for use in practical design. The test data was in good agreement with the analytical results.

In 1946, Winter (15) reported the results of, and conclusions drawn from an extensive experimental investigation conducted at Cornell University on the strength of thin steel compression flanges. The strength, general behavior, and deformation of two types of structural elements (stiffened compression elements and unstiffened compression elements) were investigated.

In Winter's study the effective width of the compression flange for each specimen was determined at two different loads: (1) in the elastic range; and (2) as close as possible to the failure load. In all beam tests the neutral axis of the cross section was located by strain gage measurements. With the location of neutral axis known, the effective width was determined. The coefficients C were computed from the original von Karman equation.

Winter's (15) coefficients C have been plotted against the parameter $\sqrt{E/\sigma_y}\ (\frac{t}{w})$ and compared with the results of Sechler's tests. Even though different methods were used, good agreement has been obtained from the results of the two independent investigations. The results of tests have been used to develop formulas and charts by which the strength and deformation of such members can be predicted under various loading conditions.

A theoretical and experimental investigation of the compressive strength of thin plates were also performed by Dwight and Ractliffe (16). Their work was concerned with individual plates, supported along both longitudinal edges and loaded in compression. An attempt was made to develop an accurate theory for predicting the strength of post-buckled plates, but this method proved to be rather extravagent in computer time and had to be abandoned in favor of a relatively crude analysis. The method furnishes a relation between out-of-plane deflection, applied load, and strain. In this analysis, the following factors have been taken into account.

(a) initial bow in the plate

(b) residual compressive stress due to welding

(c) strain hardening

The results provided a workable theory for predicting the strength of plates with simply supported edges.

George Abdel-Sayed (17) presented an approximate theoretical approach for two cases of plates where the longitudinal edges are restrained to remain straight or are free to move in the plane of the plate. The plate is first considered flat, then the effect of initial

deviation from flatness on the effective width is examined.

The effective width of wide thin plates, under compression was examined by solving the governing differential equations. The solution was based on the assumption that, the deflected form at the instant of buckling is preserved after loading exceeds the buckling limit.

The comparison shows good agreement between a theoretical formula and Winter's formula.

In 1957, Gerard and Becker (18), prepared a "Handbook of Structural Stability." This Handbook, under the sponsorship of the then National Advisory Committee for Aeronautics, presents a comprehensive review and compilation of theories and experimental data primarily related to the buckling and failure of plate elements encountered in aircraft structures.

The factors governing buckling of flat plates are reviewed and the results are summarized in a comprehensive series of charts and tables. Numerical values are also presented for buckling coefficients of flat plates with various boundary conditions and applied loadings. The effects of plasticity are incorporated in this handbook.

Because of the mechanical behavior of stainless steel and other factors, existing design procedures for carbon and low alloy steels may not be adequate for stainless steel design. Johnson and Winter (19) have conducted an experimental investigation on austenitic stainless steel members with stiffened and unstiffened compression elements.

The design procedures developed for stainless steel are similar to those used for carbon steel except that modifications have been made to account for the pecularities of the mechanical response of stainless

steel.

Wang, Winter and Errera (20,21) also conducted an experimental investigation on the behavior of cold-rolled stainless steel members with stiffened and unstiffened compression elements.

The post-buckling behavior of thin compression elements stiffened along one or both unloaded edges by thin webs has been found to agree with von Karman's ( ) relationship as modified by Winter for carbon steel as a lower bound.

Elastic post-buckling of compressed rectangular flat plates present state of knowledge was reviewed by Supple and Chilver (22).

The review suggests that the initial phase of elastic post-buckling of a perfectly flat plate is reasonably well understood. The analysis for geometrically imperfect plates is complex. Experiments showed the such plate behavior is extremely sensitive to geometric imperfections.

Bulson (23) reviewed the state of the knowledge of local buckling of thin-walled structural sections. Existing theories for flat plates were reviewed. Next, a generalized analysis for thin-walled sections was presented.

The exact analysis for upper flanges is outlined and solutions are given for plates and channels. Interaction between local and column instability is analyzed using the fundamental equilibrium equations.

C. Compressive Strength of Perforated Cover Plates

In early 1930's, bridge designers started designing compression members by substituting perforated cover plates for lattice bars or

batten plates in built-up box type sections based on a very limited amount of test data.

Due to the great increase in concern of using perforated cover plates in built-up box type sections, the National Bureau of Standards (24) in cooperation with the American Institute of Steel Construction in 1941 conducted tests to determine load-carrying capacity of the perforated cover plates.

In this investigation, the following variables were studied to determine the stiffness and strength of perforated cover plates in columns: shape of perforation, spacing of perforation, and width of plate. All specimens were designed to fail in primary column buckling rather than local buckling.

To limit this investigation to a reasonable number of tests, only the circular and ovaloid shapes of perforation were used in column specimens. For each type of specimen, the shape and size of perforations were the same, but three different spacing of perforations were used. The plates used in the fabrication of test specimens were the same thickness with three different widths.

The effective area of the perforated plate with respect to compressive strength was evaluated on the assumption that the average compression stress at failure on the effective area of the column containing the perforated plate is the same as σ_{max}, which is the average stress obtained by dividing the maximum load on an unperforated plate column of the same width by the gross area of the unperforated plate column. Considering $A_a \sigma_{max}$ as the load carried at failure by the

angles of the perforated plate column, and P_{max} as the total load at failure, then $P_{max} - A_a \sigma_{max}$ is the load carried by the perforated plate at failure. The effective area of the plate is:

$$\frac{P_{max} - A_a \sigma_{max}}{\sigma_{max}}$$

and C, a measure of the effectiveness of the plate with respect to the compressive strength is,

$$C = \frac{P_{max}}{A_p \sigma_{max}} - \frac{A_a}{A_p} \qquad (7)$$

where A_a = area of the angles

A_p = area of the plate

The value of C ranged from 0.44 to 0.50 where C for a column with no perforation is 1.00.

The findings of this study indicated that for the specimen investigated, from 60 to 80 percent of the cross-sectional area of the plate, depending on the perforation spacing, was effective in resisting shortening under compressive load. The value of the maximum stress was only slightly affected by variation of perforation spacing. The maximum stresses varied from about 2 to 2.5 times the average stress.

Due to the limited amount of information obtained from the foregoing, a series of tests on perforated plates were conducted from 1942 through 1946 at the National Bureau of Standards to determine the stiffness and strength of perforated cover plates. The results of compressive properties of steel columns having perforated cover plates were summarized in Reference 8.

In the NBS investigation (24), tests were made on perforated cover plate columns with perforations of the following shapes:

1) Circular
2) Ovaloid with the load parallel to the long axis
3) Ovaloid with the load parallel to the short axis
4) Elliptical with the load parallel to the major axis
5) Square with the load parallel to the two sides
6) Square with the load parallel to a diagonal

The axial rigidity was represented by a factor, K, defined as a ratio of the axial rigidity of a column having perforated plates to the axial rigidity of an unperforated, but otherwise similar, column. For computation of the axial deformation of the member, the rigidity EA_g may be modified by the factor K, where E is the modulus of elasticity and A_g is the gross cross-sectional area of the column.

The axial rigidity factors determined by the results of tests on columns having angles and perforated plates, and for the perforated plate alone are shown in Equations (8) and (9):

$$K_1 = E'_p/E'_s \tag{8}$$

$$K_2 = \frac{E'_p}{E'_s}\left(1 + \frac{A_a}{A_p}\right) - \frac{A_a}{A_p} \tag{9}$$

where E'_p is the effective modulus based on gross area for a column with perforated cover plates, E'_s is the modulus for a solid column of the same material, A_a is the cross-sectional area of the angles, and A_p is the gross cross-sectional area of the perforated plate.

The values of these experimental axial rigidity factors were compared with the theoretical values given by Greenspan (6,7). The differences

between the experimental and theoretical values of K for the columns investigated were within ± 2%, except for a few scattered values. Therefore, the axial rigidity factor of columns and of perforated plates can be closely approximated by the equations given by Greenspan (6,7).

The stress ratios determined by experiments for columns having a finite cross-sectional area were compared with the theroetical values derived for an infinite plate. Good agreement between the theoretical and experimental stress distributions on the edge of the perforation has been obtained in all cases.

Nomographic charts are given for the determination of the axial rigidity factor K for all mentioned shapes of perforations.

In 1943, Martin Greenspan (6) developed approximate formulas for the computation of the axial rigidity of long tension or compression members containing a plate of constant thickness uniformly perforated with a series of circular, elliptical, or ovaloid holes. The approximate formula was verified by an experimental investigation. Greenspan concluded that the formula for circular holes gives good results.

In another paper, Greenspan (7) expanded the theory developed in Reference 6 to other shapes of perforations, including ovaloid and square holes. The formulas can be used for the computation of the axial rigidity of a long tension or compression member containing a series of constant thickness uniformly spaced perforations.

In 1956, White and Thurlimann (9) conducted a complete analytical and laboratory study of the strength of columns having perforated cover plates. The laboratory tests made by the National Bureau of Standards was reviewed in detail.

In the analytical study, the following problems were considered:

1) Axial rigidity

2) Bending stiffness

3) Buckling load of concentrically loaded columns

4) Yield load of eccentrically loaded columns

5) Design of perforated plates for shear

6) Local buckling of plate elements

7) Stress concentrations due to perforations

By an experimental investigation on three members, it was determined that K, the axial rigidity factor, contributes very little to the effective area. For design purposes, it was determined that the net area may be used with sufficient accuracy in most cases and will be on the safe side.

From the results of the experimental investigation it was also determined that the stiffness of the perforated plate can be calculated using the net section only.

An equation was derived for the determination of the critical buckling stress which included the effect of shear. This equation was verified by the experimental investigation, in which the results showed that the secondary effects due to shear are negligible and no reduction in the buckling load is necessary.

Since a perforated plate must resist shear if buckling or bending takes place about an axis perpendicular to the plates, a method for determining the maximum shear stress in perforated plates was developed by considering the column as concentrically and eccentrically loaded.

To prevent local buckling, thin plate elements of which the column is built up are required to be designed so that no local buckling is possible prior to the general buckling of the column. This condition requires that the critical buckling stress of the plate elements be equal to or greater than the critical buckling stress of the column. On this basis, the design recommendation against local buckling of flat elements are:

1) For the outstanding leg of the perforated plate at the perforation

$$b_1/t = 21 - (td/sb_1)^2 \quad \text{for } \frac{L}{r} \leq 60$$

and

$$b_1/t = [0.35 - 0.017(td/sb_1)^2](\frac{L}{r}) \quad \text{for } \frac{L}{r} > 60$$

where

b_1 = width of outstanding leg at perforation

t = thickness of cover plate

d = width of restraining flange plate

s = thickness of restraining flange plate

L = column length

r = radius of gyration of column

2) For the cover plate between perforations the following relationships should be used:

$$w/t = 48 - 12(td/sw)^2 \quad \text{for } \frac{L}{r} \leq 60$$

and

$$w/t = [0.80 - 0.20(td/sw)^2](\frac{L}{r}) \quad \text{for } \frac{L}{r} > 60$$

where w is the width of cover plate. Other symbols are previously defined.

Recommendation for the shape and spacing of perforations were also given in Reference 9. It was pointed out that elliptical or ovaloid holes with their long axis in the direction of the column axis seem to be the best suited.

However, no direct answer to the problem of stress concentration caused by the perforation was given in this reference. The analytical study is supported by test results.

D. Stability of Perforated Plates

The investigation of the stability of perforated plates seem to have been initiated by Levy, Woolley, and Kroll (25) in 1947, under the direction of the National Bureau of Standards. An energy method for determining the compressive buckling load of a simply supported elastic square plate having a central circular hole reinforced by a circular doubler plate and without reinforcement was presented. The energy method of Timoshenko (26) for determining the buckling load of rectangular plates of constant thickness under compressive loads was found to be applicable to plates of variable thickness.

Using the energy method, a numerical procedure was developed for estimating the buckling stress of simply supported square plates with circular holes and doubler plate reinforcement. The analysis indicated that the buckling stress of a square plate is reduced by a small amount due to the presence of unreinforced holes. For the cases considered,

the greatest reduction, for a square plate with a hole diameter 0.5 times the width of the plate was found to be 14 percent. The critical buckling stress for a simply supported square plate, as presented by Timoshenko (26), was compared with the critical buckling stress of a square plate with unreinforced holes, having a diameter of 1/8, 1/4 and 1/2 of the width of the square plate. The result shows that the reduction in buckling load to be only 1, 4, and 14 percent respectively.

Computations indicated that reinforcement by the doubler plate will cause a marked increase in the buckling stress. The buckling stress seems to be insensitive to change in shape of reinforcements for a given volume.

In 1952, Kumai (27) applied the energy method to perform approximate calculations for the critical load of a square plate with a central circular hole subjected to edge compression, in which he used a more reasonable assumption on the deflection pattern of the perforated plate than previous investigators. Moreover, the critical loads were computed for three cases, i.e., simply supported edge, clamped edge, and clamped edge with the second mode of buckling. The experimental observations on the critical loads for all cases mentioned above were carried out by model analysis.

From this investigation, the conclusions can be drawn as follows:

1. As the diameter-to-width ratio increases, the critical load, for the case of the perforated, simply supported square plate, decreases. The theoretical and experimental values of the critical load, for a diameter-to-width ratio of 0.5, are 75 and 70 percent, respectively. The theoretical value of Levy (22) for the same case is 86 percent.

2. The minimum critical load exists for a diameter-to-width ratio of 0.2. For this case, the critical load ratio is 87 percent for the case of clamped edge with the fundamental buckling mode. When the diameter-to-width ratio exceeds 0.2, the critical load increases, and when the diameter of holes reaches to about 34 percent of the width, the critical load is almost equal to the load of a plate having no perforation. After the diameter-to-width ratio exceeds this point, the value of critical load increases rapidly.

Up to 1964, theoretical analyses concerning the elastic buckling of a simply supported square plate were based on the case of uniform edge loading along two parallel edges. This approach was considered to be impractical by Schlack (28) because a uniform load does not normally occur in practice due to the relative stiffness of the supported edges of the plate compared to its weakened central portion. The uniform edge displacement approach utilizing the Ritz energy method was used by Schlack to determine the critical edge displacement.

Displacement functions assumed for the three components of middle surface displacements was studied and the results being that the solutions without singular term was found to be valid for small holes up to 3/10 of the plate width. Excellent agreement between the experimental and theoretical buckling was presented which justifies the critical edge displacement approach.

In a paper presented by Yoshiki, Fojita, and others (29), the instability of plates with a circular hole supported at all edges and subjected to compressive forces was studied. The case investigated was a square plate with a circular central hole subjected to edge thrust

simply supported along all edges. The effect of position of the circular hole was also studied.

The buckling loads were determined by the Δ^2-method and are calculated by the energy method. It was proved theoretically and experimentally that the Δ^2-method is valid. Theoretical and experimental results showed reasonable agreement.

A method of solution for the complicated buckling problems of elastic plates was presented in a paper by Kawai and Ohtsubo (30). This method utilized the finite element method to determine the initial stress distribution. Using this distribution the well known Rayleigh-Ritz procedure was used to determine the critical stress.

The method was applied to determine the critical buckling stress of simply-supported perforated square plates with various boundary conditions. The results were compared with the results of others.

To the knowledge of the author, Hull (31) is the first to determine the elastic critical buckling stress of a square plate with a central square perforation. He used the "stability coefficient matrix" method with the finite element approach.

Hull's paper extended the stability coefficient matrix method to determine the theoretical critical elastic buckling loads for plates having non-uniform and unknown membrane stresses.

The examples given by Hull (31) indicated that the stability coefficient matrix method can be applied to determine critical buckling loads for plates having unknown in-plane stresses with reasonable accuracy. However, no experimental results were used to verify the elastic critical buckling stress of the square plate with a square

perforation.

Theoretical and experimental results on the compressive buckling of perforated plate elements was presented by Vann (32).

The results of this study indicated that unless a central unflanged hole is fairly large, it will have a very small effect on the buckling load, and that a flange hole can be expected to increase the buckling load greater than the buckling load of an unpierced plate.

E. Shear Buckling of Perforated Plates and Members

To understand more fully the effect of reinforcements in strengthening and stabilizing the structure around a hole, Kroll (33) in 1949 made a theoretical investigation of the stability of simply supported square plates with reinforced and unreinforced holes subjected to shear loading.

The critical shear buckling stresses were determined for five plates with diameter-to-width ratios of 1/8 and 1/4 using the energy method formulation presented in Reference 25.

The value given by Timoshenko and Gere (26) for a plain simply supported square plate subjected to shear loading was compared with the results of this investigation. For unreinforced holes of diameter-to-width ratio of 1/8 and 1/4, the buckling stresses was reduced by 0.2 and 22.6 percent, respectively. Reinforced holes increased the critical buckling stresses from 55 to 334 percent higher than that for a plate with the same size unreinforced hole.

Rockey, Anderson, and Cheung (34) conducted a theoretical and experimental study of the buckling and collapse load of shear webs having plain and reinforced holes of diameter-to width ratios from

0.0 to 1/2.

The finite element method was used for the determination of the critical shear buckling load. Due to symmetry, only one-quarter of the square plate was used. In this study, 56 elements were used for the idealization. For a plain square plate clamped along all edges, the finite element solution value for k was found to be equal to 13.28 as compared with the exact value of 14.71.

The experimental investigation was conducted on shear panels. These panels were restrained along the edges by very stiff members to ensure uniform restraint. The shear panels were tested in a universal testing machine by applying a tensile force across a diagonal. The buckling load was determined with the aid of dial gages.

The experimental data is shown to be in good agreement with the theoretical data.

Yoshiki, Fojita, and others (29) also studied the case of an I-beam supported at both ends and loaded by a concentrated load at the center, so that the web of the I-beam was subjected to simple shear and would buckle mainly due to the shearing stress.

The Δ^2-method was also used to determine the critical load. It was proved theoretically and experimentally that the Δ^2-method is valid for shear buckling.

F. Web Crippling

Zetlin (35) presented a theoretical analysis of the stability of a plate supported at both ends and loaded over a portion of one of the edges. The plate edges were simply supported. The total edge load was applied along the top edge and was distributed over a small width.

The buckling loads of the flat rectangular plates were obtained by using the governing partial differential equations with variable coefficients and application of the energy method.

Results of calculations have been reduced to curves suitable for design purposes. These curves are given for a wide range of plate dimensions and loading widths. The theoretical results are compared with a number of tests.

An extensive experimental investigation on the crushing strength of thin steel webs was conducted by Winter and Pian (36). This investigation gives the results of 136 web crushing tests carried out on 18 different types of beams under a variety of loading conditions. The results of these tests are given in terms of two empirical equations. These equations predict the crushing strength of webs with reasonable accuracy.

The specimens used in the tests consisted of double and single webs. Loads were applied over different bearing widths by means of steel plates. The ultimate load of each specimen was the only observation recorded.

Evaluation of the results indicated that the web depth has no influence on the crushing strength and a factor of safety of 2.5 may be used in applying the empirical equation to the design of thin-walled steel structures.

G. Current Design Provisions for Steel Sections with Perforations

To the author's knowledge, only six specifications and design guides are generally used for the analysis and the design of perforated shapes. Each of these specifications will be discussed in the following

paragraphs. Figure (2) shows the pertinent dimensions used in the specifications.

The design suggestions included in the Column Research Council Guide (1) for columns with perforated plates were derived from the AASHO Specification (3) and based mainly on a study by White and Thurlimann (9). The design suggestions are:

1. The perforations may be ovaloid, circular, or elliptical
2. $(c-a) \geq d$
3. A and I based upon the net section
4. If $a/r_f \leq 20$, and $a/r_f < L/3r_x$, the permissible load can be determined by the appropriate specification column stress applied to the column net section.
5. The net area of web at the perforation should be sufficient to resist 1/n times the transverse shear force, where n is the number of perforated plates.
6. The w/t ratio should conform to specification requirement for plates in main compression members.

The AASHO Specification (3) design suggestions are:

1. $a/m \leq 2$
2. $(c-a) \geq d$
3. The clear distance between the end perforation and the end of the cover plate shall not be less than 1.25 times the distance between points of supports.
4. The point of support shall be the inner line of fasteners or fillet welds connecting the perforated plate to the flanges.

5. The periphery of the perforation at all points shall have a minimum radius of 1-1/2 inches.

The AREA Specification (4) design suggestions are:

1. Perforations shall be ovaloid or elliptical
2. $a \leq 2m$, $a/r_f \leq 20$, $a/r_f < L/3r$.
3. $(c-a) \geq d$
4. Thickness of perforation cover plate:

   $t \geq d/50$, $t \geq b/12$
5. Splices are permitted with limitations
6. The gross section of the plate through the perforation shall be considered as a part of the area of the member.

The foregoing design suggestions are all based in part on the results of extensive experimental investigations sponsored by the National Bureau of Standards, and engineering judgement.

The design suggestions given by the AISC Specification (2) are also based on the results of National Bureau of Standards results and engineering judgements. The design suggestions are:

1. Width-to-thickness ratio at access holes is not greater than $317/\sqrt{\sigma_y}$
2. $a/m \leq 2$
3. $(c-a) \geq d$
4. The periphery of the holes at all points shall have a minimum radius of 1-1/2 in.

There are no design provisions in the AISI Specification (10) for the design of cold-formed steel sections with perforated elements. When section with perforated elements are used, special tests must be

conducted and evaluated in accordance with Section 6 of the AISI Specification for design information.

A comparison of the design suggestion of the previous guide and specifications is given in Welding Research Council Bulletin (41)

Rack Manufacturer's Institute Guide (5) gives design information for design of industrial steel storage racks. Section II-C of this guide gives design suggestions for rack posts with perforations.

The foregoing design provisions pertain primarily to the design of perforated plates loaded in compression.

Suggested design guides for beams with web holes was proposed by the Subcommittee on Beams with web openings of the Task Committee on Flexural Members of the Structural Division (38). The proposed design guides are relatable to the AISC Specification.

In Ref. 38, guides are given for both allowable-stress design and maximum strength design for members with unreinforced web holes. The design criteria were developed from the results of numerous tests. Buckling criteria is presented, but conservative because of inadequate theoretical and experimental data on the buckling of members with unreinforced web holes.

III. LOCAL BUCKLING AND POST-BUCKLING STRENGTH OF PERFORATED STIFFENED COMPRESSION ELEMENTS

A. Analytical Investigation

An analytical method for describing the structural behavior of stiffened compression elements (compression elements stiffened along both longitudinal edges) with perforations must consider the buckling behavior and post-buckling strength of the component elements. These two subjects will be discussed separately as follows:

1. Local Buckling

Critical buckling loads for perforated plates have been studied by Levy, Woolley, and Kroll (25), Kumai (27), Schlack (28), Yoshiki, Fujita, and others (29), Kawai and Ohtsubo (30), and Hull (31) using the energy method and the finite element method. Since 1964, consideration has been given to two different approaches, i.e., the uniform displacement approach and the uniform stress approach.

The uniform displacement approach is based on determining the critical edge displacement of a plate under uniform edge displacement and the uniform stress approach is based on determining the critical edge stress of a plate under uniform edge stress.

The uniform displacement approach was used by Schlack (28) in his study of buckling of perforated square plates. It has been pointed out that the uniform displacement approach is more practical than the uniform stress approach used by Levy, Woolley, and Kroll (25) and Kumai (27) because a uniform load does not normally occur in practice due to the relative stiffness of the supported edges of the plate as compared to its weakened central portion.

a. Simply Supported Square Plate Having a Central Circular Hole

For a simply-supported square plate having a central circular hole, the critical buckling stress may be determined by Eq. 4a, as shown below

$$\sigma_{cr} = \frac{k_c \pi^2 E}{12(1-\mu^2)(w/t)^2} \qquad (4a)$$

where k_c is the buckling coefficient for a perforated plate having a central circular hole. The value of k_c varies with the d/w ratio (d being the hole diameter and w being the overall width of the plate). According to the method of Kawai and Ohtsubo (30), the relationship between the buckling coefficient, k_c, and the d/w ratio is shown in Fig. 3, in which the uniform stress approach and the uniform displacement approach indicates that when the diameter of a hole is small as compared with the width of plate, the buckling load of the plate is reduced by only a small amount due to the presence of a hole. In Fig. 4a, the actual stress distribution along the loaded edges is shown for a plate with a large hole. From this figure, it can be readily seen that when a hole is considerably large in size, it may be assumed that the applied load is carried by two narrow unstiffened strips along the side boundaries as shown in Fig. 4b. For this reason, different structural behavior should be expected for plates having different sizes of holes. Kawai and Ohtsubo (30) suggested a value of d/w = 0.7 as the limiting value, above which the applied load of a circular perforated plate is assumed to be carried by two unstiffened strips.

b. Simply Supported Square Plate Having a Central Square Hole

The determination of the buckling coefficient for a simply-supported square plate having a central square hole was accomplished by using a finite element program. The finite element program used was a modified version of Yang (40). This finite element program of Yang was formulated for the stability analysis of doubly curved thin shell structures. Stiffness equations are formulated in representation of the elastic instability behavior of a doubly-curved thin shell element. The element is in the form of a shell of translation of constant thickness and constant principal radii of curvature. Modification of this finite element program consist of representation of the shell element as a plate element and where holes are to be represented, elements were deleted completely.

Due to geometric symmetry, only one-quarter of the square plate was used in the analysis. The idealization of the one-quarter plate for the cases of h_s/w ratios (h_s being the width of the square hole) of 0.0, 0.25, and 0.5, consist of 16, 15, and 12 square elements respectively. The idealization for the case of h_s/w of 0.0 is shown in Fig. 5. Element 16 is deleted from the analysis for the case of h_s/w of 0.25 and elements 11, 12, 15, and 16 are deleted from the analysis of the case of h_s/w of 0.50. The boundary freedoms deleted in this finite element solution are noted in Table I, all other degrees of freedom are not restrained from movement. The coordinate system used in this analysis is shown in Fig. 5. The z axis is perpendicular to the x-y plane and θ_x, θ_y, and θ_z are rotations about the x,y, and z axes respectively. Critical buckling loads were calculated for all three cases. The calculated buckling load for the case of $h_s/w = 0.0$ was compared with the theoretical buckling load. This comparison shows the calculated value to be

approximately 10 percent lower than the theoretical value.

The buckling coefficient ratio, k_s/k_{so} (k_{so} is the buckling coefficient for a solid plate and k_s is the buckling coefficient for a perforated plate having a central square hole), was obtained by comparing the buckling loads of perforated plates with the buckling loads of the plate having a h_s/w ratio of 0.0 as shown in Table II. The results of this analysis are compared with the finite element analysis of Hull (31) as shown in Fig. 6.

Applying the analogy used for large circular holes, where the applied load is carried by two narrow unstiffened strips along the side boundaries, a limiting value from this analogy suggests a limiting value of $h_s/w = 0.5$ be used for plates with large square holes.

A comparison of Figs. 3 and 6 is shown in Fig. 7. This comparison indicates that if the diameter of a circular hole is the same as the width of a square hole, the buckling load for the perforated plate having a square hole is less than that for a perforated plate having a circular hole. This is due to the difference in stress concentration and the shape of the two difference types of holes.

2. Post-Buckling Strength

As discussed in Part B of Chapter III, thin plates will not fail at the local buckling load, but will continue to carry additional load due to the post-buckling strength. The post-buckling strength can easily be determined by the well known "effective width" concept, which is to replace the non-uniform stress distribution which occurs after exceeding the stability limit of the plate by two rectangular blocks as shown in Fig. 1. In this figure, the solid line is the actual stress distribution over the entire width of the element, and the

dashed line represents the equivalent uniform stress distribution.

For thin plates without holes, Equation 10 developed by Winter (15) has long been used by AISI as the basis for determination of the effective width for stiffened compression elements:

$$b = 1.9t \sqrt{\frac{E}{f_{max}}} \left[1 - 0.475\left(\frac{t}{w}\right) \sqrt{\frac{E}{f_{max}}}\right] \qquad (10)$$

where b = effective width of the stiffened compression element

t = thickness of steel

E = modulus of elasticity

f_{max} = maximum edge stress

w = overall width of the element

In 1968, Equation 10 was slightly modified as shown in Equation 11 (38):

$$b = 1.9t \sqrt{\frac{E}{f_{max}}} \left[1 - 0.415\left(\frac{t}{w}\right) \sqrt{\frac{E}{f_{max}}}\right] \qquad (11)$$

For unstiffened compression elements, the effective width may be determined by using Equation 12 (15) even though this equation has not been directly used in the AISI Specifications:

$$b = 0.8t \sqrt{\frac{E}{f_{max}}} \left[1 - 0.202\left(\frac{t}{w}\right) \sqrt{\frac{E}{f_{max}}}\right] \qquad (12)$$

With regard to perforated plates, previous discussion on local buckling indicated that the structural behavior of perforated plates is affected by the size and shape of holes. Consequently, different equations should be used for plates having circular and square holes in different sizes.

The previous discussion on local buckling indicated the buckling behavior to be different depending on the value of the d/w ratio. For the range of d/w of 0 to 0.7, the buckling behavior of the perforated plate is similar to that of a stiffened compression element, therefore Eq. 11 may be modified to determine the effective width in this range. The buckling behavior of plates with a d/w ratio equal to or greater than 0.7 was found to behave like two separate and identical unstiffened compression elements, therefore Eq. 12 may be modified to determine the effective width in this range.

Modified equations for computing the effective width must take in account the size of perforation and satisfy the suggested boundary conditions. The effective width equation for stiffened compression elements with circular perforations, Eq. 13, is the modified equation. This equation satisfies the boundary conditions at d/w = 0 and 0.7 and is identical to Eq. 11 for d/w = 0 . Also, the modified equation is equal to the modified unstiffened equation for d/w = 0.7. The effective width equation for unstiffened compression elements, Eq. 12 is modified by replacing w by w', where w' = w-d/2 and the resulting equation for b is multiplied by 2.0. Eqs. 13 and 14 are the modified equations for the two ranges discussed.

$$0 < \frac{d}{w} \leq 0.7$$

$$b = 1.9t \sqrt{\frac{E}{f_{max}}} \left(1 - 0.226 \frac{d}{w}\right) \left[1 - 0.415\left(\frac{t}{w-d}\right) \sqrt{\frac{E}{f_{max}}} \left(1 - 0.0379 \frac{d}{w}\right)\right] \qquad (13)$$

$$\frac{d}{w} \geq 0.7$$

$$b = 1.6t \sqrt{\frac{E}{f_{max}}} \left[1 - 0.202\left(\frac{2t}{w-d}\right) \sqrt{\frac{E}{f_{max}}}\right] \qquad (14)$$

The foregoing derivations were concerned with only the development of equations for computing the effective width based on the d/w ratio. Another factor affecting the effective width is the w/t ratio. The limiting width-thickness ratio $(w/t)_{lim}$ for the range of d/w = 0 to 0.7, is determined by equating b=w in Eq. 13. $(w/t)_{lim}$ can be computed as follows:

$$\left(\frac{w}{t}\right)_{lim} = \sqrt{\frac{E}{f_{max}}} \left[\frac{\alpha_c + \sqrt{\alpha^2_c - 4\beta_c}}{2}\right] \qquad (15)$$

in the above,

$$\alpha_c = 1.9\left(1-0.226 \frac{d}{w}\right)$$

$$\beta_c = 0.788\left(1-0.226 \frac{d}{w}\right)\left(1-0.0379 \frac{d}{w}\right)/\left(1 - \frac{d}{w}\right)$$

The limiting width-thickness ratio, $(w/t)_{lim}$ for the range $d/w \geq 0.7$ is $63.3/\sqrt{f_{max}}$. This value is used by AISI for unstiffened compression elements.

Upon examining Eq. 15, a limiting value for d/w can be obtained by equating the discriminant in Eq. 15 to zero as follows:

$$\alpha_c^2 - 4\beta_c = 0$$

making the proper substitutions,

$d/w = 0.11$

The addition of the above range of d/w indicates that three ranges of d/w may be used. On the basis of d/w ratios, the following equations may be used to determine the effective width of perforated stiffened compression elements having circular holes: (39)

(A) $\frac{d}{w} \leq 0.11$

1. $w/t \leq (w/t)_{lim}$

$$b = w \tag{16}$$

2. $w/t > (w/t)_{lim}$

$$b = 1.9t \sqrt{\frac{E}{f_{max}}} \left(1-0.226 \frac{d}{w}\right) \left[1-0.415\left(\frac{t}{w-d}\right) \sqrt{\frac{E}{f_{max}}} \left(1-0.0379 \frac{d}{w}\right)\right] \tag{13}$$

(B) $0.11 < \frac{d}{w} < 0.7$

Use Equation 13 provided that $\frac{w-d}{2t} > \frac{63.3}{\sqrt{f_{max}}}$.

If $\frac{w-d}{2t} \leq \frac{63.3}{\sqrt{f_{max}}}$

$$b = w - d \tag{17}$$

(C) $\frac{d}{w} \geq 0.7$

1. $\frac{w-d}{2t} > \frac{63.3}{\sqrt{f_{max}}}$

$$b = 1.6t \sqrt{\frac{E}{f_{max}}} \left[1-0.202\left(\frac{2t}{w-d}\right) \sqrt{\frac{E}{f_{max}}}\right] \quad (14)$$

2. $\frac{w-d}{2t} \leq \frac{63.3}{\sqrt{f_{max}}}$

Use Equation 17

where d is the diameter of circular holes, b, t, E, f_{max} and w were previously defined.

Based on Equations 13,14,16, and 17, the influence of size of circular holes on the effective width of stiffened compression elements can be shown in Fig. 8.

For perforated plates having square holes, a study of local buckling indicated that a value of 0.5 may be used for the specific $\frac{h_s}{w}$ ratio, beyond which the applied load can be assumed to be carried by two narrow unstiffened strips. Consequently, Equations 18 to 21 may be used for the determination of the effective width of perforated stiffened compression elements having square holes (39):

(A) $\frac{h}{w} \leq 0.11$

1. $w/t \leq (w/t)_{lim}$

$$b = w \quad (18)$$

2. $w/t > (w/t)_{lim}$

$$b = 1.9t \sqrt{\frac{E}{f_{max}}} (1-0.316 \frac{h}{w}) \left[1-0.415\left(\frac{t}{w-h}\right) \sqrt{\frac{E}{f_{max}}} (1-0.053 \frac{h}{w})\right] \quad (19)$$

(B) $0.11 < \frac{h_s}{w} < 0.5$

Use Equation 19 provided that $\frac{w-h_s}{2t} > \frac{63.3}{\sqrt{f_{max}}}$.

If $\frac{w-h_s}{2t} \leq \frac{63.3}{\sqrt{f_{max}}}$ (20)

$$b = w - h_s$$

(C) $\frac{h_s}{w} \geq 0.5$

1. $\frac{w-h_s}{2t} > \frac{63.3}{\sqrt{f_{max}}}$

$$b = 1.6t \sqrt{\frac{E}{f_{max}}} \left[1-0.202\left(\frac{2t}{w-h_s}\right) \sqrt{\frac{E}{f_{max}}}\right] \quad (21)$$

2. $\frac{w-h_s}{2t} \leq \frac{63.3}{\sqrt{f_{max}}}$

Use Equation 20

where h_s is the width of square holes.

$$(w/t)_{lim} = \sqrt{\frac{E}{f_{max}}} \left[\frac{\alpha_s + \sqrt{\alpha^2_s - 4\beta_s}}{2}\right] \quad (22)$$

$$\alpha_s = 1.9\left(1-0.316 \frac{h_s}{w}\right)$$

$$\beta_s = 0.788\left(1-0.316 \frac{h_s}{w}\right)\left(1-0.053 \frac{h_s}{w}\right)/\left(1 - \frac{h_s}{w}\right)$$

Other symbols were previously defined.

It should be noted that Equations 13 and 19 are the modified formulas for stiffened compression elements, while Equations 14 and 21 are based on the formula for the effective width of two narrow unstiffened elements along side boundaries. When "d" or "h_s" is equal to zero (i.e., for solid plates), Equations 13 and 19 will be identical to Equation 11.

B. Experimental Investigation

In order to properly verify the effect of holes on the buckling load and the post-buckling strength of the perforated stiffened elements as discussed in the analytical investigation, short column tests and beam tests have been conducted in the laboratory of the Department of Civil Engineering to cover the following parameters:

a) Shape of holes: circular and square holes

b) Overall width-to-thickness ratio: 36.6 to 73.8

c) Hole opening-to-overall width ratio (d/w or h_s/w): 0 to 0.722

d) Yield point of steel: 34.4 to 59.3 ksi

The experimental investigation and the evaluation of the results of tests will be presented in this section. The discussion deals with the preparation and testing of the specimens. The critical buckling strains and the post-buckling strength of stiffened compression elements are analyzed and presented.

1. Column Tests

a. Fabrication of Test Specimens

Twenty-eight short column specimens were tested in this study. The members were selected to give a practical range of the design parameters used for perforated stiffened compression elements.

Test specimens were fabricated by connecting two C-shaped channels through the simple lips by ten 1/4" ϕ bolts. Dimensions of the test specimens are listed in Tables III and IV and the cross section of test specimens is shown in Fig. 9. Each C-shaped channel (6-1/2 x 2-1/2 in., nominal size) was cut to a length of 20 in. in accordance with the Appendix on Compression Testing of the AISI Specification (10). At the center of each stiffened element, a 1/4-in. hole was drilled. Next, each specimen was unfastened for ease in making the perforation. To further assure that the perforations would be centered and true in shape, 1/4 in. thick plates, machined circular and square were fastened to the stiffened element by 1/4 in. ϕ bolts. Circular and square holes were then cut in the stiffened element by a sabre saw. After all perforations were cut, paired C-shaped channels were then refastened. Both ends of specimens were ground flat and parallel, and were perpendicular to the longitudinal axis.

b. Location of strain gages

To properly make the precise measurements required in this type of an investigation, 1/4 in. foil strain gages were used. Paired strain gages were placed as close as practicable to the edge of the perforation. These paired strain gages were used to determine the critical buckling strains. The single strain gages located at the edge were used for centering the specimen and determining the post-buckling strength. For determining the critical buckling strains for the unperforated specimens, paired strain gages were located at mid-height along the centerline of the stiffened element. The strain gage locations are shown in Fig. 9.

c. Mechanical Properties

The mechanical properties of steel were determined by using tensile specimens cut from the center of the unused stiffened elements. All tensile specimens complied with ASTM Designation A 370-68 (42). The average values obtained from these tests were used. The mechanical properties of the steel test specimens are given in Table V.

d. Test Procedure

All column specimens were tested in the 200,000 pound Tinius Olsen universal testing machine in the flat end condition. Specimens were placed between two machined plates to insure complete bearing over the entire area. The test set-up is shown in Fig. 10.

To insure concentric loading, centering of the specimens was accomplished by using the strain gages located at four corners. During loading, small increments of load was applied. For each increment, the load was applied to the desired level, the load and strain gage readings were recorded and printed out on tape using a 40-channel Data Acquisition System. Dial gages were used for measurements of lateral deflection and axial deformation of specimens.

e. Discussion of Results

Based on the results obtained from the short column tests, the critical buckling strain was determined by using the modified strain reversal method (19,20). This was done by the application of a pair of strain gages placed on both sides of the stiffened element along both edges of perforations. The critical strain was taken as the maximum compressive strain on the convex side of the buckled stiffened element. Fig. 11. illustrates a typical load-strain diagram. The buckling

coefficient ratios were computed from the critical loads as listed in Table XI and VII. The buckling coefficient ratios for specimens with circular holes are compared favorably with the uniform stress approach as shown in Fig. 12. For specimens with square holes, the buckling coefficient ratios are close to the theoretical values determined by the modified finite element formulation of Yang (40) as shown in Fig. 13.

With regard to the post-buckling strength of the perforated stiffened compression elements, the effective width was computed on the basis of the tested ultimate loads and listed in Table VIII. For a direct comparison of the test results with the results of Winter and Sechler (15), the effect of corner properties as proposed by Karren (43) was neglected. Therefore in the calculation of effective widths, it was assumed that the stresses in lips, corners, and the 2-1/2 in. stiffened elements reached to the yield point of steel because their width-thickness ratios are less than the governing limits for local buckling and are therefore fully effective. In Fig. 14. the values of the effective width determined from the column tests are compared with the results obtained by Winter and Sechler (15).

For test specimens with the w/t ratio of 64.8, Fig. 14 indicates that the test data is in close agreement with the straight-line equation proposed by Winter (15). Test results of specimens with the w/t ratio of 36.6 are a little conservative when compared with the straight-line equation. This conservatism can be attributed to neglecting the true corner properties.

The difference in failure modes between members with small and large holes can readily be seen in Fig. 15. The failure mode for the specimen with the smaller hole is less pronounced than the failure modes for the specimens with the larger holes.

2. Beam Tests

a. Fabrication of Test Specimens.

Eight beam specimens were tested in this study. The beam specimens used in the test program were track sections. Dimensions of beam test specimens are listed in Table IX and shown in Fig. 16. Each track section was cut to a length of 100 inches. Circular holes ranging from 1 to 4 inches in diameter were cut in the stiffened compression flanges by Greenlee punches.

b. Location of Strain Gages

1/4-in. foil strain gages were used for determining the critical buckling strains and the post-buckling strength. For the perforated specimen, 15 strain gages were used. Paired strain gages for determining the critical buckling strains were placed close to the edge of the perforation and along the centerline of the specimen. Strain gages were also placed at the edge of the stiffened compression flange, on the unstiffened lip, and on the specimen webs. Strain gage locations are shown in Fig. 16.

c. Mechanical Properties

Tensile tests were conducted to determine the mechanical properties of the steel specimens. The tensile specimens complied with ASTM Designation A 370-68 (42). Average values of the mechanical properties obtained from these tests were used. The mechanical properties of steel test specimens are also given in Table V.

d. Test Procedures

The 10,000 pound Tinius Olsen beam testing machine was used to test all beam specimens. Fig. 17 shows the set-up of beam test. The specimens were loaded at the quarter points of the span as shown in Fig. 16. This quarter point loading provided a constant bending moment in the center half of the beam, thereby providing a uniformally compressed stiffened compression flange. Bearing plates were provided at load points and reactions to prevent premature failure by web crippling.

During loading strain gage readings were recorded and printed out on tape by the Data Acquisition System. Deflections were measured at midspan by dial gages located under each tension flange.

e. Discussion of Results

The buckling loads and bulking coefficient ratios were determined from the results of tests by using the modified strain reversal method. These values are listed in Table X and compared with the analytical results as shown in Fig. 12. The beam test results also compared favorably with the uniform stress approach.

The effective width was determined from the loads and measured strains. First, the position of the neutral axis was determined from the strain readings. With the neutral axis known, the effective width was calculated from the condition that, in pure bending, the sum of the axial forces equals zero:

$$\int_A \sigma dA = 0 \qquad (23)$$

Knowing the effective width and the location of the neutral axis, the internal bending moment was calculated:

$$\int_A \sigma y dA = M \tag{24}$$

The moment calculated by Eq. 24 provides a check on the computed effective width. Verification of the method for determining the effective width was obtained by comparing the calculated moments and the experimental moments. The results obtained from this investigation are also compared with the test results of Winter and Sechler in Fig. 14.

With regard to the verification of the tested yield moments, Eq. 13 and 14 were used to compute the effective widths of the compression flanges. Good agreement between the computed yield moments and the tested values were obtained. The comparison is shown in Table XI.

A comparison of the beam-test centerline deflections are shown in Table XII for different load levels. This comparison indicates that a beam having a single perforation, regardless of the d/w ratio has essentially the same deflection. A load deflection curve is shown in Fig. 18. The straight line is the calculated elastic deflection for the full section. The experimental load deflection curve in linear for small loads and becomes non-linear at larger loads. The shape of the load deflection curve is caused primarily by local buckling. For any particular load level, the calculated elastic deflection underestimates the experimental deflection. This illustrates very clearly the necessity for an analysis method taking this difference into account.

For determining the deflection of a beam having a single hole, the effective cross-sectional area may be determined using the unperforated section. For a beam with multiple holes, deflection may be conservatively determined by using the appropriate modified effective width equation derived in the analytical section to calculate the effective cross sectional area.

This study does not take in the effect of multiple holes. Multiple holes will affect the effective width depending on the hole spacing. Current design specifications and guides discussed in Part G of Chapter II are based on extensive experimental investigation and engineering judgement, indicate that the effective width is not affected as long as the clear distance between perforations is equal to or greater than the flat width.

According to the AISC design provision (2), the limiting width-thickness ratio, $(\frac{w}{t})_{lim}$, for perforated cover plates is equal to $317/\sqrt{\sigma_y}$. When the $\frac{w}{t}$ ratio of a steel plate is less than or equal $(\frac{w}{t})_{lim}$, the net width of the plate at the perforation is to be taken as being fully effective. Effective widths are computed for test specimens with circular perforations on the basis of the limiting width-thickness ratio and the modified effective width equations. A comparison of the computed effective widths and the AISC effective width is given in Table XII. Good agreement has been obtained for values of $\frac{w}{t}$ less than $(\frac{w}{t})_{lim}$. No comparison can be made for specimens with values of $\frac{w}{t}$ greater than $(\frac{w}{t})_{lim}$.

The above discussion indicates that design provisions presently being used are limited and pertains primarily to heavy steel sections.

The modified effective width equations may be used for a practical range of width-thickness ratios.

C. Summary

Based on this investigation, the following summary on stiffened compression elements with circular and square holes may be made from the analytical and experimental results:

1. The presence of holes may reduce the buckling load of the stiffened compression elements.
2. The reduction of buckling load of the stiffened compression elements is more pronounced for square holes than for circular holes due to the difference in stress concentration and the shape of holes.
3. Test data indicated that for stiffened compression elements with circular holes, the uniform stress approach may be used to predict the buckling load.
4. Winter's effective width equation for solid plates can be modified for determination of the effective width of perforated stiffened elements.
5. Even though the buckling load for the perforated stiffened elements is affected more by the square holes than circular holes, the post-buckling strength of the elements with square and circular holes are found to be nearly the same if the diameter of a circular hole is the same as the width of a square hole.

IV. BEHAVIOR OF UNSTIFFENED COMPRESSION ELEMENTS WITH CIRCULAR PERFORATIONS

In order to properly describe the structural behavior of unstiffened compression elements (compression flange with only one longitudinal edge stiffened) with circular perforations, the buckling behavior must first be known. Previous investigations (15,19,20,41) of plain unstiffened elements indicated that local distortions of the unstiffened element severly limited their service load capacity, particularly for elements with large width-thickness ratios.

Based on these established results of plain unstiffened compression elements, this study deals primarily with the experimental determination of the critical buckling stresses for structural members with circular perforated unstiffened elements. An analytical study was also conducted to determine the critical buckling stresses for an unstiffened plate with square perforations.

A. Analytical Investigation

The modified finite element program discussed in Chapter III was used in this study to determine the critical buckling stresses for an unstiffened plate with a central square perforation. The unstiffened plate was idealized by using 16 square elements as shown in Fig. 19. Only one-half of the plate was used in the finite element analysis due to geometric symmetry. The idealization for the case of h_s/w of 0.0 is shown in Fig. 19. For the case of h_s/w of 0.5, elements 7,8,11,12 were deleted from the analysis.

The boundary conditions prescribed are based on the displacement functions given by Timoshenko and Gere (26). The displacement functions are:

$$w = f(y) \sin \frac{m\pi x}{a}$$

$$f(y) = A \sinh \alpha y + B \sin \beta y$$

The boundary freedoms deleted in this solution are noted in Table XIV. All other degrees of freedom are not restrained from movements.

The critical buckling coefficient, k, for the case of $h_s/w = 0.0$ was calculated to be 0.655 as compared with the theoretical value of 0.698 given by Timoshenko and Gere (26). This comparison shows the calculated value to be about 7 percent lower than the theoretical value. Since the purpose of this investigation is to determine the reduction of the critical buckling stress due to a perforation, only relative values of the critical buckling stresses are of primary interest.

Stress reduction factor, S.R.F., was calculated by comparing the critical buckling stress of a perforated plate with the critical buckling stress of an unperforated plate. The results of this analytical investigation are verified by the experimental investigation.

B. Experimental Investigation

To determine the effect of holes on the buckling strength, eighteen short column tests have been conducted to cover the following parameters:

a) Width-to-thickness ratio: 10.7 to 27.4

b) Hole opening to overall width ratio (d/w): 0 to 0.30

c) Yield point of steel: 59.7 psi

d) Column length: 6.0 in. to 12.0 in.

The experimental investigation and the analysis of the results of tests will be presented and discussed. The discussion will cover the fabrication and testing of the specimens and determination of the critical strains and stresses.

1. Fabrication of Test Specimens

Test specimens were fabricated by connecting identical channels placed back-to-back. Dimensions of the test specimens are listed in Table XV and the test specimen cross-section is shown in Fig. 20. The lengths for all three series of test specimens are determined in accordance with the Appendix on Compression Testing of the AISI Specification (10). After channels were cut to the required lengths, identical channels were fastened back-to-back by 5/32" in diameter steel rivets spaced 1-1/2 in. apart. Next, circular perforations were drilled at the center of all four unstiffened compression elements.

2. Location of Strain Gages

Paired foil strain gages, 1/4-in. long were placed as close as possible to the edge of the unstiffened flange adjacent to the perforation. Fig. 20 also shows the strain gage locations. These paired strain gages were used for centering the specimen and determining the critical buckling strains.

3. Mechanical Properties

Tensile tests were conducted to determine the mechanical properties of steel used in this investigation. All tensile specimens compiled with ASTM designation A 370-69 (42). The average value of the yield point was found to be 59.7 ksi

4. Test Procedure

All specimens were tested in the 200,000 pound Tinius-Olsen universal testing machine in the flat end condition in the same manner as stiffened compression elements.

Loads and strain gage readings were recorded by a 40-channel Data Acquisition System.

5. Discussion of Results

Waving of the perforated unstiffened compression elements of the test specimens were observed. For unstiffened elements with large width-thickness ratios, waving was observed at loads as low as one-half of the failure load. For unstiffened compression elements with small width-thickness ratios, waving was observed just prior to the failure load.

Figure 21 shows three photographs of the same test specimen under different magnitudes of load. The width-thickness ratio of the unstiffened compression elements of the test specimen shown in the photographs was 27.4. A visual inspection of Fig. 21 indicates that the test specimen was initially imperfect. The unstiffened elements started developing waves prior to the critical buckling stress. These waves were more pronounced in the vicinity of the hole. Waving became more pronounced as loading continued. When the failure load was reached, the unstiffened elements wave spread into the web and the specimen collasped. The failure load was approximately 3 times the experimental critical buckling load. The behavior described is typical of structural members which contain perforated unstiffened compression elements.

Stress reduction factors were introduced in the analytical investigation as a means for determining the effect of a hole on the buckling stresses, therefore stress reduction factors are also used in this study.

Experimental stress reduction factors were derived on the basis of the experimental study. The critical buckling strain was determined by using the strain reversal method (19,20) as described in Chapter III. The critical buckling loads and stresses were computed from the critical strains.

Test designed to determine the critical buckling stresses are quite prone to experimental scatter. The scatter of the experimental data can be attributed to initial imperfections, residual stresses, and difficulty in obtaining ideal edge support conditions.

The experimental stress reduction factors, q_{ub}, are given in Table XVI and are compared with the analytical stress reduction factors in Fig. 22. It can readily be seen in Fig. 22 that the experimental reduction factors for circular perforated unstiffened compression elements are in agreement with the analytical stress reduction factors of the square perforated unstiffened plate. The experimental reduction factors are:

1. When the design stress is based on yielding

$$q_{uy} = \left(1 - \frac{d}{w}\right) \tag{25}$$

2. When the design stress is based on local buckling

$$q_{ub} = \left(1 - 0.80\,\frac{d}{w}\right) \tag{26}$$

Equation 25 is based on the reduction in cross sectional area and Equation 26 is derived from the experimental investigation.

Design criteria for plain unstiffened compression elements is given in the AISI Specification (10). The three equations represent the behavior of unstiffened compression elements in the yield, inelastic buckling, and elastic buckling ranges. Width-thickness ratios are used to define these ranges. Equations 27, 28, and 29 are the AISI design equations for unstiffened compression elements.

1. For w/t ratio not greater than $63.3/\sqrt{F_y}$

$$F_c = 0.60\ F_y \qquad (27)$$

2. For w/t ratio greater than $63.3/\sqrt{F_y}$ but not greater than $144/\sqrt{F_y}$

$$F_c = F_y\ [0.767 - (2.64/10^3)(w/t)\ \sqrt{F_y}\ ] \qquad (28)$$

3. For w/t ratio greater than $144/\sqrt{F_y}$ but not greater than 25.

$$F_c = 8{,}000/(w/t)^2 \qquad (29)$$

4. For w/t ratio from 25 to 60

For angle struts

$$F_c = 8{,}000/(w/t)^2 \qquad (30)$$

For all other sections

$$F_c = 19.8 - 0.28\ (w/t) \qquad (31)$$

where

F_c = maximum allowable compression stress on an unstiffened element

F_y = yield point

Based on the results obtained from the analytical and experimental investigations, the present AISI design Equations 27, 28, 29, 30 and 31 may be modified to take in account the effect of a circular hole. The

stress reduction factor based on the experimental investigation are used to modify the design equations. The modified equations are:

1. For w/t ratio not greater than $63.3/\sqrt{F_y}$

$$F_c = 0.60\ F_y\ (q_{uy}) \tag{32}$$

2. For w/t ratio greater than $63.3/\sqrt{F_y}$ but not greater than $144/\sqrt{F_y}$

$$F_c = F_y\ [0.767-(2.64/10^3)(\tfrac{w}{t})\sqrt{F_y}\ ]\ (q_{ub}) \tag{33}$$

3. For w/t ratio greater than $144/\sqrt{F_y}$ but not greater than 25

$$F_c = \frac{8{,}000}{(w/t)^2}\ (q_{ub}) \tag{34}$$

4. For w/t ratio from 25 to 60

For angle struts

$$F_c = \frac{8{,}000}{(w/t)^2}\ (q_{ub}) \tag{35}$$

For all other sections

$$F_c = [19.8 - 0.28(w/t)](q_{ub}) \tag{36}$$

C. Summary

The following summary may be made for unstiffened compression elements with circular holes based on the analytical and experimental results:

1. The critical buckling load of unstiffened compression element may be reduced due to the presence of holes.
2. Present AISI design equations may be modified by using a stress reduction factor.

V. BUCKLING BEHAVIOR OF WEBS HAVING A CIRCULAR HOLE

A. General

During the past several years, researchers (44,45,46,47) have studied the influence of the presence of holes in plates subjected to shear. Even though much analytical data is available for determining the changes in the stress distribution due to the presence of a hole, it was not until the advent of the computer along with the finite element method that a rigorous analytical solution to the complex shear buckling of web with perforations problem could be obtained.

Analytical and experimental investigations on the behavior of perforated shear webs have been conducted by Kawai and Ohtsubo (30), Kroll (33), and Rockey (34). Kroll (33) conducted only an analytical investigation. The results of the analytical investigation are shown in Fig. 23, in which the experimental results were found in good agreement with the analytical investigations.

The experimental investigation by Rockey, Anderson and Cheung (34) involved the testing of plates rather than structural members. Hot-rolled sections were used in the experimental study of Kawai and Ohtsubo (30). In developing design procedures applicable to cold-formed steel members, it is desirable to conduct tests of cold-formed members to determine the effect of the presence of a hole on the critical buckling load.

B. Experimental Investigation

1. Fabrication of Test Specimens

Twelve tests have been conducted for the range of h/t ratios from 66.2 to 99.5 and for d/h ratios from 0 to 0.504. Each specimen was fabricated by first, cutting the channels to the required length.

Paired channels were then placed back-to-back and temporarily fastened. Holes, 1/4-in. in diameter were drilled in the center of the webs at the quarter points, so that the perforations of each channel would be aligned properly with each other. The channels were unfastened and the perforations were cut in the webs. Identical channels were next placed back-to-back and fastened together with 5/32" in diameter steel rivets. Fig. 20 shows the cross-section of specimens. The dimensions of test specimens are given in Table XVII.

2. Test Procedures

Each specimen was tested in the 200,000 pound Tinius Olsen universal testing machine as a simply-supported beam loaded at the center of the span as shown in Fig. 24. To prevent premature failure by web crippling, steel bearing plates were provided at load points.

At small increments of loading, web lateral deflection readings were recorded by dial gages.

3. Discussion of Results

The critical buckling load was determined by using dial gages and the experimental method employed by Rockey (34) was applied. In this method, the buckling load is defined by the intersection of the two tangents drawn to the load lateral deflection plot as shown in Fig. 25. The critical loads obtained by this method are shown in Table XVIII.

The experimental results are compared with the analytical result of Kawai and Ohtsubo (30), Kroll (33), and Rockey (34). As shown in Fig. 23, it can be seen that the presence of holes will reduce the shear buckling load. The test data correlated better with the analytical solution for the simple support condition.

Based on the test data plotted in Fig. 23, Eq. 33 is the derived load reduction factor, q_s, for shear buckling in the elastic and inelastic ranges.

$$q_s = (1.0 - 1.1\ d/h) \tag{35}$$

where d is the diameter of holes and h is the clear distance between flanges measured along the plane of the web.

The present design equations used by AISI (10) for shear buckling in the elastic and inelastic ranges are shown below. The elastic and inelastic ranges are defined by the h/t ratio.

1. For h/t not greater than $547/\sqrt{F_y}$

$$F_v = \frac{152\sqrt{F_y}}{h/t} \text{ with a maximum of } 0.40\ F_y \tag{36}$$

2. For h/t greater than $547/\sqrt{F_y}$

$$F_v = \frac{83200}{(h/t)^2} \tag{37}$$

where F_v = maximum allowable average shear stress on the gross area of the flat web.

The experimental results indicated that holes will reduce the shear buckling load and that the reduction in load may be determined by using the load reduction factor, q_s. Based on the previous statement, it seems feasible to modify the present design Equations 36 and 37 used by AISI (10) for shear buckling in the elastic and inelastic ranges. The modified equations are:

$$0 < \frac{d}{h} \leq 0.5$$

1. For h/t no greater than $547/\sqrt{F_y}$

$$F_v = \frac{152\sqrt{F_y}}{h/t} (q_s) \text{ with a maximum of } 0.40\ F_y \qquad (38)$$

2. For h/t greater than $547/\sqrt{F_y}$

$$Fv = \frac{83,200}{(h/t)^2} (q_s) \qquad (39)$$

C. Summary

The following conclusions can be made for perforated shear webs.

1. Holes may reduce the critical web buckling load.
2. Stress reduction factor, q_s, may be used for shear buckling in the elastic and inelastic ranges.
3. Present AISI design equations may be modified by using a load reduction factor.

VI. CRIPPLING STRENGTH OF PERFORATED WEBS

A. General

When thin-walled steel members with perforated webs are subjected to concentrated loads, failure occurs primarily by the local weakening of the web adjacent to the load. Previous investigation (36) of the crippling strength of plain webs indicated that a theoretical investigation of the crippling strength is extremely complex, since an analysis would have to account for:

a) the non-uniform distribution of stresses in the web,

b) elastic and plastic instability due to the non-uniform distribution of stresses,

c) local yielding in the immediate region of the application of load, and

d) web bending produced by eccentric application of the load caused by the curved transition from web to bearing flange.

With the presence of a hole, the analysis becomes even more complex.

Due to the complexity of the problem of web crippling, an experimental investigation has been carried out to determine the effect of holes on the crippling strength of perforated webs.

B. Experimental Investigation

In this investigation, twenty tests have been conducted to cover the following parameters:

a) Shape of holes: circular and square holes

b) Overall height-to-thickness ratio: 66.7 to 101

c) Hole opening to overall height ratio: 0 to 0.642

d) Yield point of steel: 59.7 to 70.7

1. Fabrication and Testing of Specimen

Test specimens were composed of either back-to-back channels or two C-shaped channels connected through the simple lips as shown in Fig. 26. At the center of each specimen, a single hole was cut in the web. Test specimen dimensions are given in Tables XIX and XX.

The test were confined to the loading condition of a beam that is continuous over interior supports and/or subject to concentrated load. This condition was simulated as shown in Fig. 27. The bearing length, N, was held constant at 3.5 in. The 200,000 pound Tinius-Olsen universal testing machine was used to test all specimens. Loads were transmitted from the machine to the steel bearing plates by a roller as shown in Fig. 27. The ultimate loads at which the specimens failed are the only recorded results. Ultimate loads are listed in Tables XXI and XXII.

2. Discussion of Results.

To properly evaluate the test results, test values of specimens with plain webs were compared with the results of an extensive experimental investigation of Winter and Pian (36). For test specimens composed of back-to-back channels, the test values were lower than the values of the case of a beam having a single unreinforced web. This can be attributed to thin narrow flanges of the test specimens, which provide essentially no restraint against the rotation of the web. However, the reduction of load-carrying capacity due to the presence of holes can be obtained by comparing the relative test results. Test values for specimens composed of C-shaped channels were found to be higher than the case of a beam having a single unreinforced web. Comparison of the test results with the test values of Winter and Pian (36) is given in Table XXIII.

Bending of the webs out of the vertical plane was unavoidable in the tests. This was caused by slight eccentricity of the applied load with respect to the plane of the specimens, for which the corners were rounded at the web-flange intersection.

The results obtained from the twenty test specimens indicated that the presence of a hole in a web reduces the web crippling load. Load reduction factors were derived for steel members with circular and square perforations. Load reduction factors were derived by comparing the ultimate loads of perforated webs with the ultimate load for plain webs. Figures 28 and 29 show the load reduction factors versus the perforation opening-to-web height ratio for members with circular and square holes respectively.

The results of tests discussed above provide the background information on development of the following reduction factors to be used for web crippling:

For webs having circular perforations and when

$$0 < d/h \leq 0.5$$

$$q_{wcc} = (1.0 - 0.6\ d/h) \tag{40}$$

For webs having square perforations and when

$$0 < h_s/h \leq 0.642$$

$$q_{wcs} = (1.0 - 0.77\ h_s/h) \tag{41}$$

A comparison of the foregoing equations and the test data shown in Figs. 28 and 29 indicates that the reduction of the web crippling load is more pronounced for square holes than circular holes.

Design equations for plain webs are given in the AISI Specification (10) for the test loading condition and are summarized below:

1. Beams having single unreinforced webs for reactions of interior supports or for concentrated loads located anywhere on the span:

   For inside corner radius equal to or less than the thickness of sheet

   $$P_{max} = t^2[305+2.30(N/t)-0.009(N/t)(h/t)-0.5(h/t)] \times [1.22-0.22(F_y/33)](F_y/33) \quad (42)$$

   For other corner radii up to 4t, the value P_{max} given by the above equation is to be multiplied by

   $(1.06 - 0.06\ R/t)$

   For corner radii larger than 4t, tests shall be made in accordance with Section 6.

2. For I-beams made of two channels connected back-to-back or for similar sections which provide a high degree of restraint against rotation of the web, such as I-sections made by welding two angles to a channel.

   For reactions of interior supports or for concentrated load located anywhere in the span.

   $$P_{max} = t^2F_y(6.66 + 1.446\sqrt{N/t}\ ) \quad (43)$$

   P_{max} is the load or reaction for one solid web. N is the actual length of bearing.

Based on the results obtained from the experimental investigation, Equations 42 and 43 may be modified to account for the effect of a hole using the load reduction factors derived. The modified equations for webs with circular holes are:

$$0 < \frac{d}{h} \leq 0.5$$

1. Beams having single unreinforced webs for reactions of interior supports or for concentrated loads located anywhere on the span:
   For inside corner radius equal to or less than the thickness of sheet

$$P_{max} = t^2[305+2.30(N/t)-0.009(N/t)(h/t)-0.5(h/t)] \times [1.22-0.22(F_y/33)](F_y/33)\{q_{wcc}\} \quad (44)$$

2. For I-beams made of two channels connected back-to-back or for similar sections which provide a high degree of restraint against rotation of the web, such as I-sections made by welding two angles to a channel.
   For reactions of interior supports or for concentrated load located anywhere in the span.

$$P_{max} = t^2F_y(6.66+1.446\sqrt{N/t})\{q_{wcc}\} \quad (45)$$

For webs with square holes, the modified equations are:

$$0 < h_s/h \leq 0.642$$

1. Beams having single unreinforced webs for reactions of interior supports or for concentrated loads located anywhere on the span:
   For inside corner radius equal to or less than the thickness of sheet

$$P_{max} = t^2[305+2.30(N/t)-0.009(N/t)(h/t)-0.5(h/t)] \times [1.22-0.22(F_y/33)](F_y/33)\{q_{wcs}\} \quad (46)$$

2. For I-beams made of two channels connected back-to-back or for similar sections which provide a high degree of restraint against rotation of the web, such as I-sections made by welding two angles to a channel.

   For reactions of interior supports or for concentrated load located anywhere in the span.

$$P_{max} = t^2(6.66+1.446\sqrt{N/t}\,)\{q_{wcs}\} \qquad (47)$$

C. Summary

The following conclusions can be made for perforated webs subjected to failure by web crippling.

1. Holes may reduce the ultimate loads of perforated webs.
2. The stress reduction, q_{wc}, is greater for a web having a square hole than a web with a circular hole providing h_s/h ratio is the same as the d/h ratio.
3. Present AISI design equations may be modified by using a stress reduction factor.
4. The modified equations pertain to the loading case for reactions of interior supports or for concentrated loads located anywhere on the span.

D. Stability of Perforated Plate Subjected to Equal and Opposite Point Loads

An analytical study of the elastic stability of a simply-supported plate loaded at the center by equal and opposite point loads was conducted. The modified finite element program discussed in Chapter III, was used in this study. The simply-supported plate was idealized by using 16 square elements as shown in Fig. 30. Due to geometric symmetry, only one-quarter of the plate was used in the analysis. For

the case of h_s/h of 0.25, element 16 was deleted from the analysis. Elements 11, 12, 15 and 16 were deleted for the case of h_s/h of 0.50. No elements were deleted for the case of h_s/h of 0.0. Deleted boundary freedoms are noted in Table XXIV. Other degrees of freedom are not restrained.

For the case of $h_s/h = 0$, the critical buckling coefficient was calculated to be 6.66 as compared with the theoretical value of 6.00 given by Yamaki (48). The calculated buckling load is about 11 percent higher than the theoretical value. Only relative values of the critical buckling loads are of primary interest, since the purpose of this investigation is to determine the load reduction due to the presence of a hole.

Load reduction factors, q_{wbs}, were computed by comparing the critical buckling load for a perforated web with the critical load for plain webs. The critical buckling loads and load reduction factor are given in Table XXV.

The case studied is somewhat impracticable, since a point load does not normally occur in practice. For the case of a simply supported plate subjected to equal and opposite locally distributed loads, which is more practicable, the critical buckling load may be determined by using Fig. 31.

The finite element solution was for the case of $\frac{\ell}{a} = 0$ as shown in Fig. 31. The load reduction factors, q_{wbs}, obtained in this analysis are shown in Fig. 29 with the experimental results. Inspection of Fig. 29 reveals that the trend of the analytical results is in good

VII. SUMMARY AND CONCLUSIONS

The objective of this investigation was to investigate the structural behavior of beams and columns with perforated elements and to develop design recommendations for use by engineers.

Summary and design recommendations are presented based on the investigations in Chapters III through VI.

A. Local Buckling and Post-Buckling Strength of Perforated Stiffened Compression Elements

The buckling behavior and post-buckling strength of perforated stiffened compression elements was investigated analytically and experimentally.

The study on the critical buckling loads of perforated plates indicated that perforations reduce the buckling load of stiffened compression elements. Reduction of the critical buckling load was found to be more pronounced for square holes than for circular holes. This reduction was attributed to the difference in stress concentration and the shape of holes. Test results for stiffened compression elements with circular holes compared favorably with the uniform stress approach. Therefore, the uniform stress approach may be used to predict the critical buckling load.

The post-buckling strength of stiffened compression elements with perforations was investigated. The comprehensive experimental investigation consisted of testing short columns and beam members. The results of these tests were compared with the experimental results of Winter and Sechler (15). Based on the well defined results for plain stiffened compression elements and the study on perforated stiffened

compression elements, Winter's effective width equation for plain plates was modified for the determination of the effective width of circular and square perforated stiffened elements. Post-buckling strength of elements with circular and square holes were found to be nearly the same if the diameter of a circular hole is the same as the width of a square hole, even though the buckling behavior is quite different.

B. Behavior of Unstiffened Compression Elements with Circular Perforations

Critical buckling stresses for perforated unstiffened compression elements was determined analytically and experimentally. A series of tests on short compression members containing unstiffened elements was performed. The results of these tests indicated that for design of cold-formed steel members with circular perforated unstiffened compression flanges, the modified design equations developed in this study may be used.

C. Buckling Behavior of Webs Having a Circular Hole

An experimental investigation was conducted to determine the effect of a hole on the critical buckling load. This investigation involved the testing of structural members instead of plates.

The test data was compared with the analytical results of other authors and was found to be in good agreement. The test data correlated best with the analytical solution for the simple support condition. Test data indicated that for determination of the shear buckling load in the elastic and inelastic ranges, a load reduction factor, q_s, may be used for designing webs with a circular hole. A

modified equation for use in design of perforated shear webs is presented.

D. Crippling Strength of Perforated Webs

The reduction in crippling strength of perforated webs was determined experimentally. Tests were confined to the loading condition of a beam that is continuous over interior supports and/or subject to concentrated load. Test results were verified by comparing the results of plain webs with results of early studies of crippling strength of plain webs.

Based on the results of the test, reduction factors for web crippling were derived for use in the design of square and circular perforated webs. The reduction factors were used in modifying present AISI design equations to take into account the effect of circular and square holes.

Critical buckling loads were determined analytically for a simply supported plate subjected to equal and opposite point loads at the center. Load reduction factors, q_{wbs}, were derived and compared favorably with the trend of the load reduction factor, q_{wcc}.

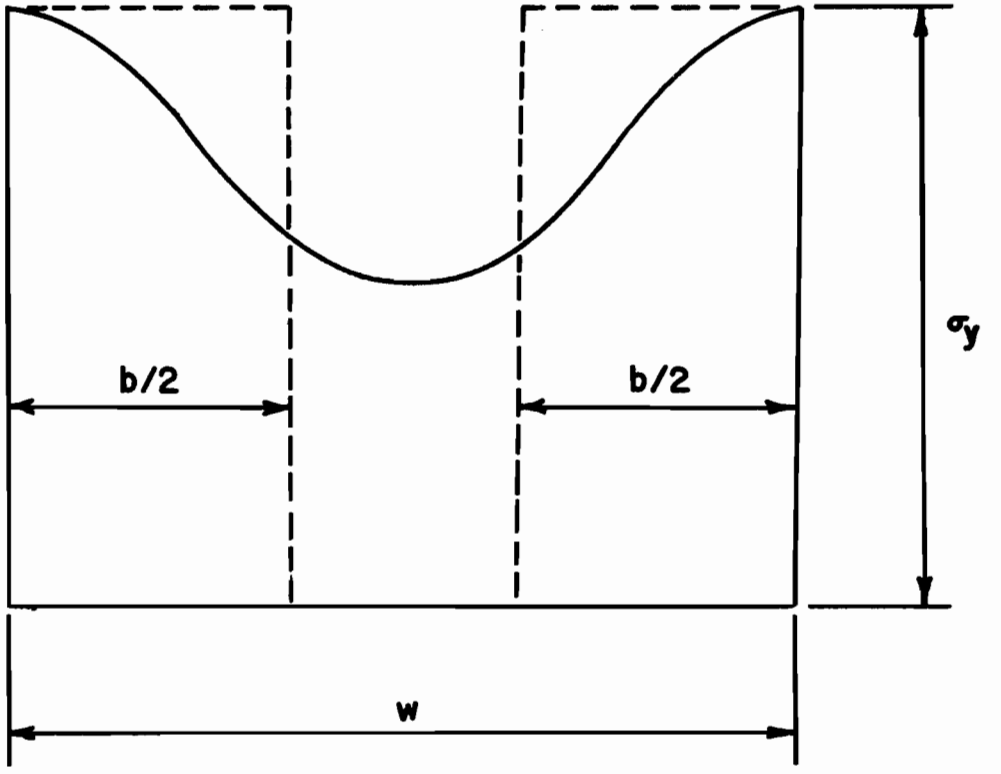

Figure 1. Effective Width of Stiffened Compression Elements

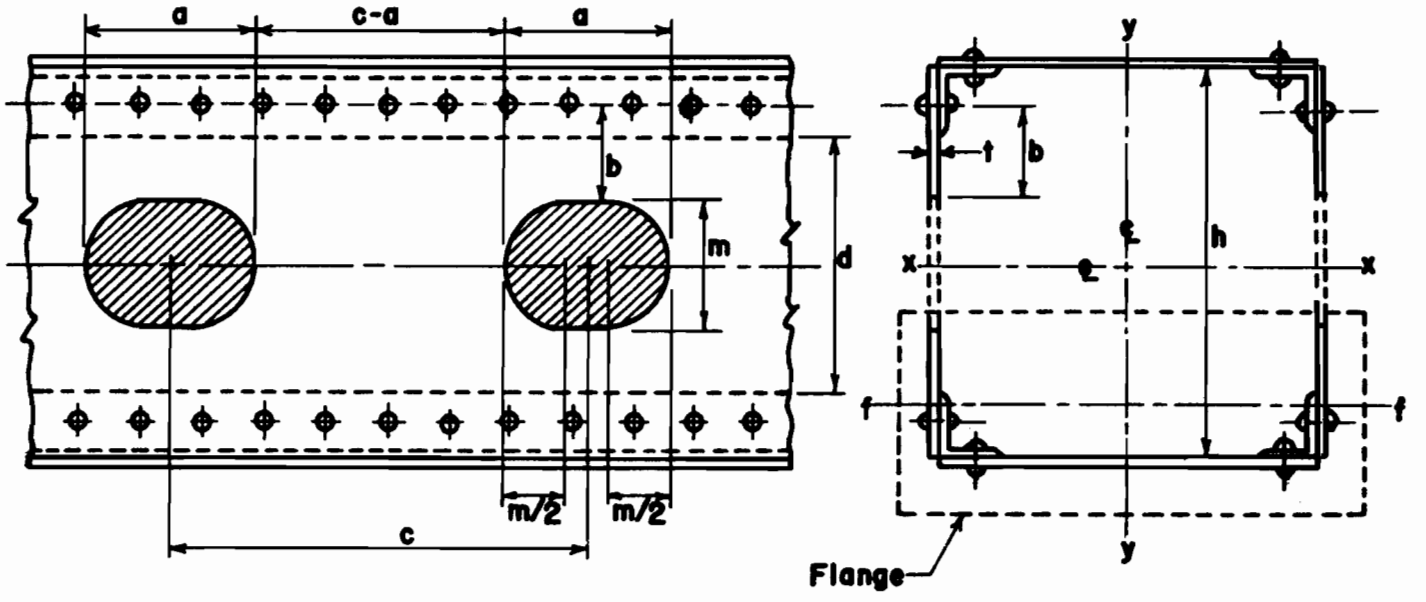

Figure 2. Dimensions Used in the Specifications

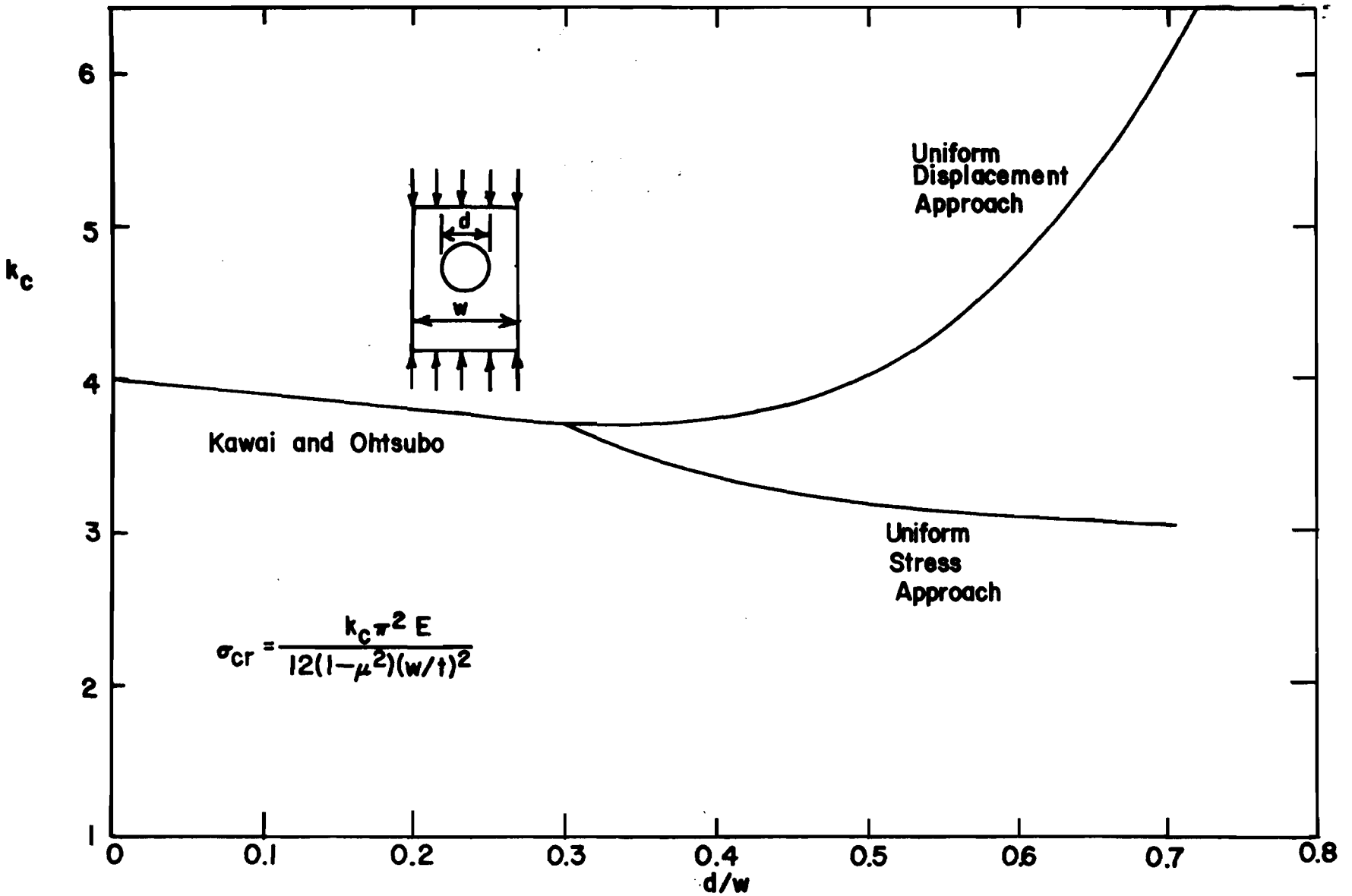

Figure 3. Buckling Coefficient VS. d/w Ratio

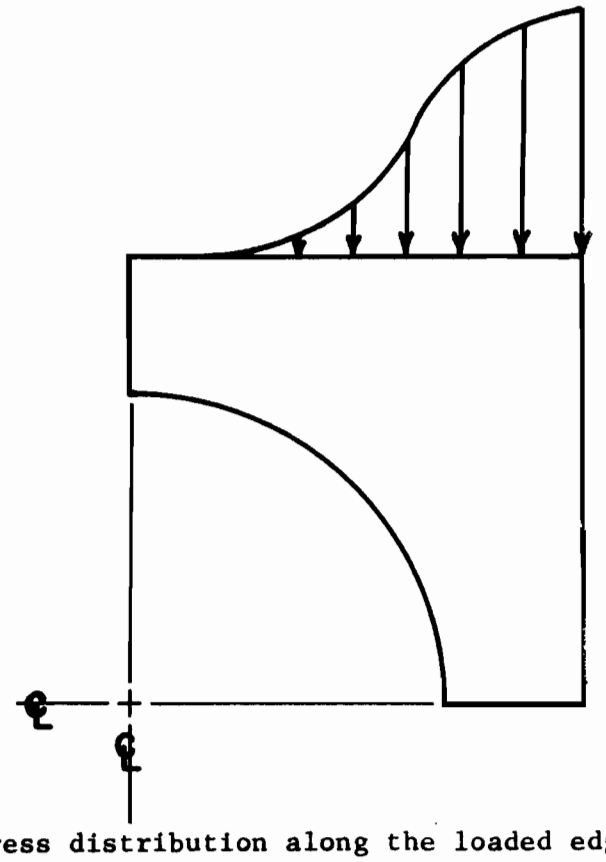

a. Stress distribution along the loaded edges for a plate having a large hole.

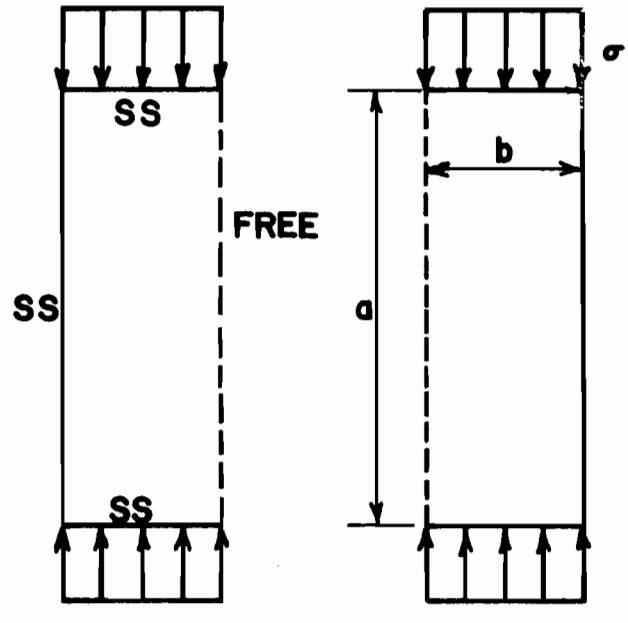

b. Simplified model for perforated plate with a large hole.

Figure 4. Perforated Plate Stress Distributions (30)

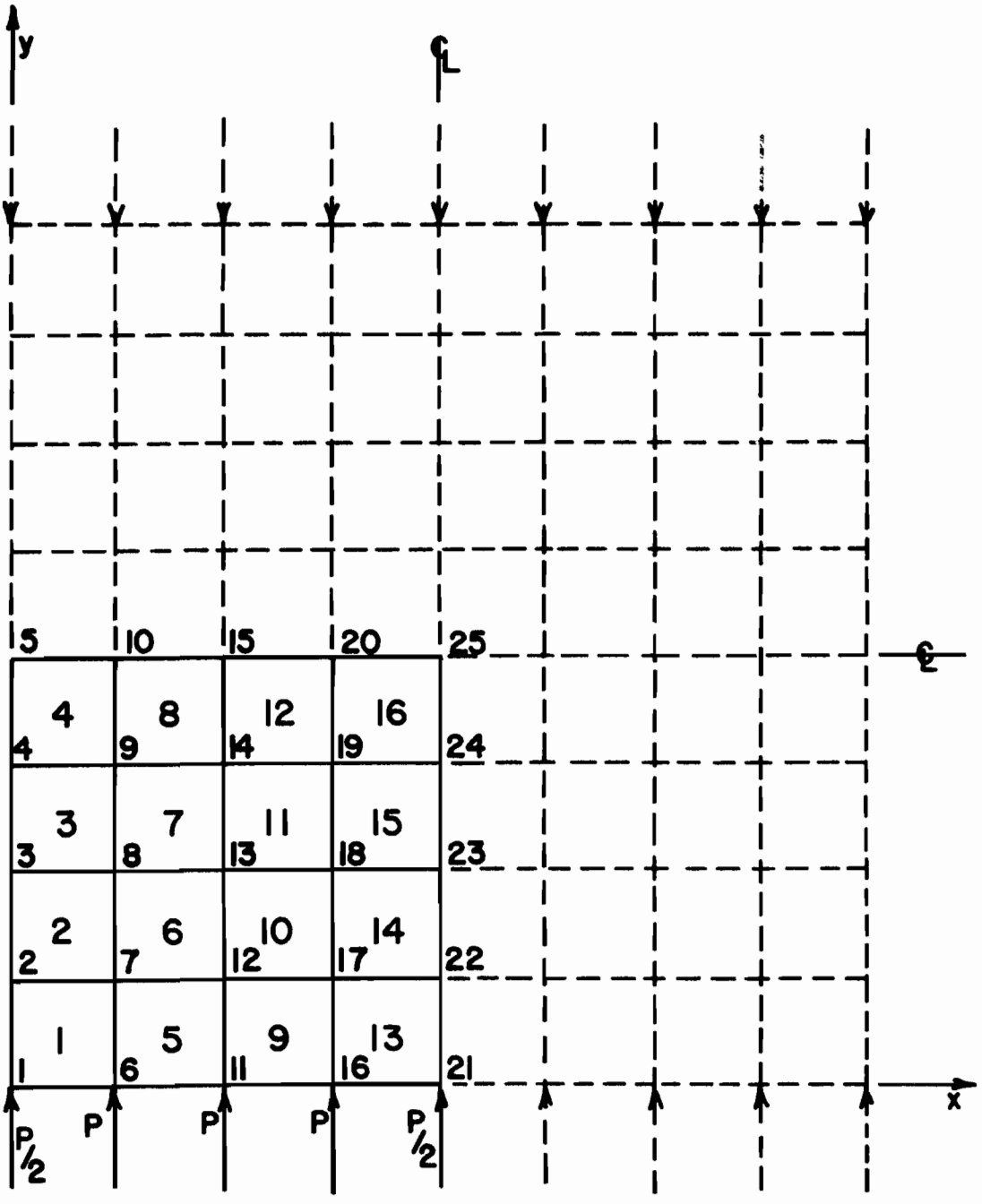

Figure 5. Finite Element Idealization for a Simply Supported Square Plate

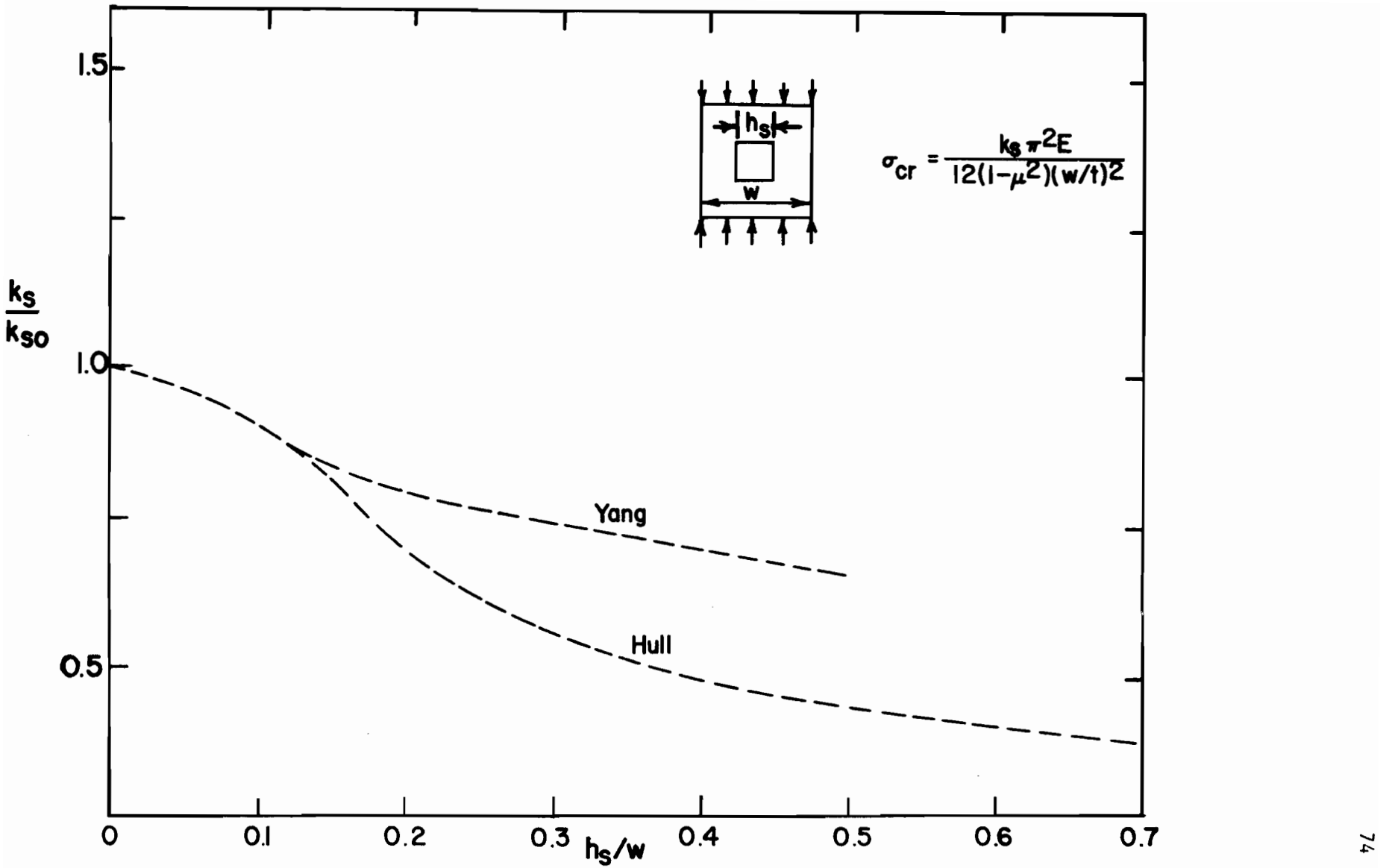

Figure 6. Buckling Coefficient VS. h_s/w Ratio

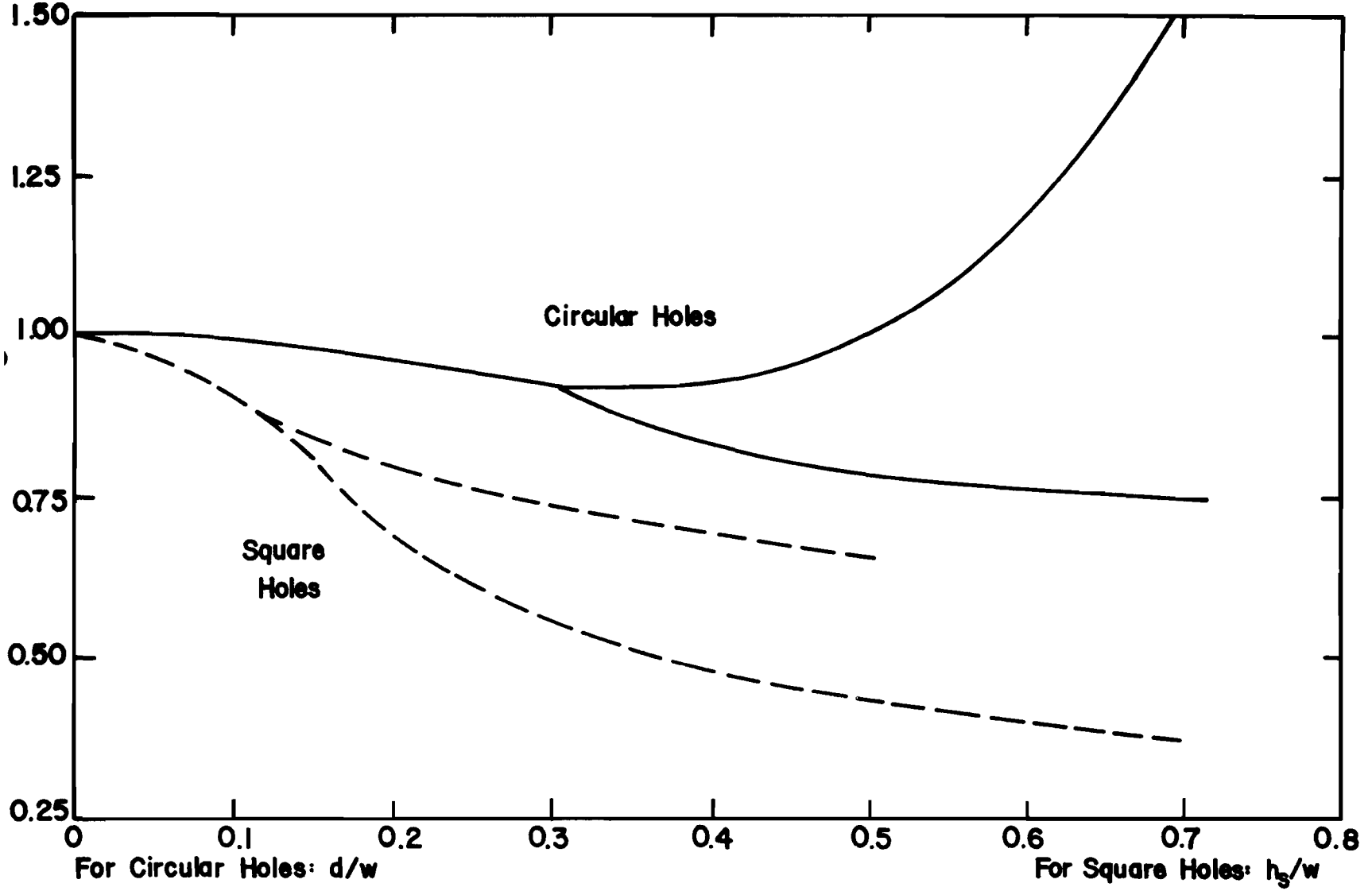

Figure 7. Effect of Shapes of Holes on Buckling Coefficient

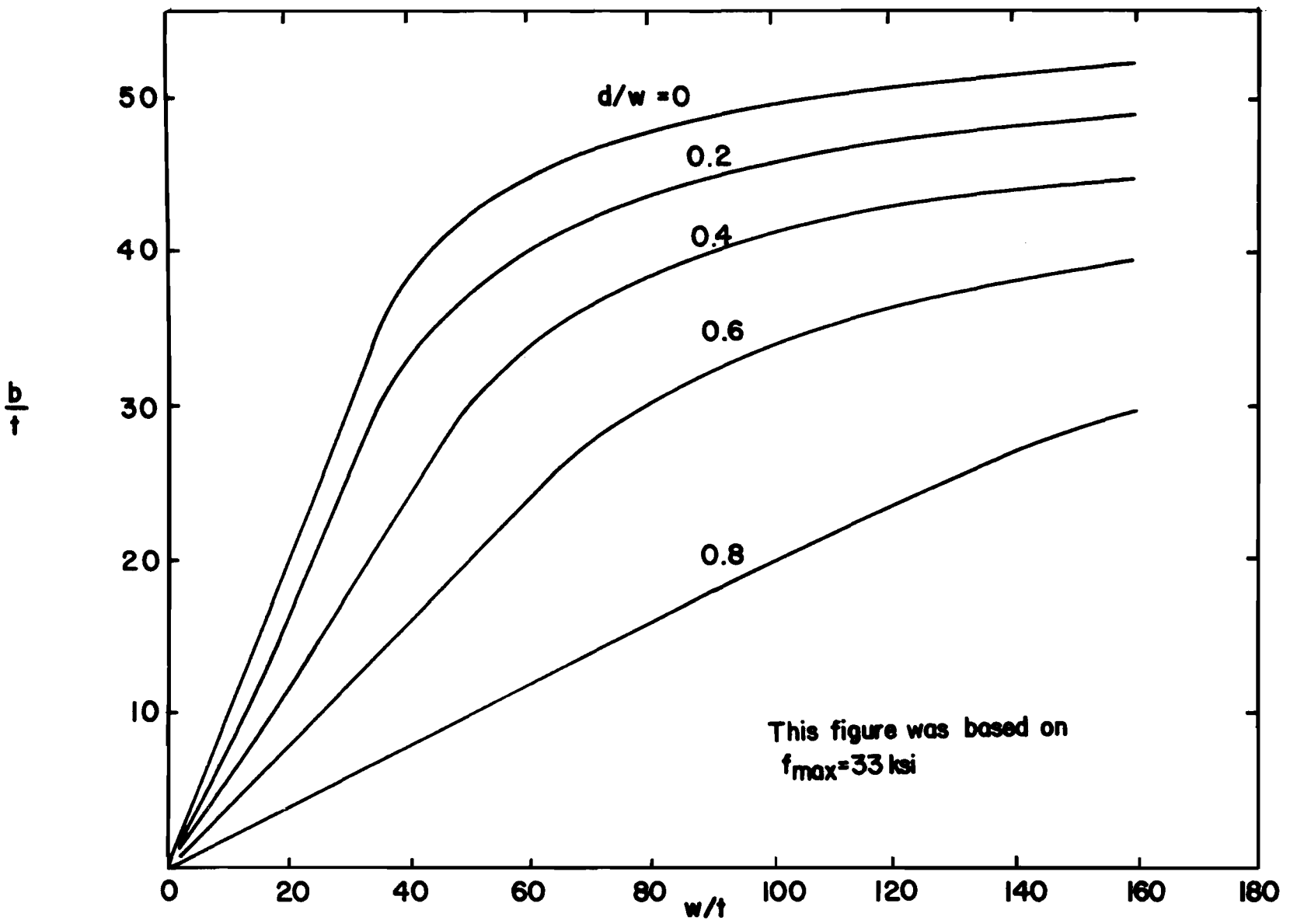

Figure 8. Influence of Holes on Effective Width of Stiffened Elements

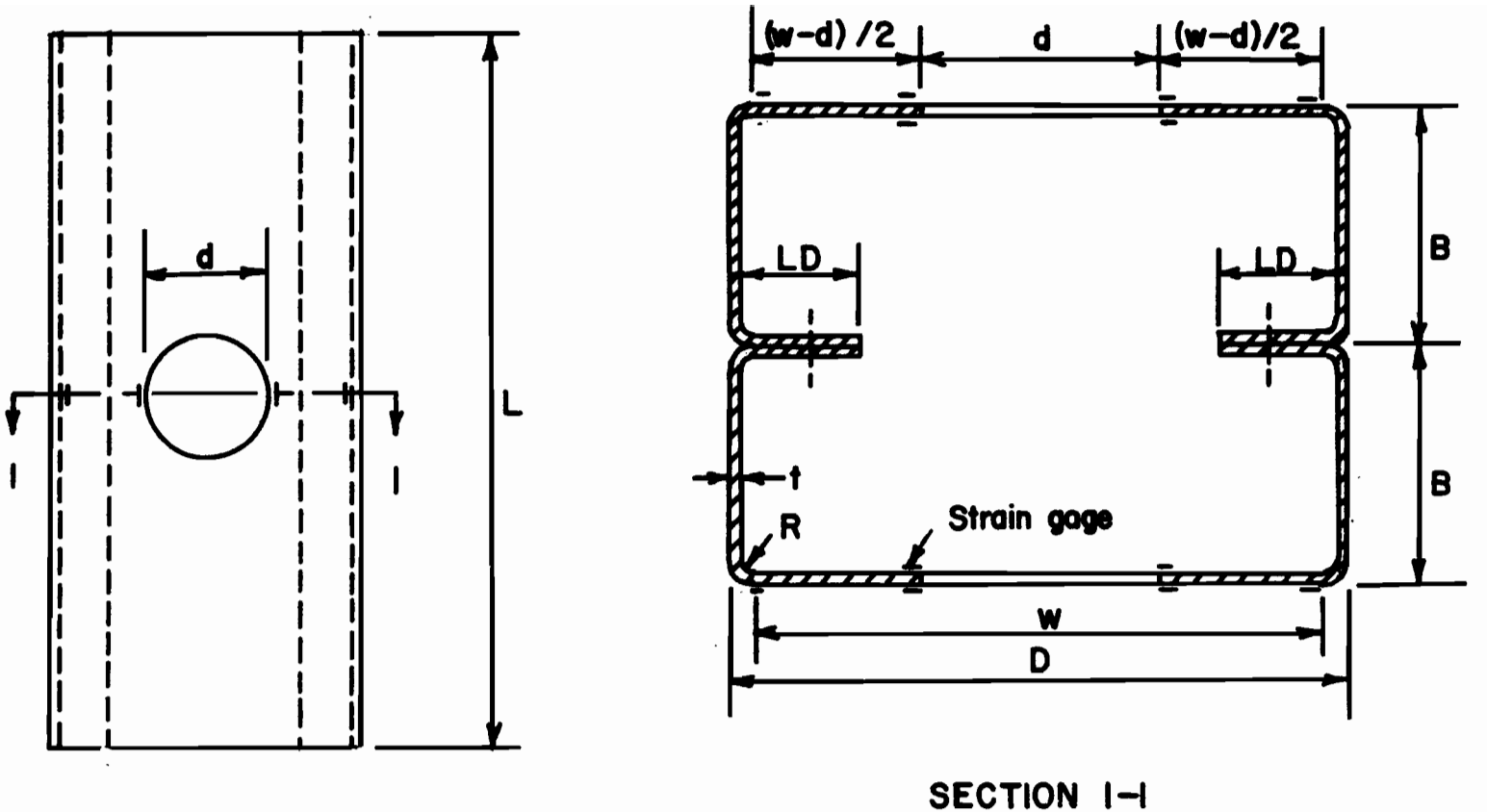

Figure 9. Dimensions of Test Specimens

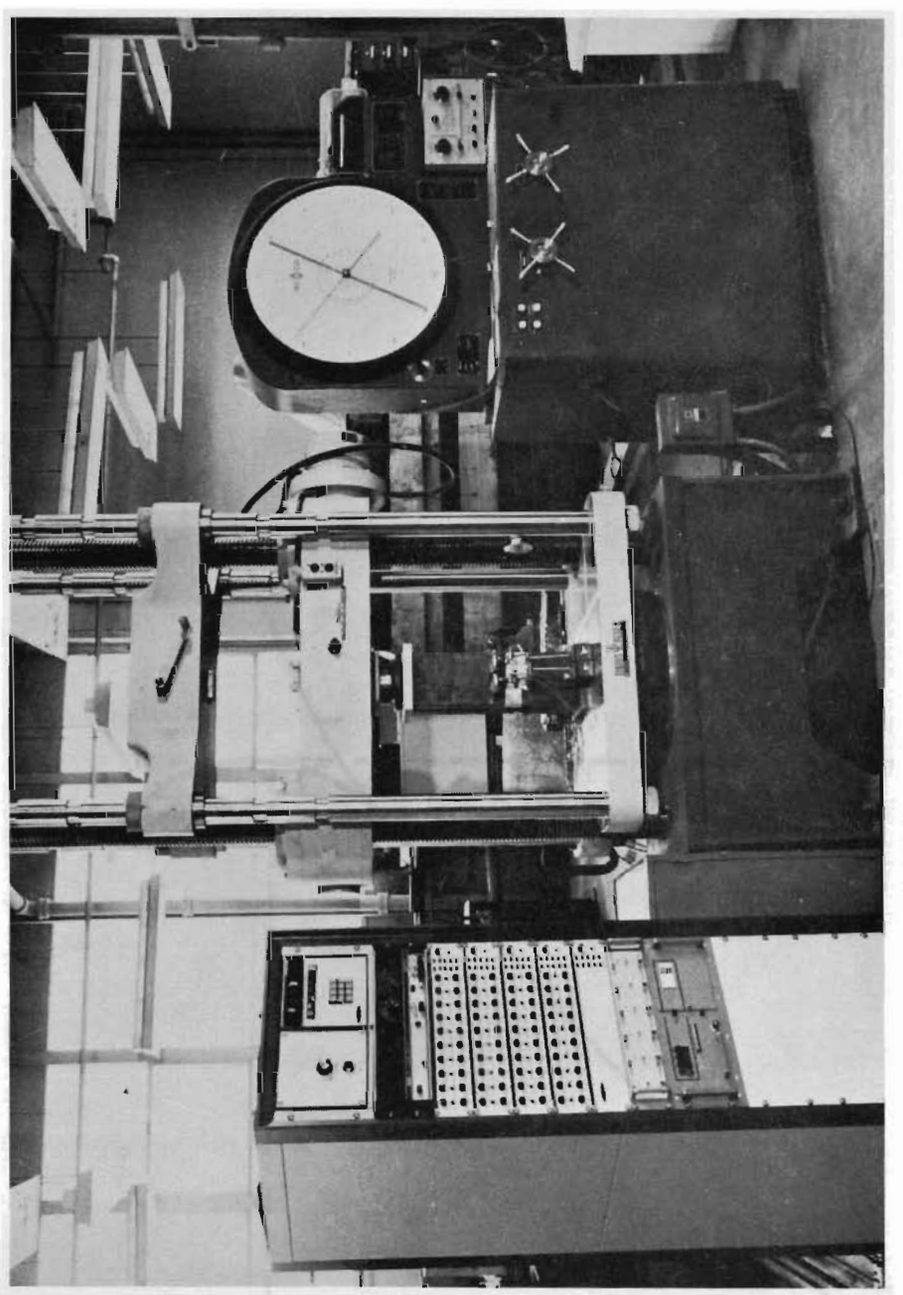

Figure 10. Test Set-Up

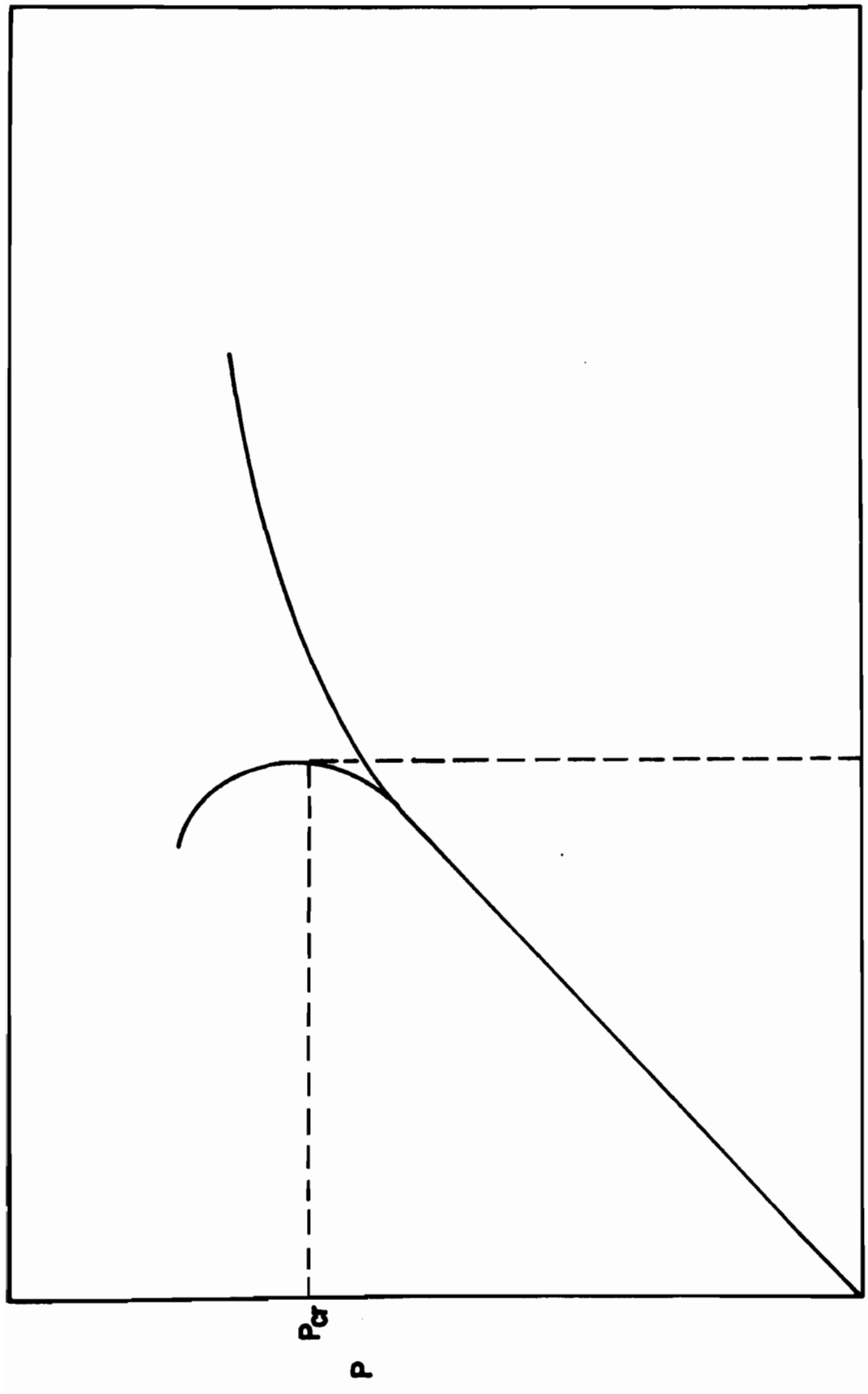

Figure 11. Typical Load-Strain Diagram

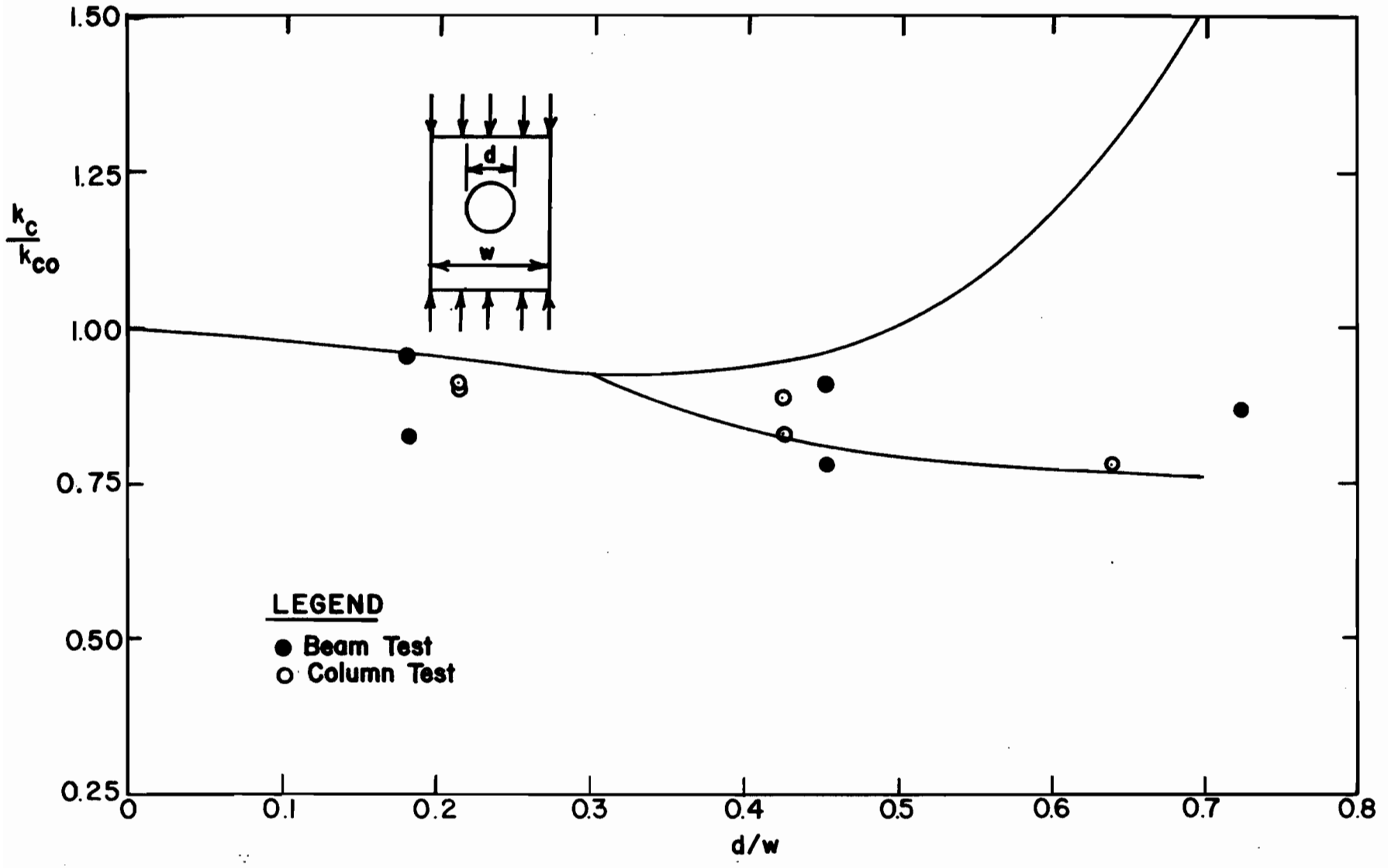

Figure 12. Comparison of Test Data with Theoretical Buckling Coefficients

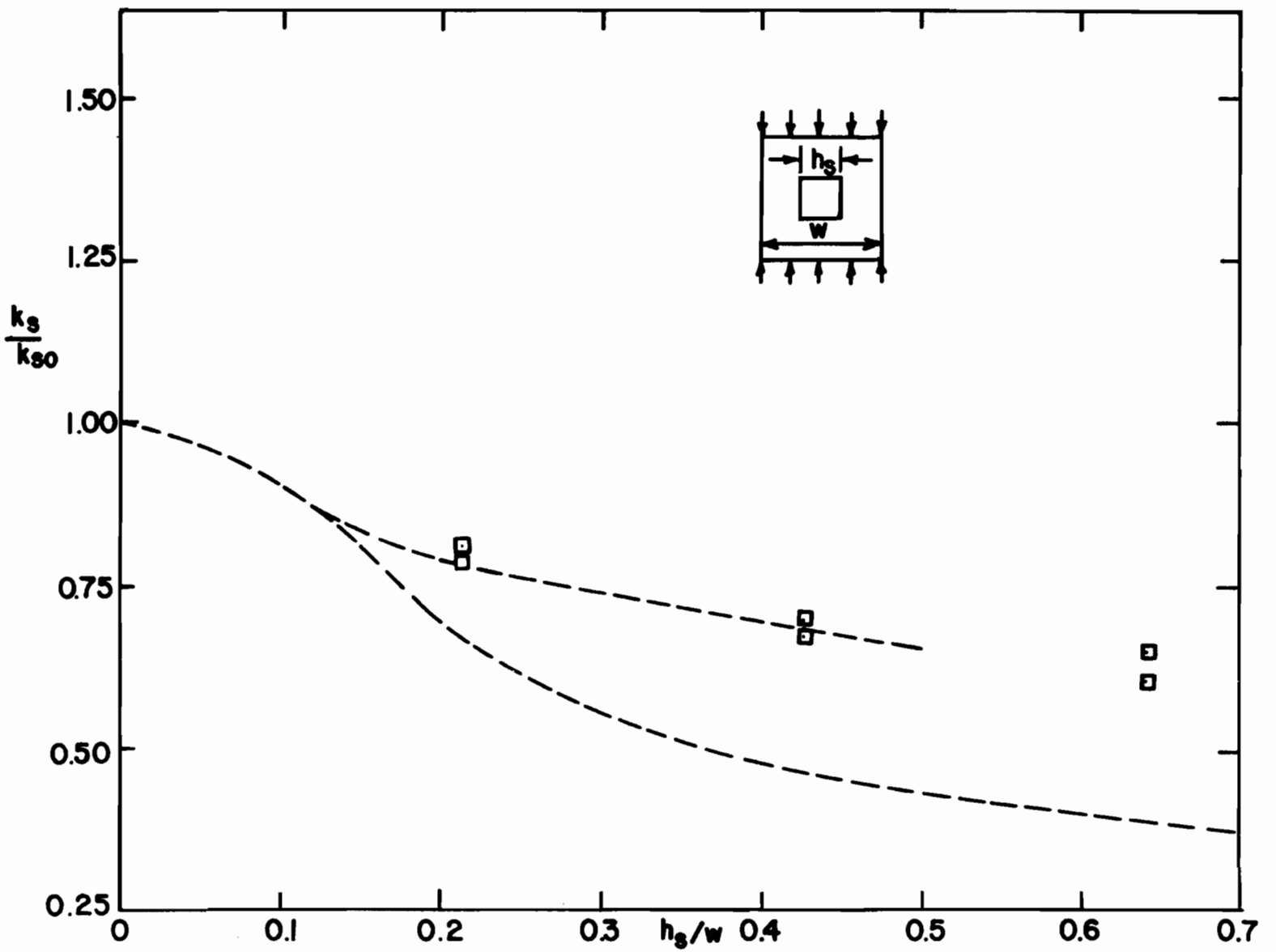

Figure 13. Comparison of Test Data with Theoretical Buckling Coefficients

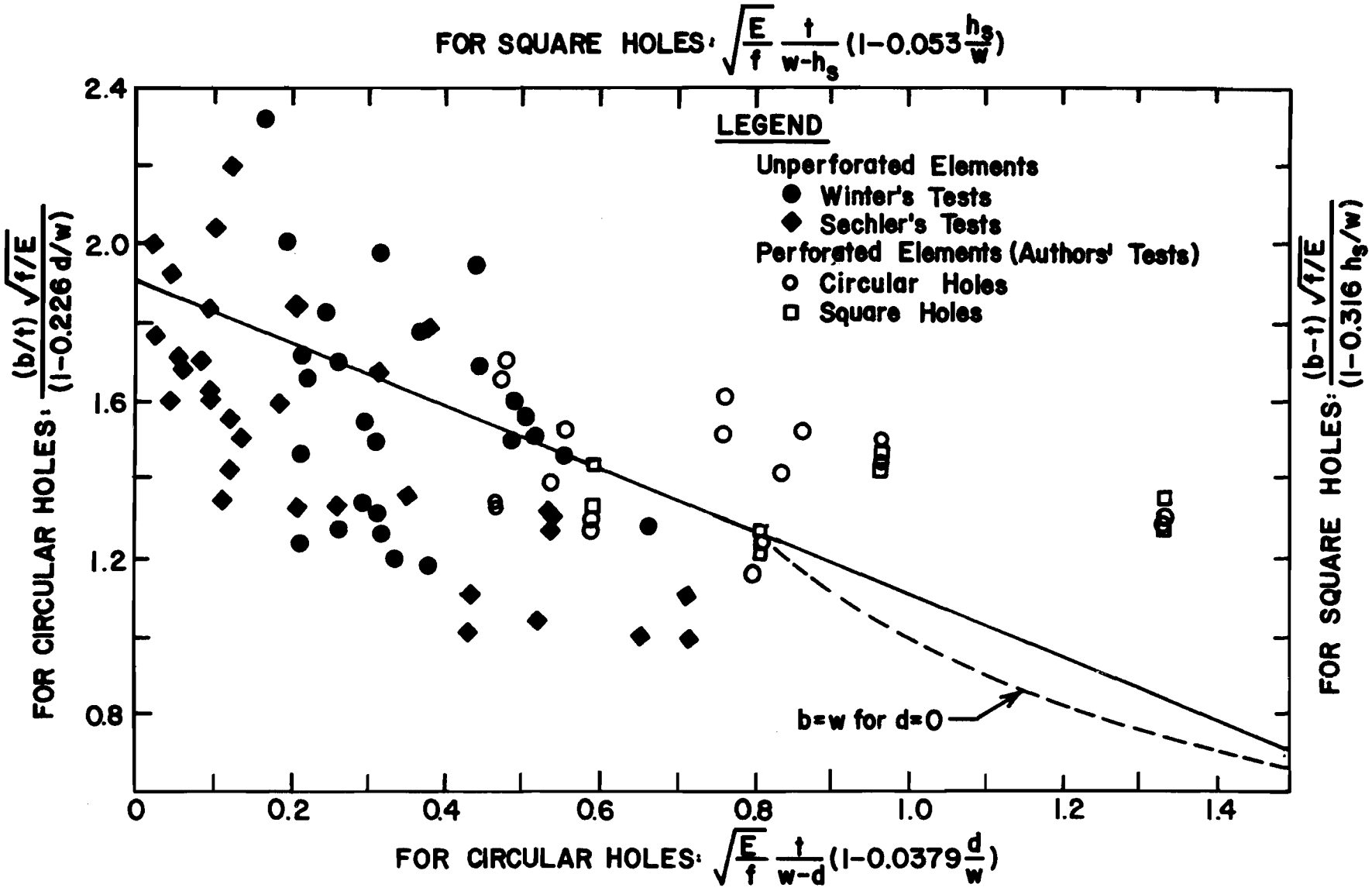

Figure 14. Comparison of Effective Width

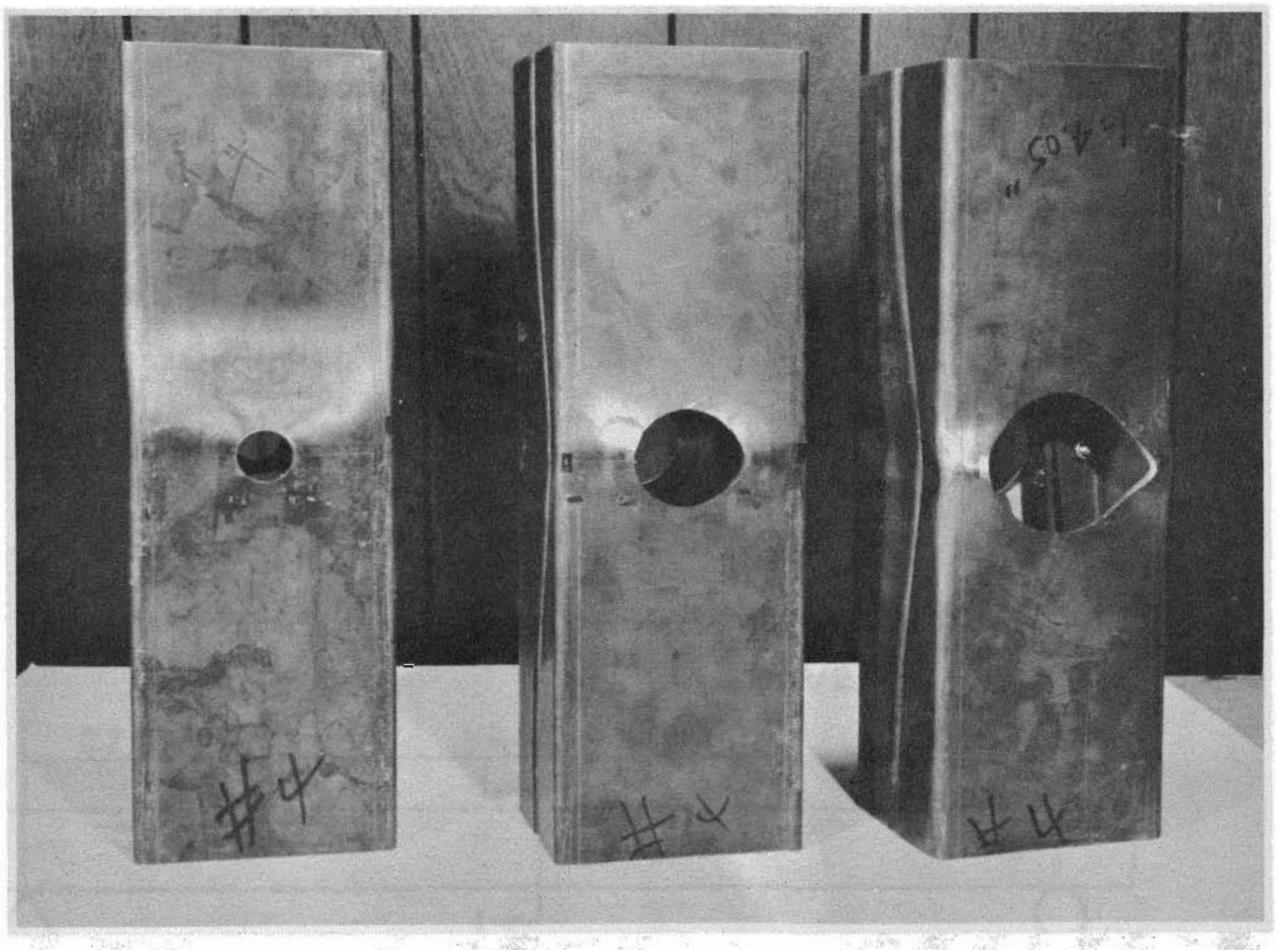

Figure 15. Comparison of Failure Modes

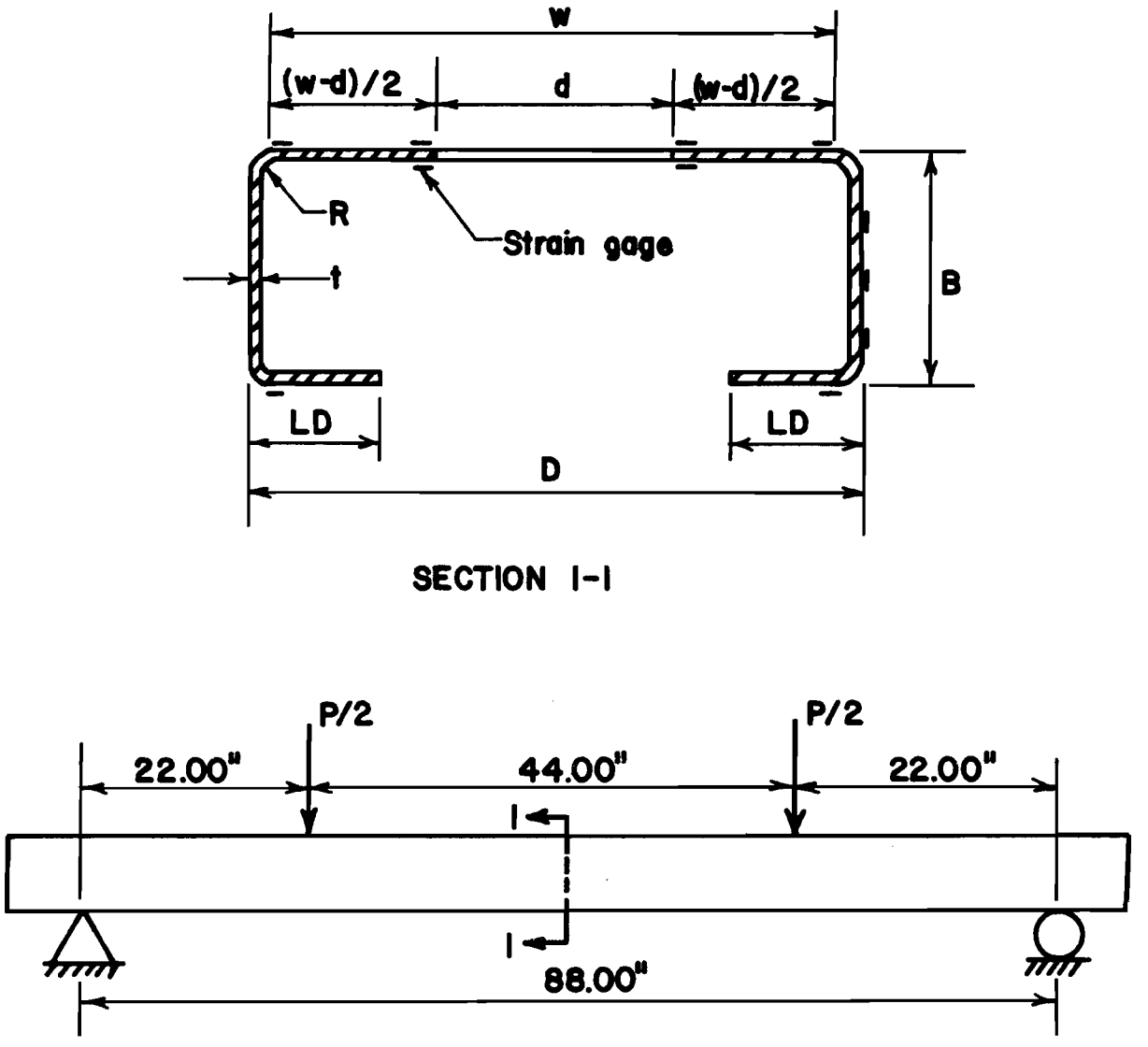

Figure 16. Dimensions of Beam Specimens

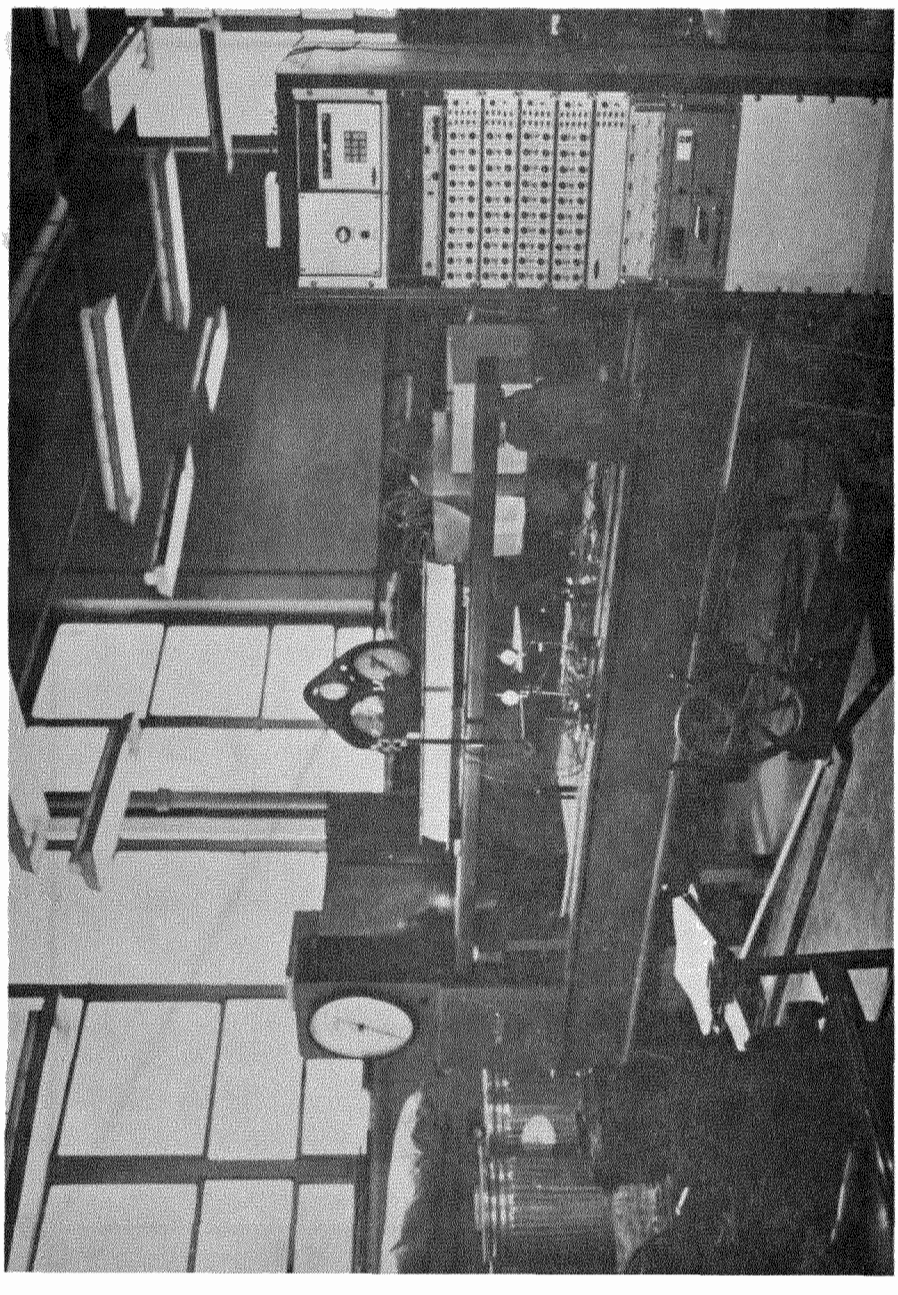

Figure 17. Set-Up for Beam Tests

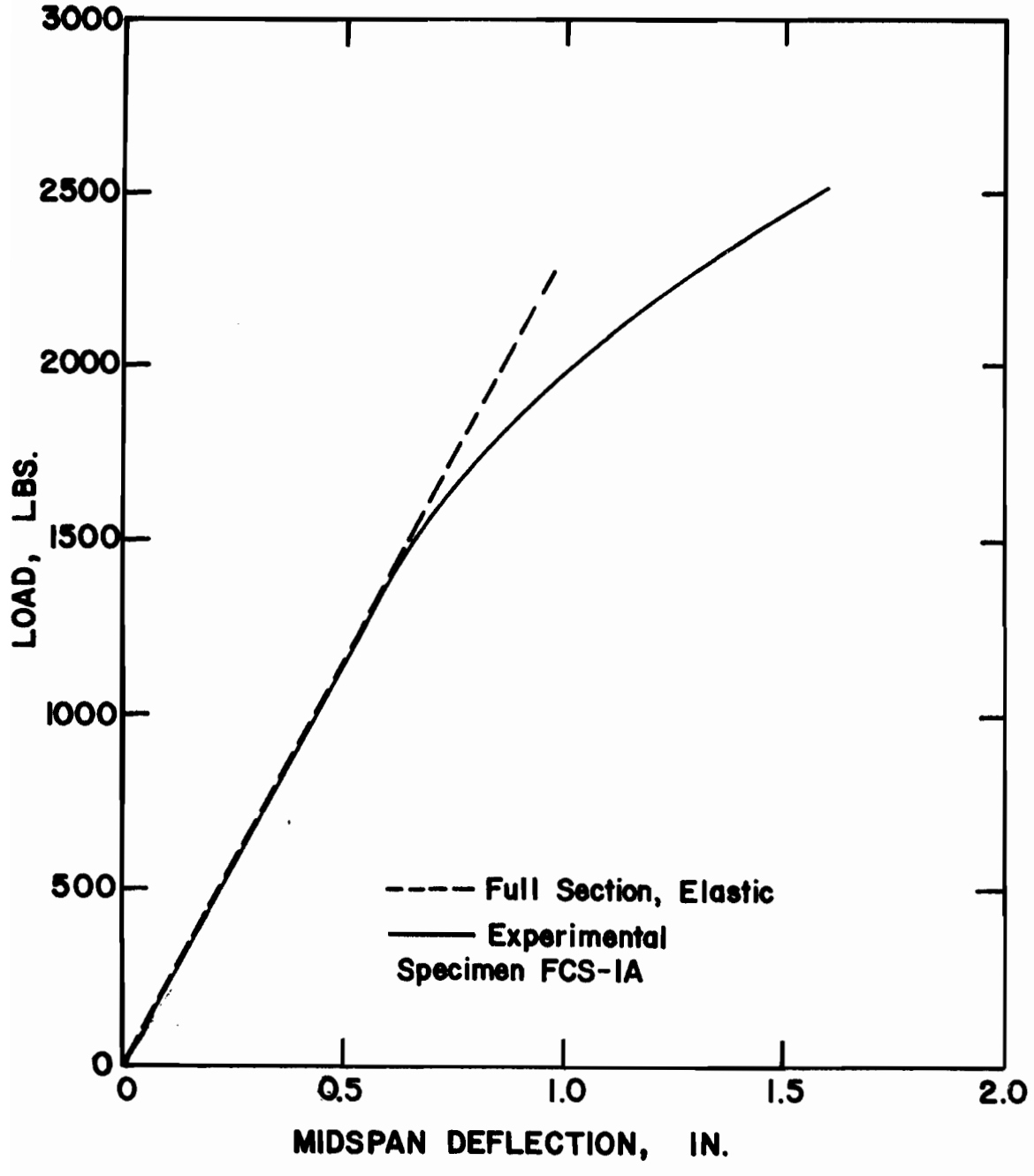

Figure 18, Load VS. Midspan Deflection

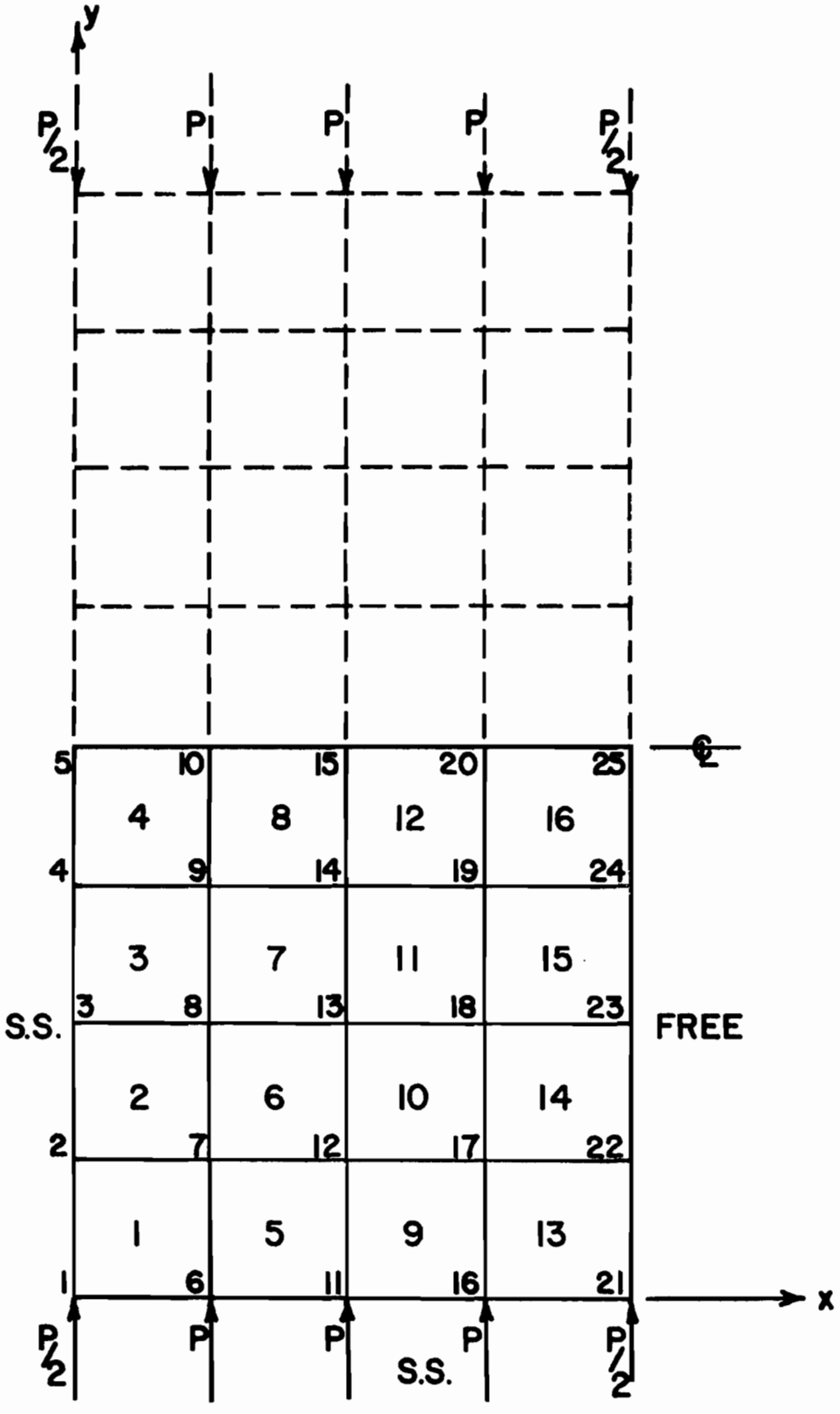

Figure 19. Finite Element Idealization for Unstiffened Plate

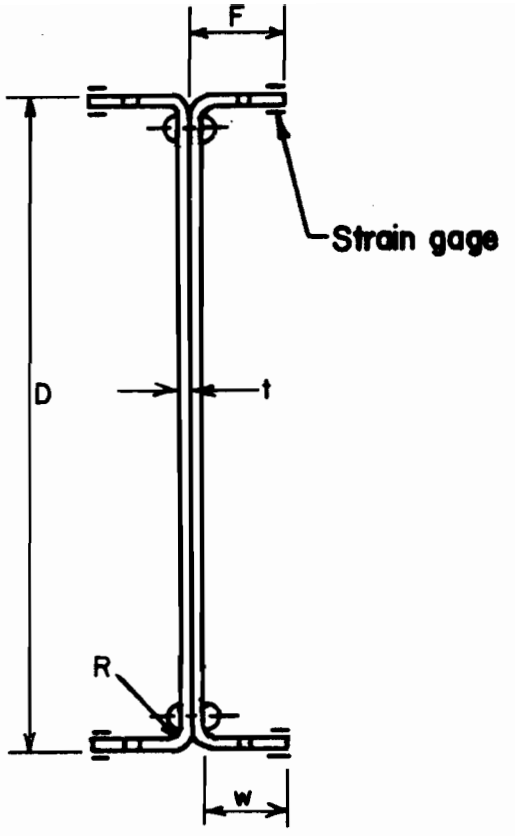

Figure 20. Cross-Section of Test Specimen

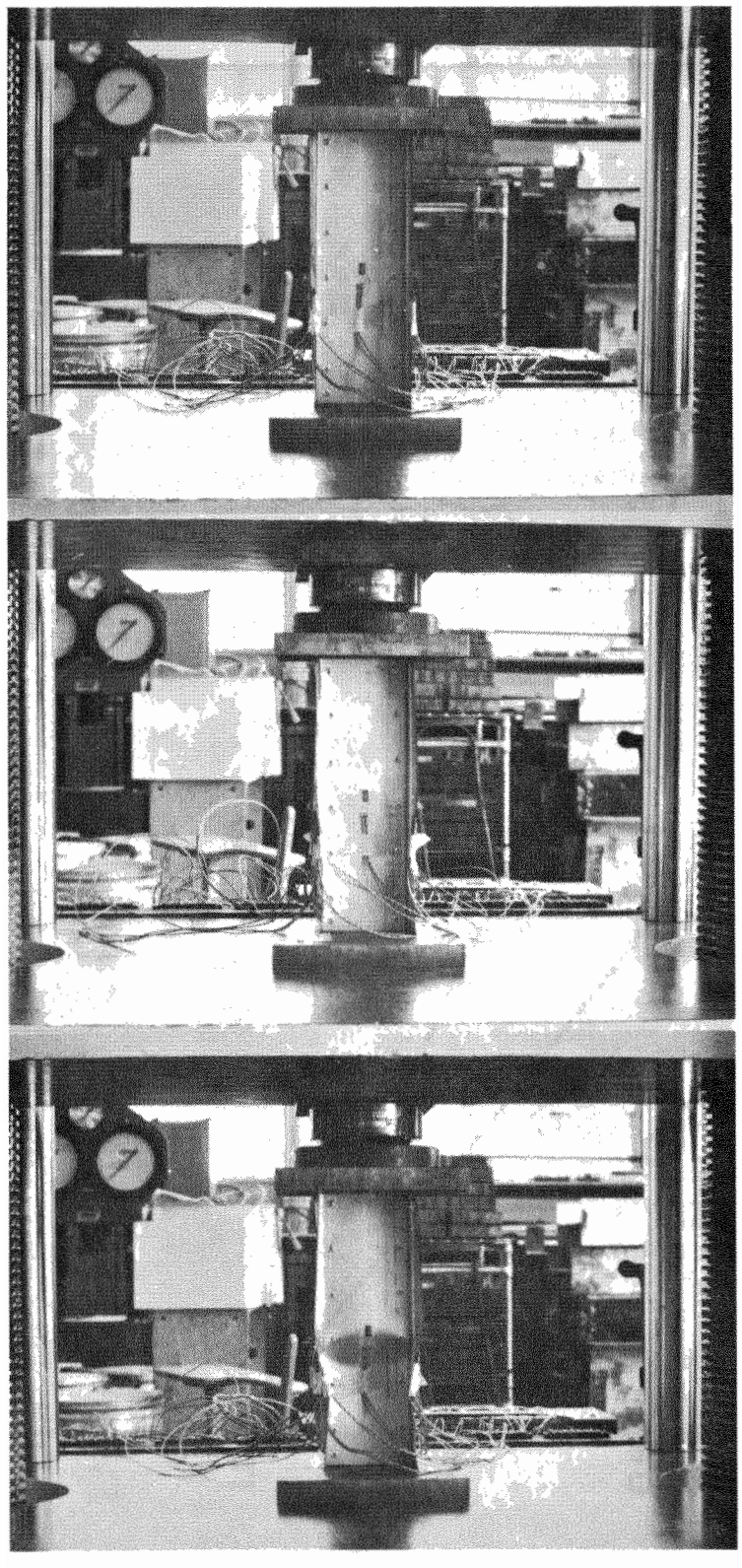

Figure 21. Perforated Unstiffened Element Test at Three Stages of Loading

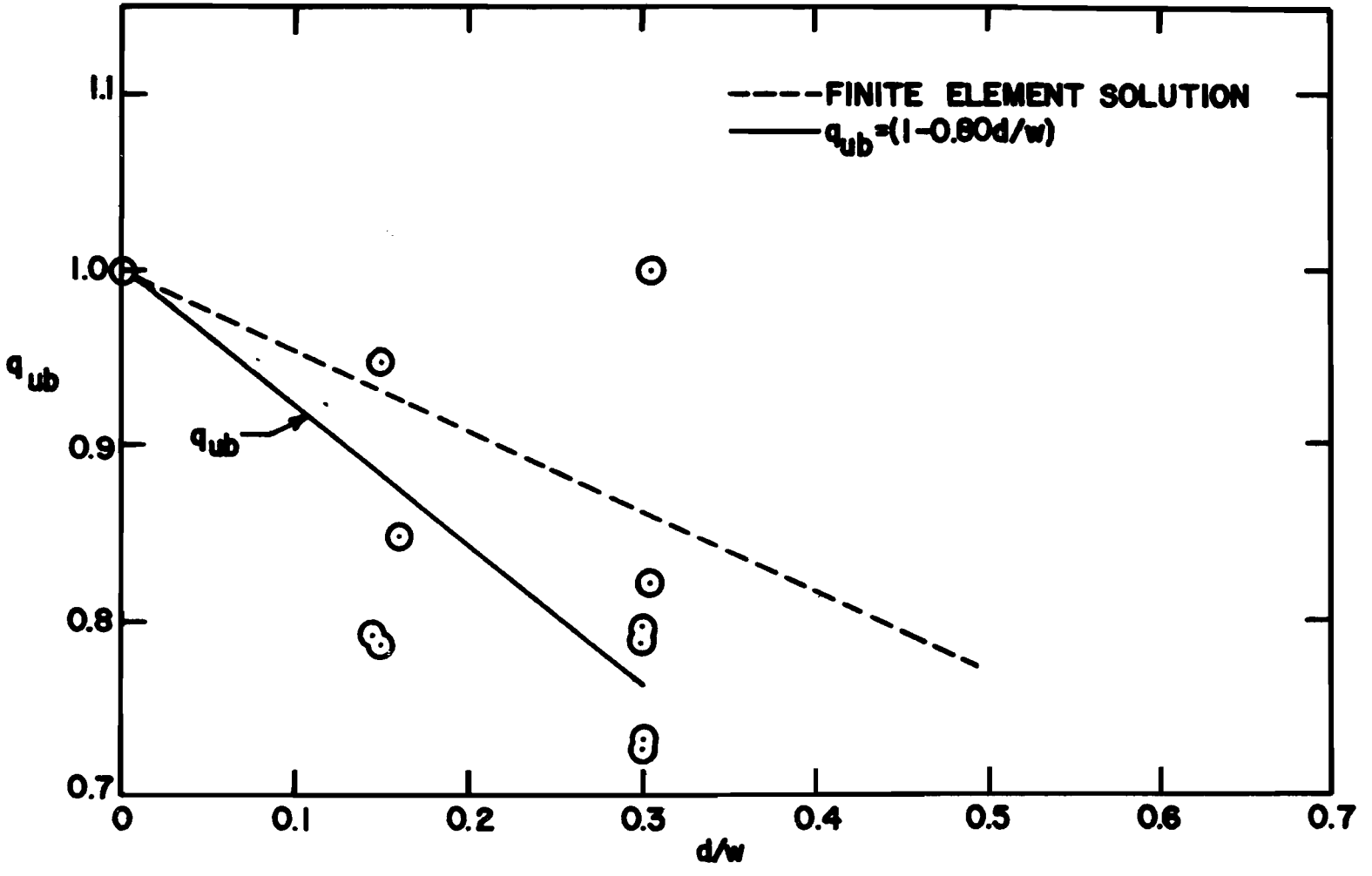

Figure 22. Reduction Factor q_{ub} for Perforated Unstiffened Compression Element

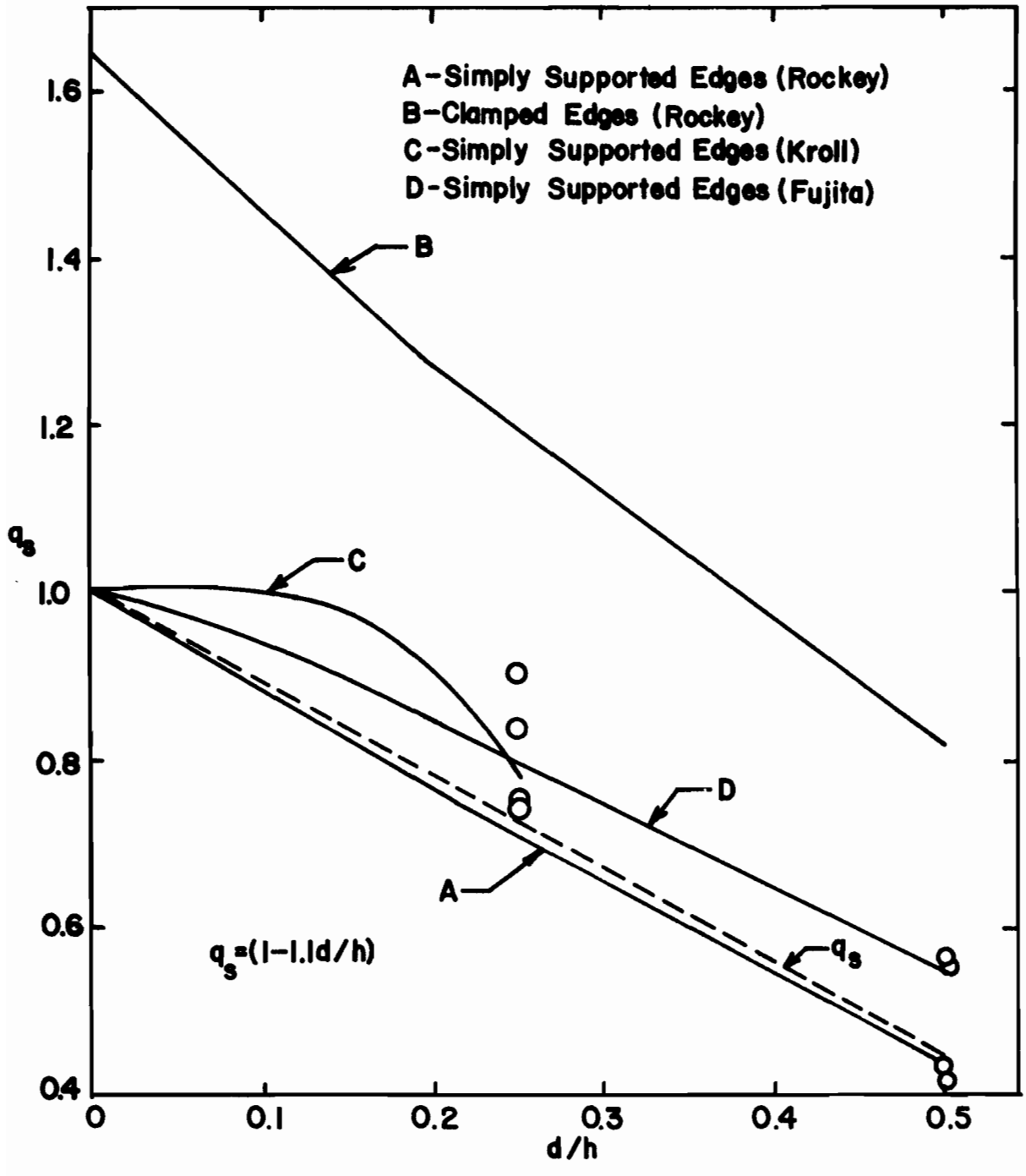

Figure 23. Comparison of Test Data with Analytical Shear Buckling Reduction Factor q_s

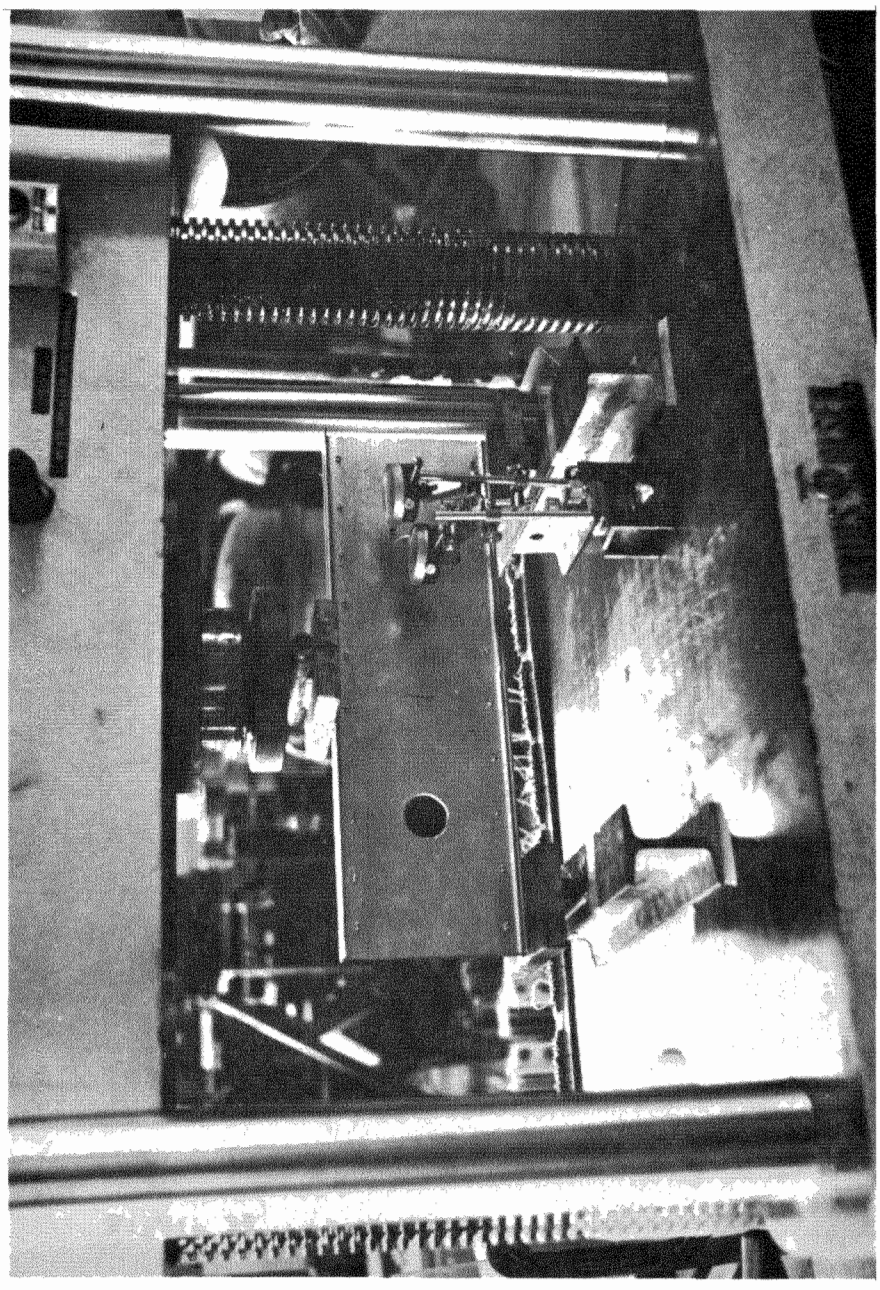

Figure 24. Shear Buckling Test Set-Up

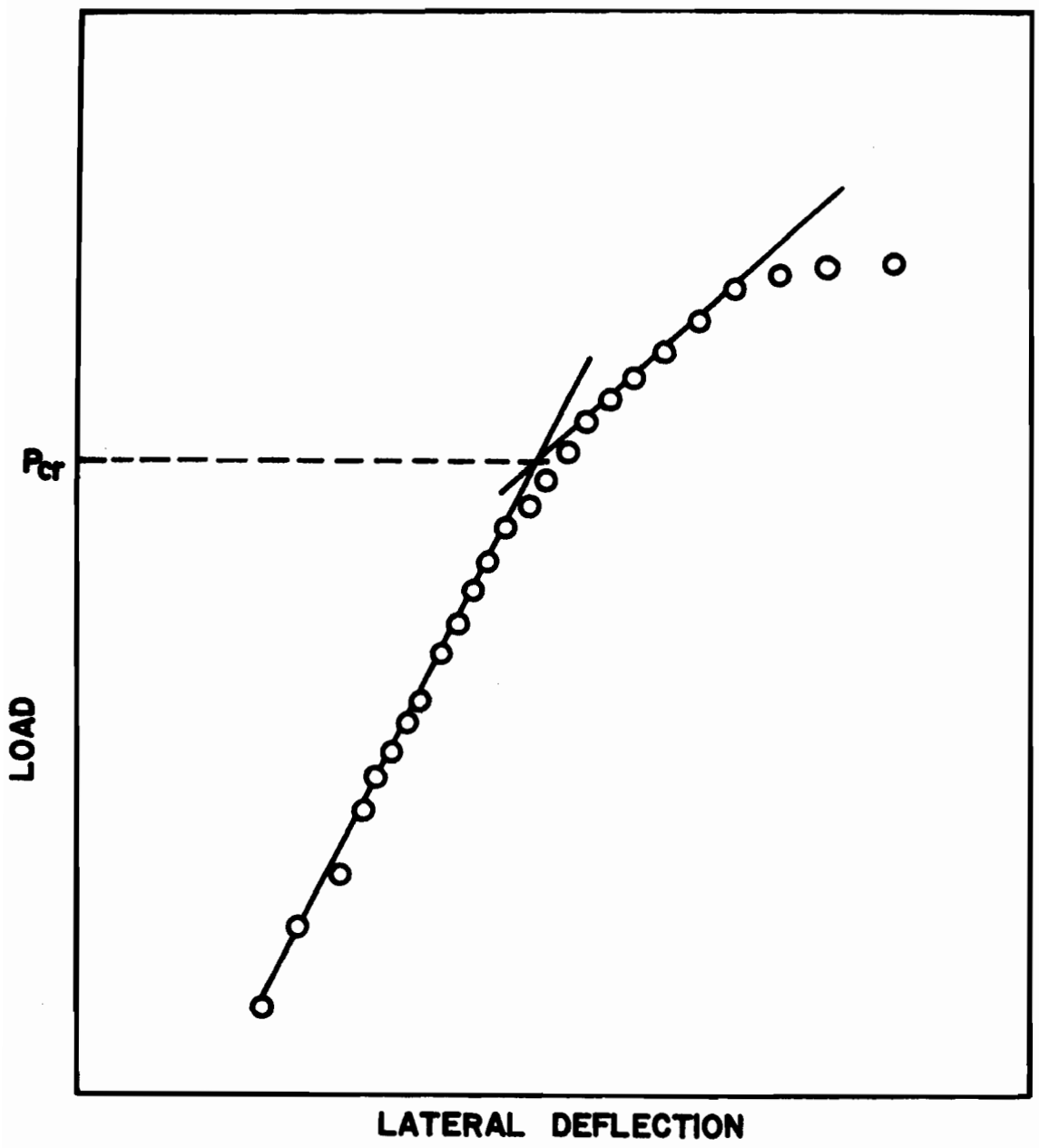

Figure 25. Load VS. Lateral Deflection Diagram

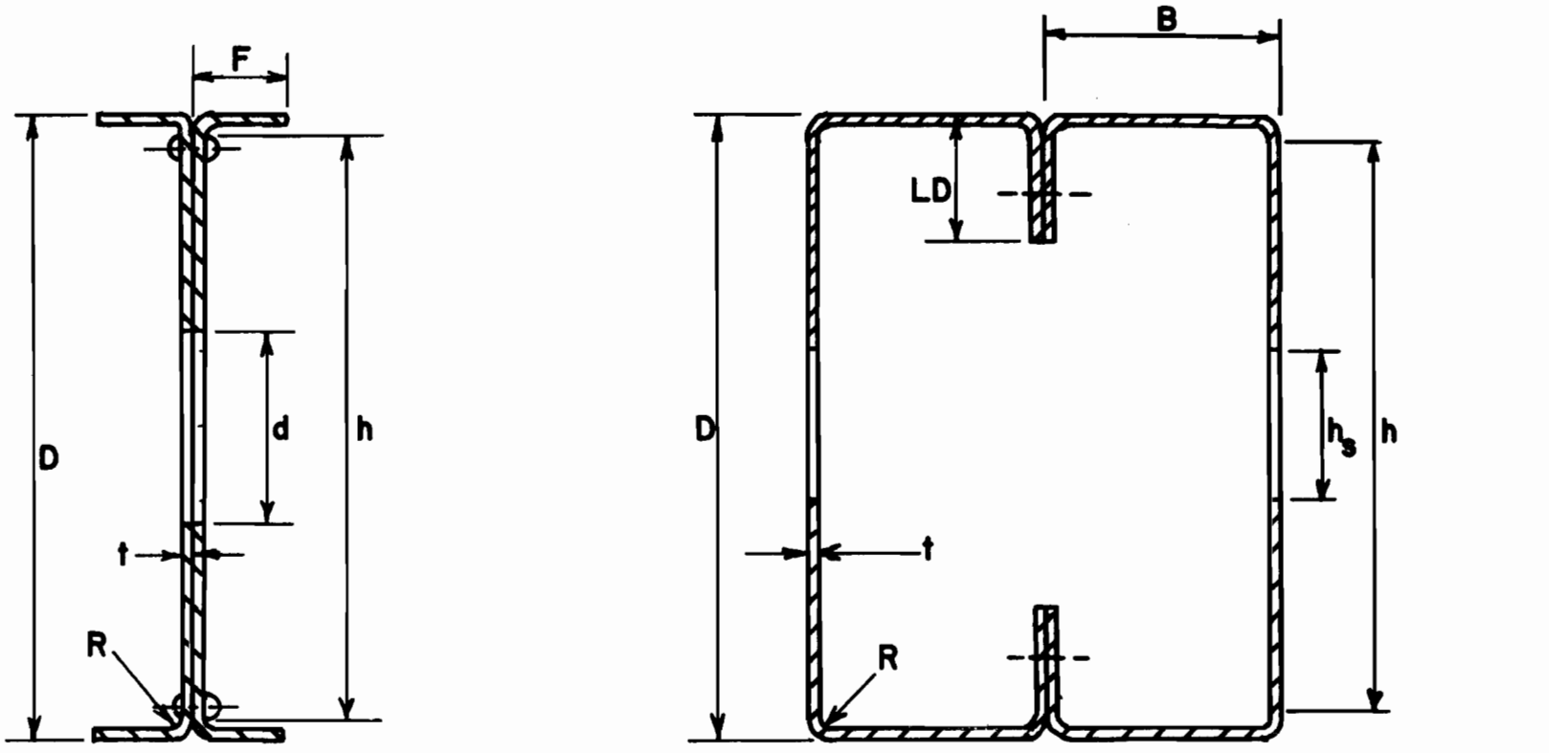

Figure 26. Crippling Test Specimens

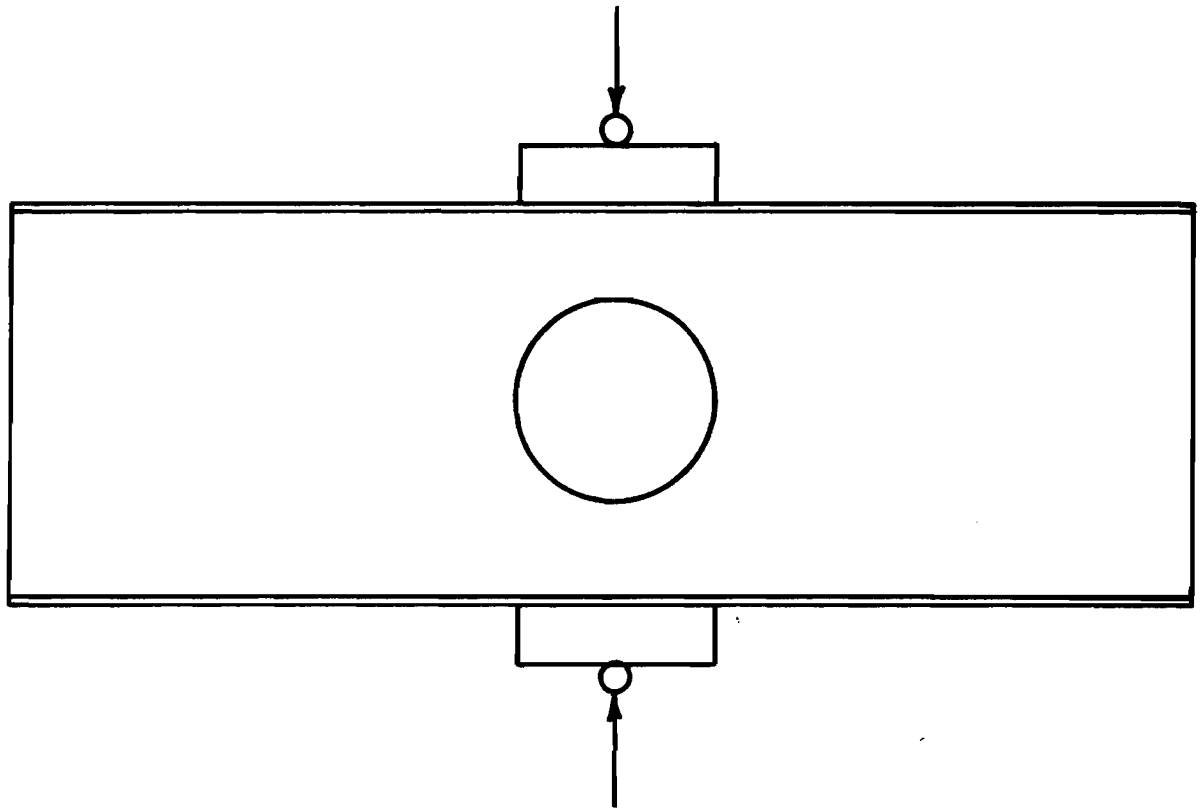

Figure 27. Crippling Test Loading Condition for I-Beams

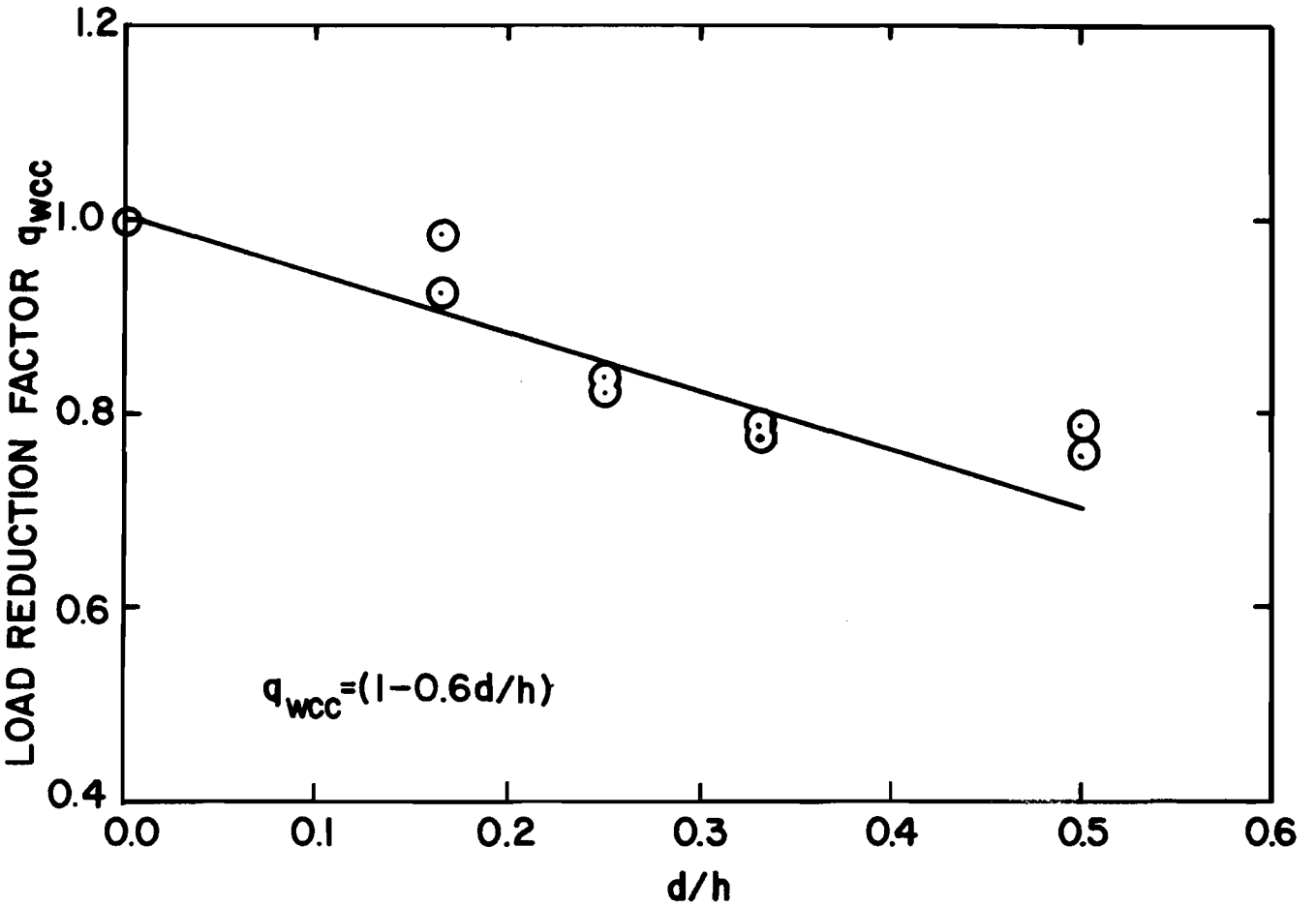

Figure 28. Load Reduction Factor q_{wcc} VS d/h Ratio for Circular Perforations

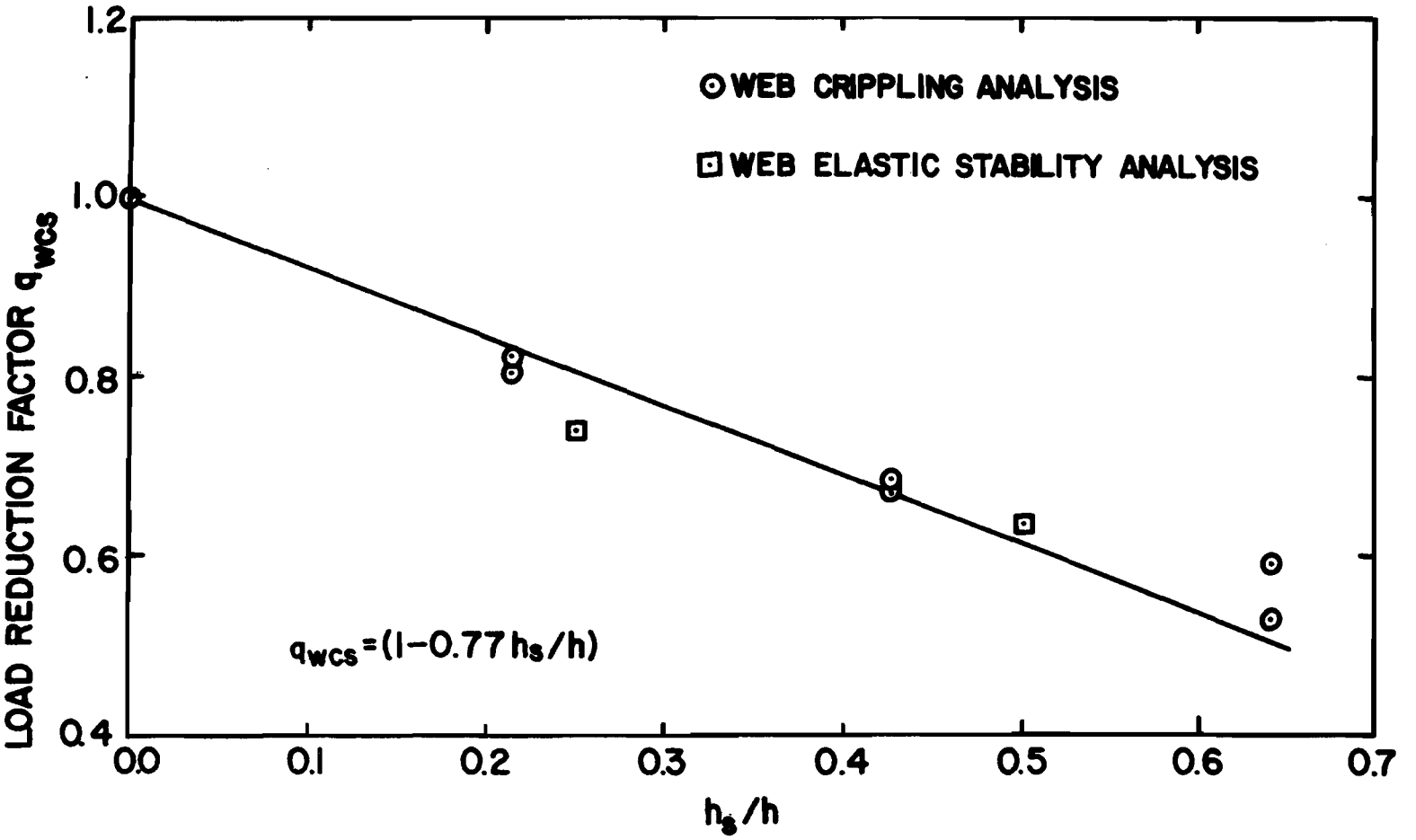

Figure 29. Load Reduction Factor q_{wcs} VS. h_s/h Ratio for Square Perforations

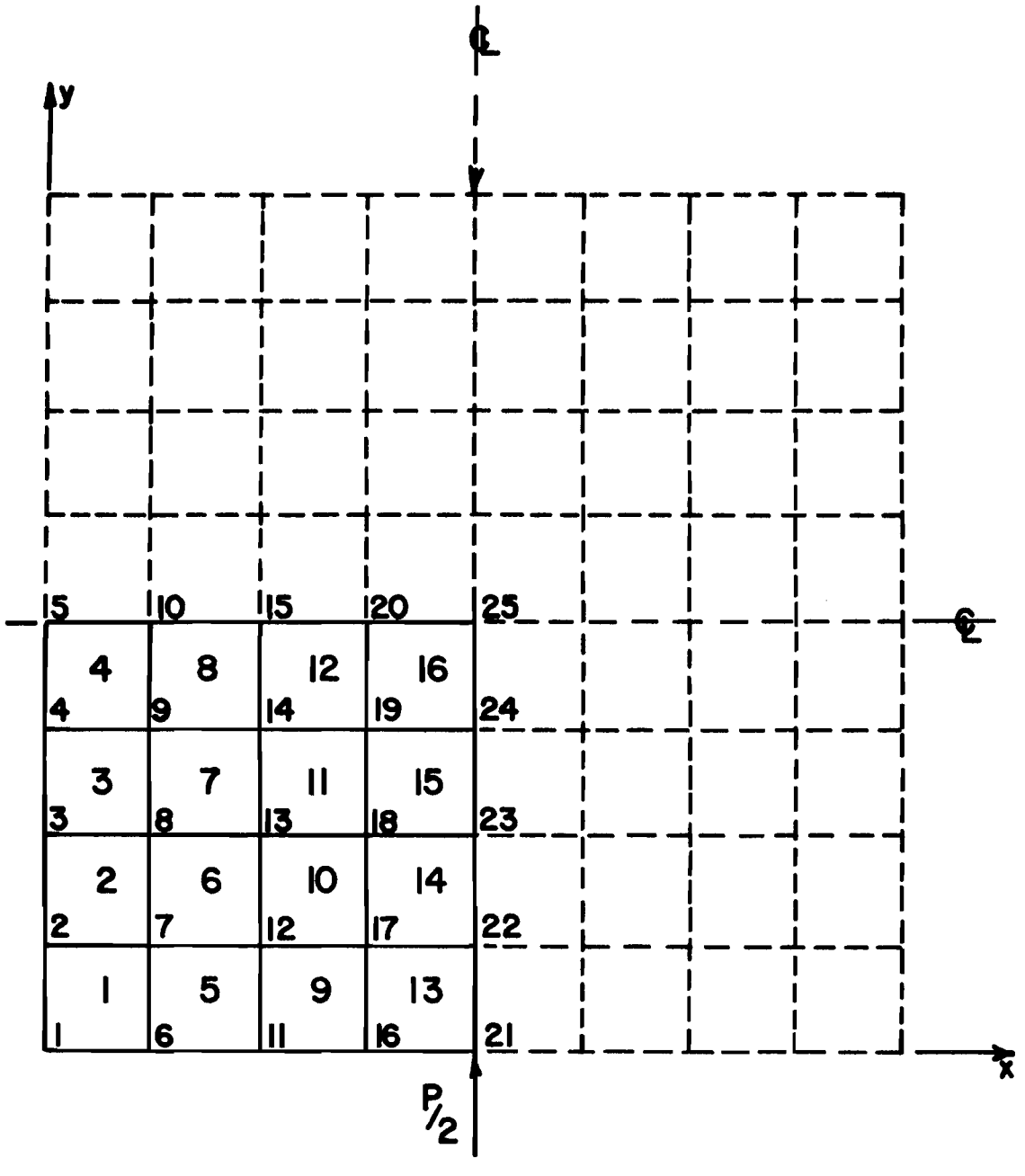

Figure 30. Finite Element Idealization for a Simply Supported Square Plate Subjected to Equal and Opposite Point Loads at the Center

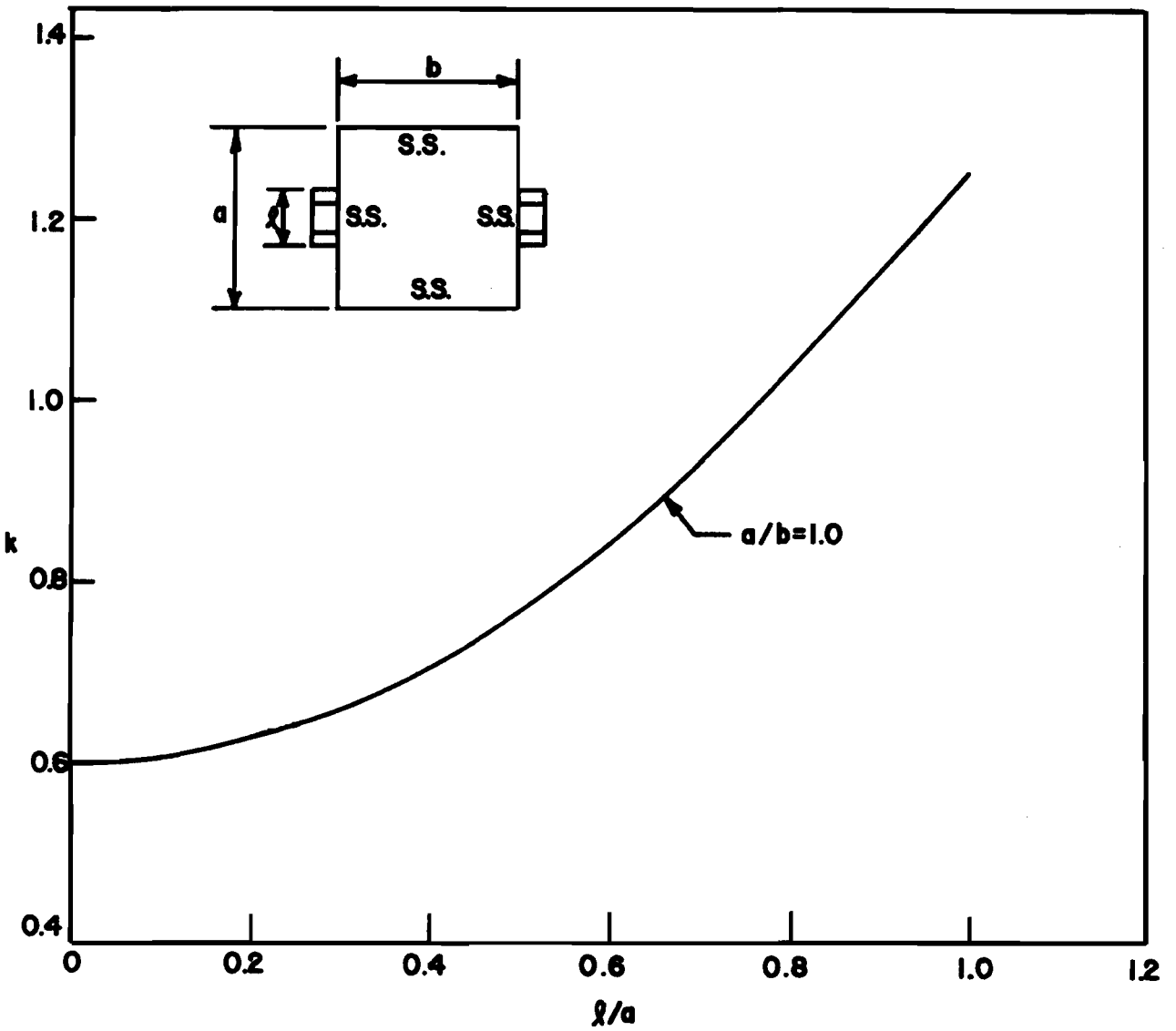

Figure 31. Effect of Locally Distributed Loads on Simply Supported Plates

Table I. Stiffened Compression Plate Boundary Conditions

Node No.	x	y	z	θ_x	θ_y	θ_z
1	(1)	2	(3)	4	5	6
2	(7)	8	(9)	10	11	12
3	(13)	14	(15)	16	17	18
4	(19)	20	(21)	22	23	24
5	(25)	(26)	(27)	28	29	30
6	31	32	(33)	34	35	36
7	37	38	39	40	41	42
8	43	44	45	46	47	48
9	49	50	51	52	53	54
10	55	(56)	57	(58)	59	60
11	61	62	(63)	64	65	66
12	67	68	69	70	71	72
13	73	74	75	76	77	78
14	79	80	81	82	83	84
15	85	(86)	87	(88)	89	90
16	91	92	(93)	94	95	96
17	97	98	99	100	101	102
18	103	104	105	106	107	108
19	109	110	111	112	113	114
20	115	(116)	117	(118)	119	120
21	(121)	122	(123)	124	125	126
22	(127)	128	129	130	(131)	132
23	(133)	134	135	136	(137)	138
24	(139)	140	141	142	(143)	144
25	(145)	(146)	147	(148)	(149)	(150)

( ) Deleted freedoms

Refer to Fig. 5

Table II. Buckling Coefficient Ratio for a Simply Supported Square Plate Having a Central Square Hole

Plate Dimensions	h_s In.	$\frac{h_s}{w}$	P_{cr} kips	k_s/k_{so}
40"x40"x0.1"	0.00	0.00	2.408	1.000
40"x40"x0.1"	10.00	0.25	1.840	0.764
40"x40"x0.1"	20.00	0.50	1.590	0.660

Table III. Dimensions and Sectional Properties of Column Specimens with Circular Perforations

Specimen	D In.	B In.	LD In.	w In.	t In.	d In.	$\frac{w}{t}$	$\frac{w-d}{t}$	A $In.^2$	L In.
FTFP-1	6.50	2.50	1.125	6.0932	0.094	0.0	64.8	64.8	2.4638	19.85
FTFP-2	6.40	2.50	1.375	5.8612	0.160	0.0	36.6	36.6	4.2192	19.85
FTFC-1	6.50	2.50	1.125	6.0932	0.094	1.30	64.8	51.0	2.2198	19.85
FTFC-2	6.50	2.50	1.125	6.0932	0.094	2.60	64.8	37.2	1.9758	19.85
FTFC-3	6.50	2.50	1.125	6.0932	0.094	3.90	64.8	23.35	1.7318	19.85
FTFC-4	6.40	2.50	1.375	5.8612	0.160	1.30	36.6	28.5	3.8032	19.85
FTFC-5	6.40	2.50	1.375	5.8612	0.160	2.60	36.6	20.4	3.3872	19.85
FTFC-6	6.40	2.50	1.375	5.8612	0.160	3.90	36.6	12.25	2.9712	19.85

Notes:

R = Inside corner radius = 0.1094 in. for all specimens
FTFP = Specimens with no perforations
FTFC = Specimens with circular perforations

Refer to Fig. 9

Table IV. Dimensions and Sectional Properties of Column Specimens with Square Perforations

Specimen	D In.	B In.	LD In.	w In.	t In.	h In.	$\frac{w}{t}$	$\frac{w-h}{t}$	A $In.^2$	L In.
FTFS-1	6.50	2.50	1.125	6.0932	0.094	1.30	64.8	51.0	2.2198	19.85
FTFS-2	6.50	2.50	1.125	6.0932	0.094	2.60	64.8	37.2	1.9758	19.85
FTFS-3	6.50	2.50	1.125	6.0932	0.094	3.90	64.8	23.35	1.7318	19.85
FTFS-4	6.40	2.50	1.375	5.8612	0.160	1.30	36.6	28.5	3.8032	19.85
FTFS-5	6.40	2.50	1.375	5.8612	0.160	2.60	36.6	20.4	3.3872	19.85
FTFS-6	6.40	2.50	1.375	5.8612	0.160	3.90	36.6	12.25	2.9712	19.85

Notes:

R = Inside corner radius = 0.1094 in. for all specimens
FTFS = Specimens with square perforations

Refer to Fig. 9

Table V. Mechanical Properties of Steel Test Specimens

Specimen	t	F_y	F_u	Average Mechanical Properties		
	In.	Ksi.	Ksi.	F_y Ksi.	F_u Ksi.	Elong.* Percent
1	0.094	34.00	50.00	(34.4)	(50.4)	(32.5)
2	0.094	35.10	50.20			
3	0.094	33.50	51.10			
4	0.094	35.10	50.30			
5	0.160	43.20	56.60	(41.9)	(57.3)	(25.0)
6	0.160	40.70	57.00			
7	0.160	41.80	57.10			
8	0.160	41.80	58.30			
9	0.075	58.70	74.00	(59.3)	(72.9)	--
10	0.075	60.20	72.50			
11	0.075	58.70	72.50			
12	0.075	59.70	72.80			

* Based on a 2 in. gage length

Table VI. Experimental Buckling Coefficient Ratio for Column Specimens with Circular Perforations

Specimen	d In.	$\frac{d}{w}$	P_{cr} Kips	$\frac{k_c}{k_{co}}$
FTFP-1	0.00	0.000	61.00	1.000
FTFC-1A	1.30	0.213	55.50	0.910
FTFC-1B	1.30	0.213	55.00	0.900
FTFC-2A	2.60	0.426	54.00	0.886
FTFC-2B	2.60	0.426	50.67	0.031
FTFC-3A	3.90	0.639	38.00	0.624
FTFC-3B	3.90	0.639	47.50	0.779

Table VII. Experimental Buckling Coefficient Ratio for Column Specimens with Square Perforations

Specimen	h In.	$\frac{h_s}{w}$	P_{cr} Kips	$\frac{k_s}{k_{so}}$
FTFP-1	0.00	0.000	61.00	1.000
FTFS-1A	1.30	0.213	48.50	0.795
FTFS-1B	1.30	0.213	49.00	0.803
FTFS-2A	2.60	0.426	41.00	0.672
FTFS-2B	2.60	0.426	42.50	0.697
FTFS-3A	3.90	0.639	37.00	0.607
FTFS-3B	3.90	0.639	39.50	0.650

Table VIII. Tested Ultimate Loads and Computed Effective Widths Based on Short Column Tests

Specimen	t In.	Area $In.^2$	d or h In.	Ultimate Load Kips	b* In.
FTFP-1A	0.094	2.4638	0.00	69.8	3.781
FTFP-1B	0.094	2.4638	0.00	70.0	3.812
FTFC-1A	0.094	2.2198	1.30	68.2	3.533
FTFC-1B	0.094	2.2198	1.30	67.5	3.425
FTFC-2A	0.094	1.9758	2.60	66.0	3.193
FTFC-2B	0.094	1.9758	2.60	67.7	2.992
FTFC-3A	0.094	1.7318	3.90	61.4	2.482
FTFC-3B	0.094	1.7318	3.90	61.8	2.544
FTFS-1A	0.094	2.2198	1.30	68.1	3.518
FTFS-1B	0.094	2.2198	1.30	70.0	3.812
FTFS-2A	0.094	1.9758	2.60	65.6	3.131
FTFS-2B	0.094	1.9758	2.60	64.9	3.023
FTFS-3A	0.094	1.7318	3.90	59.4	2.173
FTFS-3B	0.094	1.7318	3.90	60.5	2.343
FTFP-2A	0.160	4.2192	0.00	179.8	6.952
FTFP-2B	0.160	4.2192	0.00	181.8	7.101
FTFC-4A	0.160	3.8032	1.30	169.0	6.146
FTFC-4B	0.160	3.8032	1.30	172.1	6.377
FTFC-5A	0.160	3.3872	2.60	155.5	5.138
FTFC-5B	0.160	3.3872	2.60	156.8	5.235
FTFC-6A	0.160	2.9712	3.90	148.1	4.586
FTFC-6B	0.160	2.9712	3.90	149.0	4.653
FTFS-4A	0.160	3.8032	1.30	166.3	5.922
FTFS-4B	0.160	3.8032	1.30	167.2	6.011
FTFS-5A	0.160	3.3872	2.60	156.4	5.205
FTFS-5B	0.160	3.3872	2.60	152.3	4.899
FTFS-6A	0.160	2.9712	3.90	144.0	4.280
FTFS-6B	0.160	2.9712	3.90	143.2	4.220

* For the 0.160 inch thick specimens, the computed effective width is greater than the actual width.

Table IX. Dimensions and Properties of Beam Specimens with Circular Perforations

Specimen	D In.	B In.	LD In.	w In.	d In.	$\frac{w}{t}$	$\frac{w-d}{t}$	Span,L In.
FCS-1	6.00	2.50	0.50	5.538	0.00	73.8	73.80	88.00
FCS-2	6.00	2.50	0.50	5.538	1.00	73.8	59.20	88.00
FCS-3	6.00	2.50	0.50	5.538	2.50	73.8	40.50	88.00
FCS-4	6.00	2.50	0.50	5.538	4.00	73.8	20.50	88.00

Notes: R = Inside corner radius = 0.156 in. for all specimens
t = 0.075 for all specimens

Refer to Fig. 16

Table X. Experimental Buckling Coefficient Ratio for Beam Specimens with Circular Perforations

Specimen	d In.	$\frac{d}{w}$	P_{cr} Kips	$\frac{k_c}{k_{co}}$
FCS-1	0.00	0.000	1.150*	1.000*
FCS-2A	1.00	0.181	1.100	0.957
FCS-2B	1.00	0.181	0.950	0.826
FCS-3A	2.50	0.451	0.900	0.783
FCS-3B	2.50	0.451	1.050	0.913
FCS-4A	4.00	0.722	1.000	0.870
FCS-4B	4.00	0.722	1.000	0.870

* Average of two tests

Table XI. Comparison of the Computed and Tested Yield Moments

Specimen	Computed Yield Moment M_{comp}, In.-K	Tested Yield Moment M_{test}, In.-K	$\frac{M_{comp}}{M_{test}}$
FCS-1A	20.65	21.55	0.96
FCS-1B	20.65	21.85	0.95
FCS-2A	20.42	21.70	0.94
FCS-2B	20.42	21.80	0.94
FCS-3A	19.94	21.10	0.95
FCS-3B	19.94	20.80	0.96
FCS-4A	18.31	19.45	0.94
FCS-4B	18.31	19.80	0.92

Table XII. Comparison of Centerline Deflections for Beam Tests

Load lbs	d/w Ratios			
	0.0	0.181	0.452	0.723
0	0	0	0	0
500	0.257	0.267	0.262	0.273
1000	0.530	0.545	0.522	0.545
1500	0.829	0.857	0.795	0.825

Table XIII. Comparison of Effective Widths

Specimen	AISC Limiting Value[1] for $(\frac{w}{t})_{lim}$	Specimen $\frac{w}{t}$	AISC Effective Width b_{AISC} In.	Computed[2] Effective Width b. In.	$\frac{b_{AISC}}{b}$
FTFP-1	54.0	64.8	--	4.26	--
FTFC-1	54.0	64.8	--	3.94	--
FTFC-2	54.0	64.8	--	3.33	--
FTFC-3	54.0	64.8	--	2.29	--
FTFP-2	49.0	36.6	5.86	5.66	1.03
FTFC-4	49.0	36.6	4.56	4.74	0.96
FTFC-5	49.0	36.6	3.26	3.41	0.96
FTFC-6	49.0	36.6	1.96	1.96	1.00
FCS-1	41.0	73.8	--	2.78	--
FCS-2	41.0	73.8	--	2.58	--
FCS-3	41.0	73.8	--	2.21	--
FCS-4	41.0	73.8	--	1.50	--

[1] $(\frac{w}{t})_{lim} = 317/\sqrt{F_y}$

[2] Computations based on modified effective width equations.

Table XIV. Unstiffened Compression Plate Boundary Conditions

Node No.	x	y	z	θ_x	θ_y	θ_z
1	(1)	2	(3)	(4)	(5)	6
2	(7)	8	(9)	10	(11)	12
3	(13)	14	(15)	16	(17)	18
4	(19)	20	(21)	22	(23)	24
5	(25)	(26)	(27)	28	(29)	30
6	31	32	(33)	(34)	35	36
7	37	38	39	40	41	42
8	43	44	45	46	47	48
9	49	50	51	52	53	54
10	55	(56)	57	58	(59)	60
11	61	62	(63)	(64)	65	66
12	67	68	69	70	71	72
13	73	74	75	76	77	78
14	79	80	81	82	83	84
15	85	(86)	87	88	(89)	90
16	91	92	(93)	(94)	95	96
17	97	98	99	100	101	102
18	103	104	105	106	107	108
19	109	110	111	112	113	114
20	115	(116)	117	118	(119)	120
21	121	122	(123)	(124)	125	126
22	127	128	129	130	131	132
23	133	134	135	136	137	138
24	139	140	141	142	143	144
25	145	(146)	147	148	(149)	150

( ) Deleted freedoms

Refer to Fig. 19

Table XV. Dimensions of Unstiffened Elements Test Specimens

Specimen	D In.	F In.	t In.	w In.	w/t	d In.	d/w	L In.
UCE 1	4.187	0.75	0.060	0.643	10.7	0.000	0.00	6.0
UCE 2	4.187	0.75	0.060	0.643	10.7	0.000	0.00	6.0
UCE 3	4.187	0.75	0.060	0.643	10.7	0.096	0.145	6.0
UCE 4	4.187	0.75	0.060	0.643	10.7	0.096	0.145	6.0
UCE 5	4.187	0.75	0.060	0.643	10.7	0.193	0.300	6.0
UCE 6	4.187	0.75	0.060	0.643	10.7	0.193	0.300	6.0
UCE 7	6.187	0.75	0.048	0.655	13.65	0.000	0.00	6.5
UCE 8	6.187	0.75	0.048	0.655	13.65	0.000	0.00	6.5
UCE 9	6.187	0.75	0.048	0.655	13.65	0.098	0.150	6.5
UCE 10	6.187	0.75	0.048	0.655	13.65	0.098	0.150	6.5
UCE 11	6.187	0.75	0.048	0.655	13.65	0.196	0.300	6.5
UCE 12	6.187	0.75	0.048	0.655	13.65	0.196	0.300	6.5
UCE 13	4.187	1.75	0.060	1.643	27.40	0.000	0.000	12.0
UCE 14	4.187	1.75	0.060	1.643	27.40	0.000	0.000	12.0
UCE 15	4.187	1.75	0.060	1.643	27.40	0.265	0.161	12.0
UCE 16	4.187	1.75	0.060	1.643	27.40	0.265	0.161	12.0
UCE 17	4.187	1.75	0.060	1.643	27.40	0.500	0.304	12.0
UCE 18	4.187	1.75	0.060	1.643	27.40	0.500	0.304	12.0

Note: R = Inside corner radius = 0.047 in. for all specimens

Table XVI. Experimental Critical Buckling Loads and Stress Reduction Factor, $q_{ub_{exp}}$

Specimen	d/w	P_{cr} Kips	$q_{ub_{exp}}$	q_{ub}	$\frac{q_{ub}}{q_{ub_{exp}}}$
UCE 2	0.00	16.500*	1.000	1.000	1.000
UCE 3	0.145	13.000	0.788	0.884	1.120
UCE 4	0.145	13.000	0.788	0.884	1.120
UCE 5	0.300	12.000	0.727	0.760	1.045
UCE 6	0.300	13.000	0.788	0.760	0.963
UCE 8	0.00	18.100*	1.000	1.000	1.000
UCE 9	0.150	17.150	0.947	0.880	0.928
UCE 10	0.150	14.200	0.785	0.880	1.120
UCE 11	0.300	13.250	0.732	0.760	1.035
UCE 12	0.300	14.400	0.796	0.760	0.954
UCE 14	0.00	8.929*	1.000	1.000	1.000
UCE 16	0.161	7.575	0.848	0.871	1.025
UCE 17	0.304	7.325	0.820	0.757	0.923
UCE 18	0.304	8.925	0.999	0.757	0.757

* Average of two identical tests

Table XVII. Shear Buckling Test Specimens Dimensions

Specimen	D In.	F In.	t In.	d In.	h In.	d/h	L In.
SB 1	4.187	1.75	0.060	0.00	3.973	0.00	15.00
SB 2	4.187	1.75	0.060	0.00	3.973	0.00	15.00
SB 3	4.187	1.75	0.060	1.00	3.973	0.252	15.00
SB 4	4.187	1.75	0.060	1.00	3.973	0.252	15.00
SB 5	4.187	1.75	0.060	2.00	3.973	0.504	15.00
SB 6	4.187	1.75	0.060	2.00	3.973	0.504	15.00
SB 7	6.187	0.75	0.060	0.00	5.973	0.00	20.00
SB 8	6.187	0.75	0.060	0.00	5.973	0.00	20.00
SB 9	6.187	0.75	0.060	1.50	5.973	0.25	20.00
SB 10	6.187	0.75	0.060	1.50	5.973	0.25	20.00
SB 11	6.187	0.75	0.060	3.00	5.973	0.50	20.00
SB 12	6.187	0.75	0.060	3.00	5.973	0.50	20.00

Notes: h = The web height
R = Inside corner radius = 0.047

Table VXIII. Experimental Shear Buckling Loads and Shear Buckling Reduction Factor, $q_{s_{exp}}$

Specimen	d/h	P'_{cr} Kips	$q_{s_{exp}}$	q_s	$\frac{q_s}{q_{s_{exp}}}$
SB 2	0.00	4.975*	1.000	1.000	1.000
SB 3	0.252	4.175	0.840	0.723	0.860
SB 4	0.252	4.500	0.905	0.723	0.798
SB 5	0.504	2.175	0.437	0.446	1.020
SB 6	0.504	2.075	0.417	0.446	1.065
SB 7	0.00	3.825*	1.000	1.000	1.000
SB 9	0.251	2.850	0.745	0.724	0.971
SB 10	0.251	2.825	0.738	0.724	0.981
SB 11	0.502	2.125	0.555	0.448	0.808
SB 12	0.502	2.150	0.562	0.448	0.788

* Average of two identical tests

Table XIX. Dimensions of Web Crippling Test Specimens with Circular Perforations

Specimen	D In.	F In.	t In.	h In.	d In.	d/h	L In.
WC 1	6.187	0.75	0.060	5.973	0.00	0.00	12.00
WC 2	6.187	0.75	0.060	5.973	0.00	0.00	12.00
WC 3	6.187	0.75	0.060	5.973	1.00	0.167	12.00
WC 4	6.187	0.75	0.060	5.973	1.00	0.167	12.00
WC 5	6.187	0.75	0.060	5.973	2.00	0.334	12.00
WC 6	6.187	0.75	0.060	5.973	2.00	0.334	12.00
WC 7	4.187	1.75	0.060	3.973	0.00	0.00	8.00
WC 8	4.187	1.75	0.060	3.973	0.00	0.00	8.00
WC 9	4.187	1.75	0.060	3.973	1.00	0.252	8.00
WC 10	4.187	1.75	0.060	3.973	1.00	0.252	8.00
WC 11	4.187	1.75	0.060	3.973	2.00	0.504	8.00
WC 12	4.187	1.75	0.060	3.973	2.00	0.504	8.00

Table XX. Dimensions of Web Crippling Test Specimens with Square Perforations

Specimen	D In.	B In.	LD In.	t In.	h In.	h_s In.	h_s/h	L In.
WC 13	6.50	2.50	1.125	0.060	6.071	0.00	0.000	19.85
WC 14	6.50	2.50	1.125	0.060	6.071	0.00	0.000	19.85
WC 15	6.50	2.50	1.125	0.060	6.071	1.30	0.214	19.85
WC 16	6.50	2.50	1.125	0.060	6.071	1.30	0.214	19.85
WC 17	6.50	2.50	1.125	0.060	6.071	2.60	0.428	19.85
WC 18	6.50	2.50	1.125	0.060	6.071	2.60	0.428	19.85
WC 19	6.50	2.50	1.125	0.060	6.071	3.90	0.642	19.85
WC 20	6.50	2.50	1.125	0.060	6.071	3.90	0.642	19.85

Note: R = Inside corner radius = 0.1094 in. for all specimens

Table XXI. Experimental Ultimate Loads and Ultimate Load Reduction Factor, $q_{wcc_{exp}}$ for Web Crippling Specimens with Circular Perforations

Specimen	d/h	P_{ult} Kips	$q_{wcc_{exp}}$	q_{wcc}	$\frac{q_{wcc}}{q_{wcc_{exp}}}$
WC 2	0.00	5.530*	1.000	1.000	1.000
WC 3	0.167	5.440	0.983	0.900	0.916
WC 4	0.167	5.100	0.922	0.900	0.976
WC 5	0.334	4.340	0.785	0.800	1.020
WC 6	0.334	4.270	0.772	0.800	1.035
WC 8	0.00	6.190*	1.000	1.000	1.000
WC 9	0.252	5.170	0.835	0.849	1.015
WC 10	0.252	5.090	0.823	0.849	1.030
WC 11	0.504	4.850	0.784	0.698	0.892
WC 12	0.504	4.670	0.755	0.698	0.925

* Average of two identical tests

Table XXII. Experimental Ultimate Loads and Ultimate Load Reduction Factor, q_{wcs} for Web Crippling Specimens with Square Perforations^{exp}

Specimen	h_s/h	P_{ult} Kips	$q_{wcs_{exp}}$	q_{wcs}	$\frac{q_{wcs}}{q_{wcs_{exp}}}$
WC 14	0.000	8.375*	1.000	1.000	1.000
WC 15	0.214	6.750	0.805	0.835	1.035
WC 16	0.214	6.900	0.824	0.835	1.010
WC 17	0.428	5.750	0.686	0.670	0.977
WC 18	0.428	5.650	0.675	0.670	0.993
WC 19	0.642	4.950	0.591	0.505	0.854
WC 20	0.642	4.450	0.531	0.505	0.950

* Average of two identical tests

Table XXIII. Comparison of Test Results with Results of Winter and Pian (36)

Test Specimen	Experimental P_{ult} Kips	Winter & Pian P_{ult} Kips
WC-2	5.530	6.680
WC-8	6.190	7.04
WC-14	8.375	6.26

Table XXIV. Boundary Conditions for Perforated Plate

Node No.	x	y	z	θ_x	θ_y	θ_z
1	(1)	2	(3)	(4)	(5)	6
2	(7)	8	(9)	10	(11)	12
3	(13)	14	(15)	16	(17)	18
4	(19)	20	(21)	22	(23)	24
5	(25)	(26)	(27)	28	(29)	30
6	31	32	(33)	(34)	35	36
7	37	38	39	40	41	42
8	43	44	45	46	47	48
9	49	50	51	52	53	54
10	55	(56)	57	58	(59)	60
11	61	62	(63)	(64)	65	66
12	67	68	69	70	71	72
13	73	74	75	76	77	78
14	79	80	81	82	83	84
15	85	(86)	87	88	(89)	90
16	91	92	(93)	(94)	95	96
17	97	98	99	100	101	102
18	103	104	105	106	107	108
19	109	110	111	112	113	114
20	115	(116)	117	118	(119)	120
21	(121)	122	(123)	(124)	125	126
22	(127)	128	129	(130)	131	132
23	(133)	134	135	(136)	137	138
24	(139)	140	141	(142)	143	144
25	(145)	(146)	147	(148)	(149)	(150)

( ) Deleted freedoms

Refer to Fig. 30

Table XXV. Critical Buckling Loads and Load Reduction Factor, q_{wbs}

h_s/h	P_{cr} Kips	q_{wbs}
0.00	37.7	1.00
0.25	27.9	0.740
0.50	23.9	0.635

BIBLIOGRAPHY

1. Column Research Council, "Guide to Design Criteria for Metal Compression Members," edited by B.G. Johnston, Second Edition, John Wiley & Sons, Inc., New York, 1966.

2. American Institute of Steel Construction, "Specification for the Design, Fabrication and Erection of Structural Steel for Buildings," February, 1969.

3. The American Association of State Highway Officials, "Standard Specifications for Highway Bridges," 10th Edition.

4. American Railway Engineering Association, "Specification for Steel Railway Bridges," 1969.

5. Rack Manufacturer's Institute, "Minimum Engineering Standards for Industrial Steel Storage Racks," September 11, 1964.

6. Greenspan, M., "Axial Rigidity of Perforated Structural Members," National Bureau of Standard Research Paper RP 1568, Dec. 1943.

7. Greenspan, M., "Theory for Axial Rigidity of Structural Members Having Ovaloid or Square Perforations," National Bureau of Standards Research Paper RP 1737, Sept. 1946.

8. Stang, A.H. and Greenspan, M., "Perforated Cover Plates for Steel Columns: Summary of Compressive Properties," National Bureau of Standards Research Paper RP 1880, May 1948.

9. White, M.W. and Thurlimann, B., "Study of Columns with Perforated Cover Plates," AREA Bull. No. 531, 1956.

10. American Iron and Steel Institute, "Specifications for the Design of Cold-Formed Steel Structural Members," 1968 Edition.

11. Murray, J.M., "Pietzker's Effective Breadth of Flange Re-examined," Engineering, V. 161, pp. 364-365, 1946.

12. von Karman, T., Sechler, E.E., and Donnell, L.H., "The Strength of Thin Plates in Compression," Transactions American Society of Mechanical Engineers, Vol. 54, 1932, pp. 53.

13. Marguerre, K., "The Apparent Width of the Plate in Compression," NACA Technical Memoranda No. 833, 1937.

14. Winter, G., "Stress Distribution In and Equivalent Width of Flanges of Wide, Thin-Wall Steel Beams," NACA Technical Note No. 784, 1940.

15. Winter, G., "Strength of Thin Steel Compression Flanges," Transactions, American Society of Civil Engineers, Vol. 112, 1947, pp. 527-554.

16. Dwight, J.B., and Ractliffe, A.J., "The Strength of Thin Plates in Compression," Thin Walled Steel Structures, Gordon and Breach Science Publishers, N.Y., 1968.

17. Abdel-Sayed, G., "Effective Width of Thin Plates in Compression," Journal of the Structural Division, ASCE, Oct. 1969, pp. 2183-2203.

18. Gerard, G., and Becker, H., "Handbook of Structural Stability, Part I - Buckling of Flat Plates," NASA Technical Note 3781, July 1957.

19. Johnson, A.L. and Winter, G., "The Structural Performance of Austenitic Stainless Steel Members," Cornell Report No. 327, November, 1966.

20. Wang, S.T. and Winter, G., "Cold-Rolled Austenitic Stainless Steel: Materials Properties and Structural Performance," Cornell Report No. 334, July, 1969.

21. Wang, S.T. and Errera, S.J., "Behavior of Cold-Rolled Stainless Steel Members," Proceedings of the First Specialty Conference on Cold-Formed Steel Structures, University of Missouri-Rolla, August 19-20, 1971.

22. Supple, W.J., and Chilver, A.H., "Elastic Post-Buckling of Compressed Rectangular Flat Plates," Thin Walled Structures, John Wiley and Sons, Inc., N.Y., 1967.

23. Bulson, P.S., "Local Stability and Strength of Structural Sections," Thin Walled Structures, John Wiley and Sons, Inc., N.Y., 1967.

24. National Bureau of Standards Progress Report No. 1, "Compressive Properties, Perforated Cover Plates for Steel Columns," Aug. 1941.

25. Levy, S., Woolley, R.M. and Kroll, W.D., "Instability of Supported Square Plates with Reinforced Circular Hole in Edge Compression," Journal Research of the National Bureau of Standards, Vol. 139, December, 1947.

26. Timoshenko, S.P. and Gere, J.M., "Theory of Elastic Stability," McGraw-Hill, New York, N.Y., 1961.

27. Kumai, T., "Elastic Stability of the Square Plate with a Central Circular Hole Under Edge Thrust," Reports of Research Institute for Applied Mechanics, Vol. 1, No. 2, April, 1952.

28. Schlack, A.L., "Elastic Stability of Pierced Square Plates," Experimental Mechanics, June 1964.

29. Yoshiki, M., Fujita, Y. and others, "Instability of Plates with Holes (1st Report)," Proceedings of the Society of Naval Architects of Japan, No. 122, December, 1967.

30. Kawai, T. and Ohtsubo, H., "A Method of Solution for the Complicated Buckling Problems of Elastic Plates with Combined Use of Rayleigh-Ritz's Procedure in the Finite Element Method," Proceedings of the 2nd Air Force Conference on Matrix Methods in Structural Mechanics, October, 1968.

31. Hull, R.E., "Buckling of Plates with Unknown In-Plane Stress Using the Finite Element Method," Master Thesis, University of Washington, August, 1970.

32. Vann, W.P., "Compressive Buckling of Perforated Plate Elements," Proceedings of the First Specialty Conference on Cold-Formed Steel Structures, University of Missouri-Rolla, August 19-20, 1971.

33. Kroll, W.D., "Instability of Simply Supported Square Plates with Reinforced and Unreinforced Holes Subjected to Shear," Journal Research, National Bureau of Standards, Vol. 43, Nov. 1949, p. 465.

34. Rockey, K.C., Anderson, R.G., Cheung, Y.K., "The Behavior of Square Shear Webs Having a Circular Hole," Thin Walled Steel Structures, Gordon and Breach Science Publishers, N.Y., 1969.

35. Zetlin, L., "Elastic Instability of Flat Plates Subjected to Partial Edge Loads," Proceedings, American Society of Civil Engineers, Vol. 81, 1955, pp. 795-1 to 795-24.

36. Winter, G. and Pian, R.H.J., "Crushing Strength of Thin Steel Webs," Cornell University Engineering Experimental Station Bulletin No. 35, Part 1, 1946.

37. Yen, B.T., Huang, P.J., Patterson, P.J., and Brozzetti, J., "Structural Stability Design Provisions - A Comparison of the Provisions of the CRC Guide and the Specification of AASHO, AISC, and AREA, Column Research Council Bulletin No. 146, Nov. 1969.

38. Subcommittee on Beams with Web Openings of the Task Committee on Flexural Members of the Structural Division, "Suggested Design Guides for Beam with Web Holes," Journal of the Structural Divsion, ASCE, Vol. 97, No. ST11, Proc. Paper 8530, Nov. 1971, pp. 2707-2728.

39. Yu, W.W. and Davis, C.S., "Buckling Behavior and Post-Buckling Strength of Perforated Stiffened Compression Elements," Proceedings of the First Specialty Conference on Cold-Formed Steel Structures, University of Missouri-Rolla, August 19-20, 1971.

40. Yang, H.T.Y., "A Finite Element Formulations for Stability Analysis of Doubly Curved Thin Shell Structures," Ph.D. Dissertation, Cornell University, January, 1969.

41. Winter, G., "Commentary on the 1968 Edition of the Specification for the Design of Cold-Formed Steel Structural Members," published by American Iron and Steel Institute, 1970.

42. American Society for Testing and Material, "Annual Book of ASTM Standards, Part 1," 1971.

43. Karren, K.W., "Corner Properties of Cold-Formed Steel Shapes," Journal of the Structural Division, ASCE, Vol. 93, No. ST1, Feb. 1967, pp. 401-432.

44. Kirsh, G., "Theory of Elasticity," 1st Edition by S. Timoshenko, p. 80, 1898.

45. Howland, R.C.J., and Stevenson, A.C. Phil Trans. R. Soc. Series A, Vol. 232, pp. 155-222, 1933-34.

46. Biskin, L., "Strengthening of Circular Holes in Plates under Edge Forces," Journal Applied Mechanics, Trans. A.S.M.E., p. A-140, 1944.

47. Wang, C.K., "Theoretical Analysis of Perforated Shear Webs," Journal Applied Mechanics, Trans. A.S.M.E., B, No. 2, pp. A77-A-S4, June 1946.

48. Yamaki, N., Rep. Inst. High Speed Mech. (Japan), Vol. 3, March 1953, p. 65.